5-1-2014

Design and Analysis of Hydrogen Powered Actuator Integrating Metal Hydride Storage System

Md Mainul Hossain Bhuiya

University of Nevada, Las Vegas, bhuiyam@unlv.nevada.edu

DESIGN AND ANALYSIS OF HYDROGEN POWERED ACTUATOR

INTEGRATING METAL HYDRIDE STORAGE SYSTEM

by

Md Mainul Hossain Bhuiya

Bachelor of Science in Mechanical Engineering
Bangladesh University of Engineering & Technology
2005

Master of Science in Mechanical Engineering
University of Nevada, Reno
2008

A dissertation submitted in partial fulfillment
of the requirements for the

Doctor of Philosophy - Mechanical Engineering

Department of Mechanical Engineering
Howard R. Hughes College of Engineering
The Graduate College

University of Nevada, Las Vegas
May 2014

THE GRADUATE COLLEGE

We recommend the dissertation prepared under our supervision by

Md Mainul Hossain Bhuiya

entitled

Design and Analysis of Hydrogen Powered Actuator Integrating Metal Hydride Storage System

is approved in partial fulfillment of the requirements for the degree of

Doctor of Philosophy in Engineering - Mechanical Engineering

Department of Mechanical Engineering

Kwang Kim, Ph.D., Committee Chair

Woosoon Yim, Ph.D., Committee Member

Brendan O'Toole, Ph.D., Committee Member

Dong-Chan Lee, Ph.D., Committee Member

Jacimaria Batista, Ph.D., Graduate College Representative

Kathryn Hausbeck Korgan, Ph.D., Interim Dean of the Graduate College

May 2014

ABSTRACT

Design and Analysis of Hydrogen Powered Actuator

Integrating Metal Hydride Storage System

by

Md. Mainul Hossain Bhuiya

Kwang J. Kim, Examination Committee Chair
Southwest Gas Professor of Energy & Matter, The Mechanical Engineering Department
University of Nevada, Las Vegas (UNLV)

The multi-fold purposes of this dissertation consists of construction, simulation and validation of a model describing hydrogen sorption kinetics in metal hydride. The project involves a comprehensive review of engineering applications involving metal hydrides and furthermore, design and investigation of a thermo-kinetically driven actuation system integrating metal hydrides for compact and soft robotic actuation. This will also shed some light on the feasibility of designing a damping system integrating metal hydride. Firstly, a mathematical model along with comprehensive simulation strategy of hydrogen absorption and desorption processes in porous metal hydride compacts was developed. A two dimensional axisymmetric model was built in COMSOL to simulate the sorption behavior of a typical metal hydride during hydrogen absorption and desorption processes. The model was formulated by considering mass conservation of hydrogen-absorbed metal alloy, Darcy flow in the porous medium, and heat generation and absorption by

exothermic and endothermic reaction for hydrogen absorption and desorption, respectively. Experiments to identify sorption characteristics during hydrogen uptake and desorption were carefully carried out for model validation purpose. The experimental data were used to validate the model describing fundamental physiochemical processes involved. Secondly, to test the plausibility of thermally driven actuator, a conventional piston type actuation system was built and integrated with $LaNi_5$ based hydrogen storage reactor. Copper encapsulation followed by compaction of particles into pellets, were adapted to improve thermal conductivity of the storage material, which minimizes thermal energy input that drives the system. The performance of the actuator was thoroughly investigated for arrays of operating temperature ranges to demonstrate smooth and noiseless actuation over the operating ranges. Consistent and smooth actuation was observed for repeated cycles of operation. Detailed performance analysis was performed along with application of Monte Carlo experiment to evaluate system efficiency and uncertainty associated with the results. The system showed actuation behavior that can be tuned to mimic a wide range of actuators including pneumatic and hydraulic actuators, artificial and biological muscles. Finally, preliminary investigation was carried out to study the feasibility of integration of hydrides in a damping system. Overall, the simulation results are in good agreement with the experimental observation for the hydrogen sorption model and the actuator showed consistent performance and very good level of efficiency within the temperature ranges of low grade waste heat.

ACKNOWLEDGEMENTS

TABLE OF CONTENTS

LIST OF TABLES

LIST OF FIGURES

NOMENCLATURE

A Constant in equation

B Constant in equation, K-1

c Concentration of hydrogen, mol/m^3

c_p Specific heat, J/kg-K

C Constant in equation, kg/m^3-s

D Diffusivity, m^2/s

E_a Activation energy, J/mol

H_a Activation enthalpy, eV

H Convective heat transfer coefficient, W/m^2-K

k Thermal conductivity, W/m-K

k_B Boltzmann constant, 8.617×10^{-5} eV/K

L Pellet height

M_{H_2} Molar mass of hydrogen gas, 2.0158 g/mol

$\dot{m}$ Hydrogen absorption rate, kg/m^3-s

p Hydrogen gas pressure, Pa

p_{eq} Equilibrium pressure, atm

r Radius

R Gas constant, 8.314 J/mol-K

R_c Reaction rate, mol/m^3-s

t Time, s

T Temperature, K

Z Compressibility factor

Greek Letters

ΔH Formation heat, J/kg

ε Porosity

κ Permeability, m^2

μ Viscosity, Pa-s

ρ Density, kg/m^3

Subscripts

a   Absorption

d   Desorption

g   Hydrogen gas

s   Metal hydride

ss   Stainless steal

sat   Saturated

o   Initial

1   Inner pellet

2   Outer pellet/inner wall

3   Outer wall

∞ Liquid pool

CHAPTER 1: Introduction & Objectives

Hydrogen is one of the most anticipated renewable energy sources of the future. Due to the unique ability of storing hydrogen at room temperature within the atomic structure and with H_2 density greater than liquid hydrogen, metal hydrides have long been established as excellent mediums for hydrogen storage [1-26]. While the kinetics of hydrogen absorption and desorption in storage material remain complex and are greatly influenced by a number of thermo-physical properties of the storage material, the processes for hydrogen storage and compression can be explained by simpler physicochemical process that takes place during the operation. Hydrogen is first absorbed into the storage material at a given supply pressure and at room temperature or lower. It remains in the hydride structure until the system is exposed to an elevated temperature or a driving pressure differential, which cause the stored hydrogen to exit from the hydride structure. It is the storage capacity of the hydrides that caught attention of the researchers for on board vehicular applications [20, 27].

1.1   Metal Hydride Fundamentals

There are at least fifty metallic elements in the periodic table, which can store hydrogen, only a handful of them are suitable for storing it at moderate temperature and pressure. The process is heavily reversible and can be expressed by Equation 1.1. Here, M and H represents metal and hydrogen respectively, x is the non-stoichiometric coefficient, and ΔH is the reaction enthalpy. The sorption process is exothermic while hydrogen is being absorbed or endothermic while hydrogen is being desorbed from the storage material.

$$M + \frac{x}{2}H_2 \leftrightarrow MH_x \pm \Delta H \qquad\qquad (1.1)$$

Hydrogen is stored in the interstitial spaces of the storage materials with densities greater than liquid hydrogen as shown in Figure 1.1. Stored mass of hydrogen in the storage systems are compared per unit mass (%) vs. per unit volume (kg H_2/m^3) basis. Additionally, regions are divided with dotted lines for grouping available hydrogen storage system in similar storage density ranges. Comparison of various metal hydrides, carbon nanotubes and other hydrocarbons is illustrated in the same graph. Except for the light weight hydrides, metal hydrides are generally heavier. On the contrary, hydrogen is the lightest gas next to helium. Thus, the weight of the hydride is mainly due to the metallic elements in the storage material, which is the reason why mass percentage of stored hydrogen in most of the hydrides are lower as shown with the black rectangles in the upper left region of the graph. Some light weight hydrides have better mass percentage as indicated in the grey rectangles. Liquid hydrogen, which require extremely cold temperature, also has very high mass percentage because of light weight composite cylinders that stores the hydrogen. Nevertheless, for mass of stored hydrogen per unit volume basis, metal hydrides are the best option for storing hydrogen at moderate temperature and pressures. Apart from the highest densities of these metal hydrides, low cost storage, maintenance and extraction made them an effective option for storage of hydrogen for practical applications.

Considering the fact that hydrogen has the smallest molecular weight (MW_{H2}=2), mass percentage of hydrides may seem very low. Nevertheless, density (mass/volume) wise, hydrides are superior to traditional storage technologies available as of today. For portable applications such as vehicular hydrogen storage, hydrides are very attractive

2

alternatives. The limiting condition for applicability of hydride material is generally related to the applicable temperature and pressure. Among different types of hydrides such as AB_5 (e.g. $LaNi_5$), AB (e.g. FeTi), A_2B (e.g. Mg_2Ni), and AB_2 (e.g. ZrV_2); AB_5 types such $LaNi_5$ are consistent in reversible sorption behavior at desirable ranges of operating temperature and pressures. It is the extremely high density with moderate operating ranges that make metal hydride a suitable candidate for portable hydrogen storage applications.
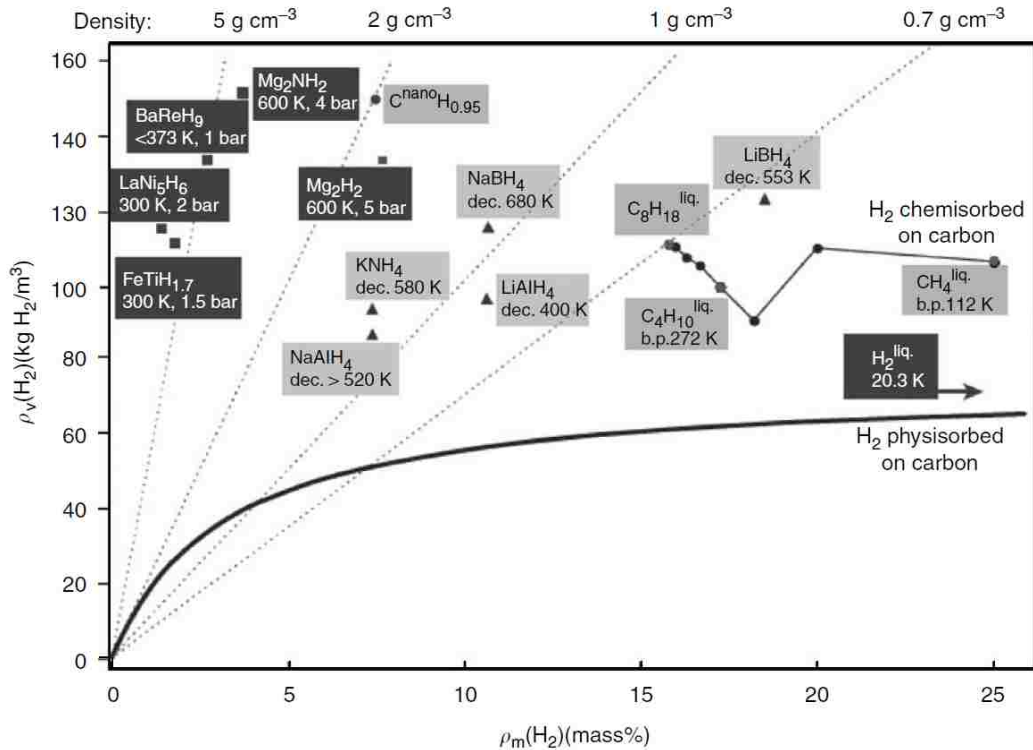
Figure 1. 1: Comparison of metal hydrides with other storage systems [14]

The most important feature of metal hydride storage system is the plateau pressure, illustrated in Figure 1.2(a), at which materials reversibly absorb/desorb hydrogen at a large quantity. For applications such as NiMH batteries, this plateau pressure is desired to be close to the ambient pressure, which allows designing the container with light weight

3

material. Higher pressure plateau would generate higher desorption pressure in the application system. Hence, the container would be required to be strong enough to withstand that pressure during operation. This would eventually increase the material cost and the cost of final product. Generally, a pressure differential between absorption and desorption is observed in the isotherms. This is indicative of the fact that, absorption requires higher pressure for the gas to permeate into the material and eventually get absorbed into the lattice structure. Desorption is likely to occur spontaneously if there is no external pressure or the system remains at atmospheric pressure level. The difference between the two plateaus is the material hysteresis. Such hysteresis can be reduced by means of mechanical means such as milling/grinding during the manufacturing procedure. It eventually homogenize the material and help to react to hydrogen, heat and pressure differential faster than usual. The pressure plateaus for a certain compound generally increases (moves up in the chart) as temperature increases as shown in Figure 1.2(b). With the increasing temperature plateau pressures in natural log scale can be plotted against inverse of corresponding temperature, which would generate a linear plot shown in Figure1.2(c). This plot is called Van't Hoff plot, which is probably the single most important piece of information required for selection of appropriate types of metal hydride.
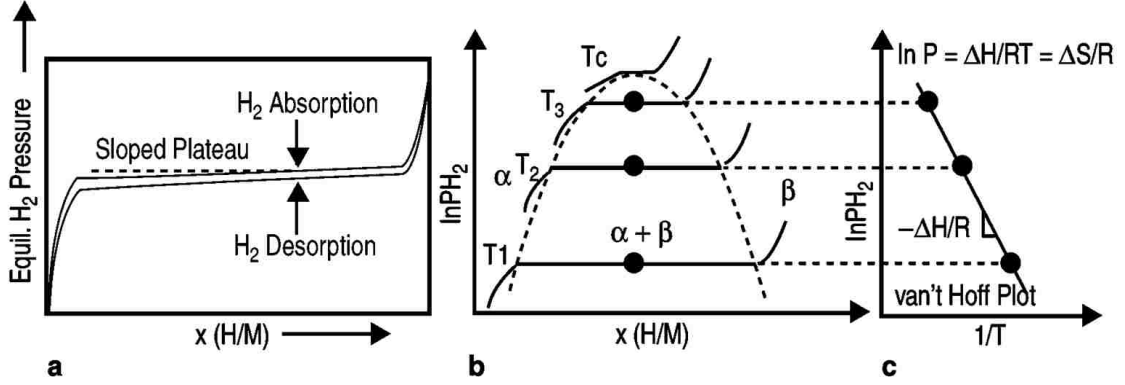
Figure 1. 2: (a) Sorption isotherm showing hysteresis (b) typical phase diagram for a metal hydride showing the transformation from α-phase to β-phase; (c) the Van't Hoff plot derived from the isotherms for various temperatures [20]

The equilibrium behavior of metal hydrides in the plateau region can be described by Van't Hoff plots, according to the relation,

$$lnP_{H_2} = \frac{\Delta H_a}{RT} - \frac{\Delta S}{R} \tag{1.2}$$

Here, R is the molar gas constant (8.314 kJ/kg-mole-K); T is the absolute temperature; ΔH_a is the heat of absorption in kJ/kg-mole of H_2; and ΔS is the standard entropy of the formation in kJ/kg-mole of H_2-K. The Van't Hoff plot and the pressure concentration isotherm data available for metal hydrides are the basis for thermo-mechanical design. Van't Hoff plot for an array of metal hydrides, as shown in Figure 1.3, allows researchers to identify design specific materials. The selection of the storage material is governed by the applicable operating temperature and pressure ranges for desired application. If a system requires operating temperature range from room temperature to about 100°C, for example, then the material falls in that window can be narrowed down by the upper and lower limit of the temperature range. The choice can be narrowed down further by identifying the limiting pressure range. For such temperature range and pressure within one atmosphere, the choice narrows down to $LaNi_5$, FeTi and NaAl alloys. Finally the

cost of the material and availability may dictate the selection of appropriate material. Hence, Van't Hoff plot plays a vital role in the design of metal hydride integrated devices.
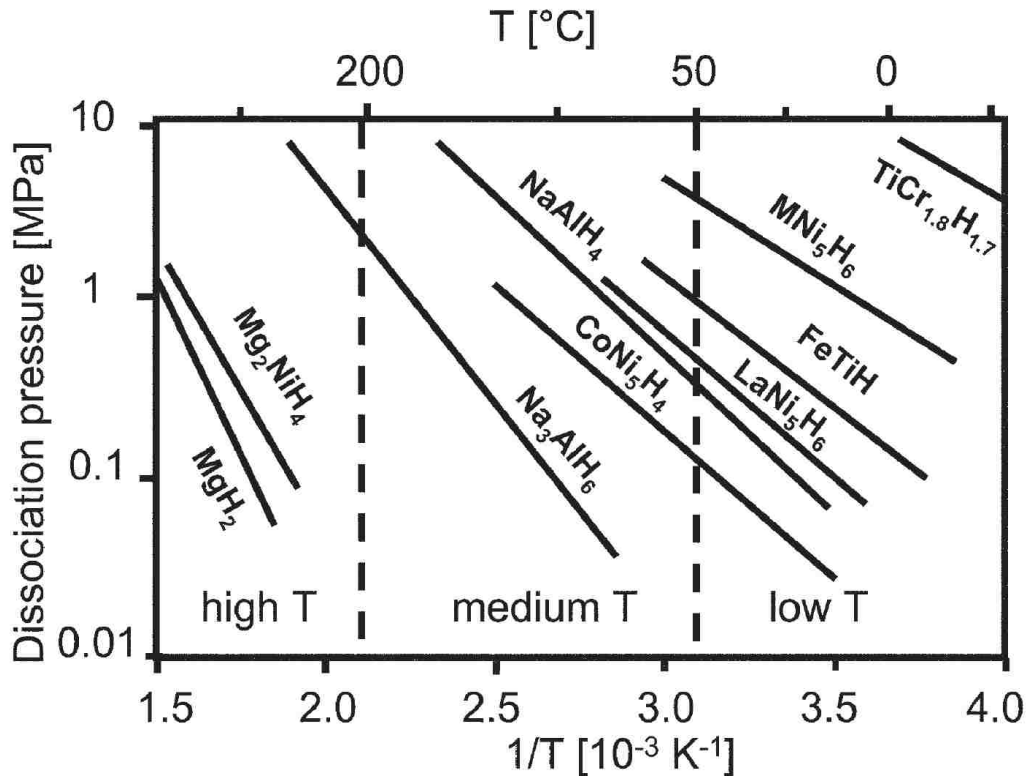
Figure 1. 3: Van't Hoff's plot for different metal hydrides [17]

1.2   Hydrides in Engineering Systems

Hydrogen can be stored reversibly in metal hydride through the removal of heat during absorption and supply of heat during desorption. The enthalpy change during the process permits a number of applications. Since the discovery of hydrogen absorbing alloys, researchers have been investigating various methodologies to improve the characteristics which would accommodate the demands of the application realm. A wide range of applications of metal hydride have already been developed. Metal hydride integrated systems such as thermally driven metal hydride compressor [3, 4, 7, 10, 11, 16, 28-37], heat pump [28, 38-53], refrigerator and air conditioning system [39, 42, 53-59],

heat transformer [8, 39, 60, 61] etc. have been developed and reported in patents and in the literatures. It can also be used for purifying hydrogen [2, 62-64] in semiconductor industry where high purity hydrogen is used. Hydrogen powered Ni-MH batteries have already been made available commercially. Fuel cells [18, 22, 27, 65-69] using metal hydride to store hydrogen are also in use in commercial forklifts because of high storage capacity of these materials in compact design.

Traditional hydrogen storage process comprises of storing hydrogen in pressurized tank or cryogenically stored liquid hydrogen in metal tank. Storing hydrogen in inter molecular spaces of metal hydrides enables safe storage of the gas at a density greater than the storage densities achieved by conventional methods. Compact storage volume with ultra-high density of hydrogen and noiseless operation using metal hydride have opened up doors to its application in robotics and industrial automation. Hydrogen powered actuator made of cylinder with metal bellows [70] as a functional part was being investigated. Copper plated hydrogen absorbing LaNi$_5$ was used for storage of hydrogen which was reversibly heated and cooled by Peltier element in that investigation. A special type of metal hydride was also used for storage and supply of hydrogen to power a similar type of actuator [5]. Both studies investigated the characteristics of the actuator for different temperature, pressure and external loads. Hydrogen powered braided artificial pneumatic muscle [71] was also investigated for compact, noiseless and smooth operation. This actuator claimed to have very high second law efficiency as well as very high force to weight ratio. Biomimetic Mckibben actuator combined with metal hydride was also being reported [72] with comprehensive simulation strategy for actuation purpose. It is evident from all these studies that the combination of actuator with metal

hydride offers compactness, high force to mass ratios and noiseless soft actuation similar to biological muscles. Solar or surplus heat driven metal hydride integrated actuator [73] was also being investigated with findings supporting the operation of the actuator without any energy consumption from sources such as electric or fossil fuel. The concept of powering up actuators with hydrogen stored in metal hydride has been getting very popular because of its unique characteristics such as biomimeticity, compact design, high force to mass ratio, and environmentally benign frictionless operation. But the concept of hydrogen powered actuator is comparatively new and still needs comprehensive research strategy to fully exploit its potential at application level.

The extremely complicated hydriding and dehydriding mechanism of metal hydride have been modeled by several researchers using nonlinear partial differential equations as well as relatively simple thermodynamic relations [10]. On top of the intricate nature of the process, the process itself is affected by the type of material, supply pressure and temperature, porosity, thermal conductivity, diffusivity etc. Mathematical model for absorption and desorption can be developed by considering mass conservation of hydrogen-absorbed metal alloy, Darcy flow in the porous medium, and heat generation by exothermic and endothermic reaction for absorption and desorption respectively. In some studies, the problem was modeled as one dimensional problem [6, 45, 74-76] where as some others considered it as two dimensional [77, 78] problem. Absorption and desorption models, however, provides an extensive base for further formulation at application level. The missing piece of the puzzle, however, is a coupling between hydrogen sorption models to the actuator design based on the performance requirements of intended field of application.

1.3 Research Objectives

Objective 1: A comprehensive review of technical background and applications involving metal hydride in engineering systems and devices.

A comprehensive review of applications involving metal hydrides in engineering systems, processes and devices was performed and summarized. The investigation into the application realm of hydrides led to classify its implementation into different categories. The fundamentals and working principles of these systems were thoroughly studied. Beside hydrogen storage, metal hydrides were being proposed and demonstrated for applications in hydrogen compressors, refrigerators and actuators. The optical and electrical properties of hydride were exploited in the design of sensors and energy efficient windows. The hydriding and dehydriding process was also demonstrated to be economic and effective in preparing implants for osseointegration. Certain hydride material such hafnium hydride was demonstrated to be more effective for being used in neutron moderators compared to the conventional boron carbide (B_4C) in the nuclear power plants. All such applications involving metal hydrides were thoroughly revised and classified. The working principles of MH integrated engineering systems were also discussed briefly.

Objective 2: Modelling and simulation of hydrogen sorption kinetics in cylindrical hollow pellets filled metal hydride reactor using COMSOL multi-physics.

The mathematical model for simulation was developed by considering mass conservation of hydrogen-absorbed metal alloy, Darcy flow in the porous medium, and heat generation and sink by exothermic and endothermic reaction during absorption and desorption respectively. A two dimensional axially symmetric model was prepared for

describing the absorption and desorption process. A series of equations governing the heat and mass transfer process, flow in porous media, diffusion of gas and sorption chemistry was fully coupled to simulate the sorption kinetics. The model proposed was simulated using COMSOL multiphysics. This effort would provide insight into the sorption behavior of metal hydrides as well as the influence of the controllable thermo-physical properties of the hydrides such as porosity, thermal conductivity, etc. in the system design. A new set of experiments was designed for verification of simulation results. Temperature response of the reactor during absorption and desorption process was used to verify simulation results. It is, however, very difficult to experimentally verify desorption temperature response due to the instability of the hydrides at higher temperature for which most of the model validation is done using a single source of previously published data. Here a unique approach was introduced to maintain the exact boundary condition for sorption experiments as modeled in the simulation. Nevertheless, the numerical results were verified experimentally for better comprehension of the mathematical model.

Objective 3: Design and analyze performance of thermally driven metal hydride integrated actuation system for soft robotic application.

This task demonstrated the feasibility of metal hydride embedded actuation system which can potentially be a part of industrial automation, soft robotics etc. Since hydrogen storage and extraction process are dominated by thermal energy extraction and supply respectively, copper encapsulation and subsequent compaction of the particles into pellets was adopted for preparing hydrogen storage reactor. Combination of the two thermal conductivity enhancement processes would greatly reduce the energy consumption to

drive the system. Such efficient and compact energy source integrated with a piston type actuator can be tuned for various actuation requirements as desired. Temperature controlled operation process, during preliminary studies, showed steady pressure and displacement responses during the forward stroke with respect to time. During return stroke, system pressure and displacement were observed to have fluctuations when those quantities were plotted with respect to temperature. But from the plots of those parameters with respect to time, proposed actuator showed steady and smooth actuation even for repeated cycles of operation. The behavior of the MH coupled actuator was found to be very similar to biological muscles in terms of stress generated inside the cylinder and actuation caused by it. Such system performance need to be investigated carefully for identification of overall efficiencies and ways to improve such actuator. Hence, a comprehensive analysis of performance of the actuator was studied to understand the system energy requirements and ways to improve system performance. A distribution propagation method, based on Monte Carlo experiments, was implemented to evaluate system efficiency and quantify associated uncertainty. Detail analysis of the performance specifications might hint toward the future development of such actuators for enhanced efficiencies.

CHAPTER 2: Applications Involving Metal Hydrides

A comprehensive review of applications involving metal hydrides in engineering systems, processes and devices was performed and summarized in this chapter. The investigation in the application realm of metal hydride led to classify its implementation into seven different categories. They are: (1) thermal system, (2) energy system, (3) actuation and sensing, (4) H_2 purification, (5) semiconductor hydrides, (6) biomedical and (7) nuclear applications. The fundamentals and working principles of these systems were briefly explained with illustration. Beside hydrogen storage, metal hydrides were proposed and demonstrated for applications in hydrogen compressors, refrigerators and actuators. The optical and electrical properties of hydride were exploited in the design of sensors and energy efficient windows. The hydriding and dehydriding process was also demonstrated to be economic and effective in preparing implants for osseointegration. Certain hydride material was demonstrated to be more effective neutron moderators compared to the conventional ones in nuclear power plants. All such applications involving metal hydrides are revised and briefly discussed along with their working principles in this segment.

2.1   MH Integrated Systems

Metal hydrides have been established as an excellent medium for on board or stationary hydrogen storage medium since the discovery of this material. The sole reason behind its superiority as a storage medium over the competing/existing technology is its capability of storing large amount of hydrogen at density greater than liquid hydrogen. Moreover, the discharge pressure can be close to atmospheric pressure at moderate temperatures for some hydrides, which makes it more suitable for portable systems.

Besides, the properties of hydrides such as storage capacity, operating pressure and temperature etc. can be altered by alloying as well as other mechanical means. Thus, metal hydrides are vigorously researched for on board vehicular hydrogen storage systems capable of storing enough hydrogen to cover approximately 300 miles of conventional driving range.

Apart from the hydrogen storage application, metal hydrides had been integrated in various engineering applications. These systems take advantage of high storage capability of metal hydrides and temperature/pressure swing dependent sorption method. The concept of temperature swing causing a low pressure absorption and high pressure desorption is utilized in designing thermally driven hydrogen compressors. Based on the fact that absorption and desorption processes are exothermic and endothermic, metal hydride storage systems can be engineered for the supply of heated or cooled air using MH integrated air conditioning, refrigeration and in heat pumps. The same properties can also be utilized in designing thermochemical heat storage system. Apart from these thermal systems, metal hydrides are also very well known for its application in energy systems such as metal hydride batteries and fuel cells. AB_5 type metal hydrides are used in the production of more than a billion batteries every year. Polymer exchange membrane fuel cells have the potential to replace the internal combustion engine in future. The chemical energy of hydrogen stored in metal hydrides is converted to dc power in these cells, which will drive the DC motor of the vehicle. The ultra-high storage capability of metal hydride can be translated to high force to weight ratio from the desorbed hydrogen, which makes it a suitable candidate for actuation of robotic arms and biomimetic muscles.

There are some metallic hydrides that exhibit optical and electrical property changes while they undergo hydrogen absorption process. Changes in such properties make them potential candidate for designing micro systems that serve for sensing gas. The optical property change in presence of hydrogen enable metal hydride to be used in smart windows. Certain metallic coatings were found to switch from transparency to opacity in presence and absence of hydrogen respectively. Hydrogen purification and isotope separation processes were also demonstrated using metal hydride storage material. From a mix of gases, only hydrogen gets absorbed in the storage material and the remaining gases can be purged by previously purified hydrogen gas. Certain metals like palladium shows affinity towards different isotopes of hydrogen at different temperature ranges. Such properties were taken advantage of to design isotope separation processes for industrial application.

Finally, comparatively newer field of applications that have been proposed or demonstrated by integrating hydride materials comprises of applications in semiconductors electronics, osseointegration and fast nuclear reactors. Certain hydrides were found to have n-type and p-type conductivity as revealed from the analysis of band structure. Such hydride opened up the potential of new era of "hydride electronics". Some biocompatible metals such as Ti are used in living systems for implantation. Very often the material needs to be transformed into powder before they are compressed into desired shape. This process is expensive and can be replaced with an economic hydrogenation and dehydrogenation process, which eventually break up crude particles or agglomerates in to finer powder after repeated cycles of sorption. The ability of hydrogen atoms in hydride to moderate fast neutrons in nuclear reactor encouraged researchers to

use hafnium hydrides as neutron moderator. Also certain actinide hydride fuels were suggested as a transmutation target of long lived nuclear wastes.

Metal hydride has been an interesting topic with ongoing research emphasis. As time progresses and hydrogen evolves as a future fuel to suffice the world's energy demand, new generation of metallic alloys will be developed to minimize the shortcomings of the contemporaries. Along the way, hydride materials have found interesting engineering applications besides storage. New applications involving hydrides will emerge as new characteristics of hydrides are discovered in the future. This chapter summarizes the fundamentals behind the applications of metal hydrides in thermal, energy, actuator and sensors, industrial, biomedical, nuclear systems, etc., as proposed and demonstrated in research and publications.

2.2 Areas of Applications

Metal hydrides have been proposed and demonstrated for numerous applications. Some of them have been commercialized while others are still in research and development phase. Nevertheless, the engineering applications of metal hydride in practical systems can be broadly classified into:

2.2.1 Thermal Systems: compressor, refrigeration, heat storage, thermal engine etc.

2.2.2 Energy Systems: battery, fuel cells.

2.2.3 Actuation and Sensing: Actuators, gas sensors, smart windows etc.

2.2.4 Purification: H_2 purification, isotope separation.

2.2.5 Semiconductors: Semiconducting hydrides for "hydride electronics"

2.2.6 Biomedical: Pre-process for implant material preparation

2.2.7 Nuclear: Neutron moderator, transmutation

15

In the following sections, fundamentals and working principles of each of these systems have been briefly reviewed.

2.2.1 Thermal Systems

2.2.1.1 Compressor:

Thermally driven metal hydride hydrogen compressor [3, 4, 7, 10, 16, 29-32, 34-36, 79] is one of the prominent systems involving hydrogen storage materials. Taking advantage of the reversibility of absorption and desorption of hydrogen by temperature swing, this compressors operates in a closed loop thermodynamic cycle. The operating cycle, illustrated in Figure 2.1, begins with the initiation of the formation of hydride phase as marked by D in the pressure concentration isotherm. Along the isotherm, the metallic storage material absorbs hydrogen till it reaches as saturation point A at a lower pressure P_L in thermodynamic equilibrium. At this point the absorption phase is complete and hydrogen is absorbed inside the metal hydride at moderately lower temperature and pressure. As the temperature of the system is subsequently increased to a higher level than the absorption temperature, desorption process initiates following a higher pressure concentration isotherm at elevated pressure. For an elevated temperature T_H the initiation of desorption process is marked by B at an equilibrium pressure higher than the absorption pressure. As such higher temperature is maintained, the system keeps desorbing the gas along the isotherm at higher equilibrium pressure. The process continues until the point C is reached where almost all the hydrogen is extracted from the storage material at an elevated equilibrium pressure P_H. Hence, thermally driven hydrogen compression systems form a closed loop where hydrogen is absorbed into the system at lower temperature (T_L) and pressure (P_L) and subsequently desorbed at an

elevated temperature (T_H) and pressure (P_H). Such compressors do not require moving part and thus they are noiseless and environmentally benign. Reported compression ratios for such system are very high ranging from 3 to 10 [3, 30, 34]. Such systems can also be assembled in series for multiple stages of compression, which can generate a compression ratio over 12 [10].
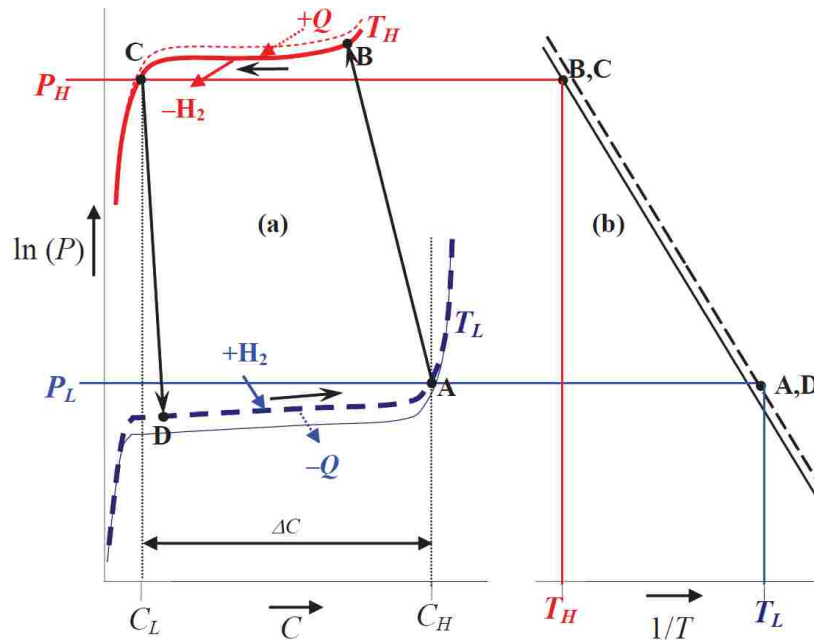
Figure 2. 1: Thermally driven metal hydride compressor operating cycle adopted from Lototskyy et al [36]. (a) Absorption isotherm in solid and desorption isotherm in dashed line shown for lower and higher operating temperatures. (b) Van't Hoff plots for illustrating temperature dependencies of the plateau pressure for the operating range

2.2.1.2   Refrigerator, Air conditioner and Heat Pump:

Metal hydrides store and desorb hydrogen through a reversible chemical reaction that incorporates evolution and absorption of heat respectively. The exothermic reaction during absorption of hydrogen can be utilized in the heat pump whereas the absorption of heat during the endothermic reaction associated with desorption can be utilized for cooling. Metal hydride refrigerator [39, 53-55, 58, 59] and heat pump [38-40, 43-53] take

advantage of the heat absorption and desorption phenomena during desorption and absorption of hydrogen into the storage reactor beds, respectively. A vivid illustration of such system was provided and prototyped by Park *et al* [50] as shown in Figure 2.2. Their system was able to attain COP of 1.8 with a half cycle time of 3 minute with the minimum cooling temperature of 6 $^{\circ}$C. For heating or cooling application, metal hydride integrated devices usually have two identical reaction beds filled with the same type of storage material. Use of similar material simplifies the cycle coordination for heating or cooling. Initially one of the beds is completely charged with hydrogen and the other is kept empty. To maintain the flow of hydrogen in such system, a compressor driven by a variable speed motor is incorporated in the design as shown in the figure. An insulated air damper regulates the flow of air over the reactors alternatively. When hydrogen is extracted from the charged reactor, the air from the room is blown over that reactor which takes up the heat of reaction from the room air. As a result, the outlet of the system discharges cold air inside the room. The discharged hydrogen from this reactor is passed on to the second reactor which absorbs hydrogen and cooled by the flow of ambient air. Once the first reactor is depleted and the second one is charged with hydrogen, the orientation of the air damper changes to allow room air to blow over the second reactor while desorption process continues in that reactor. Hence, continuous supply of cold air is maintained inside the room by alternating desorption cycle in two reactors and regulating the flow of room air using the air damper.
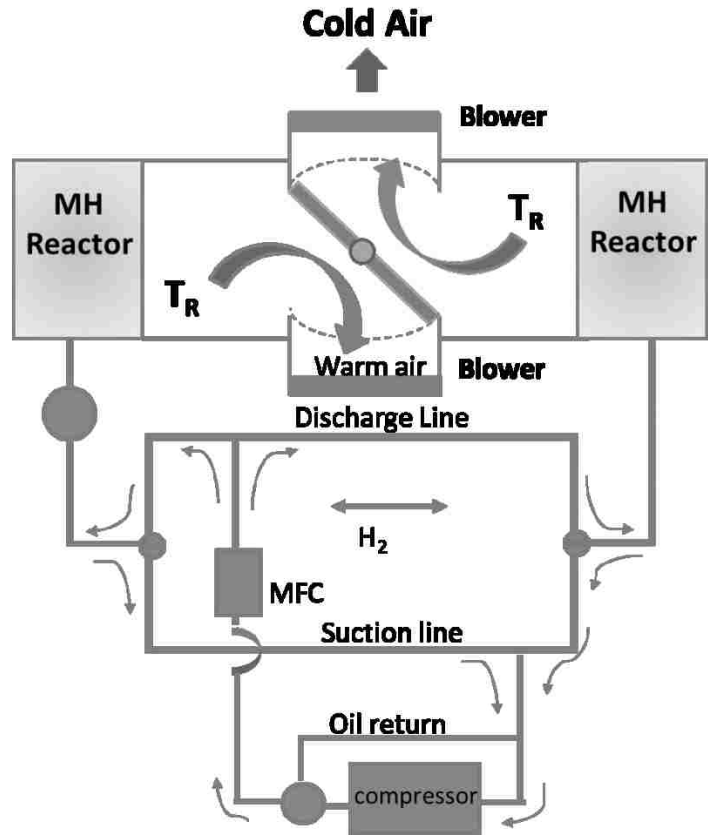
Figure 2. 2: Compressor driven metal hydride heat pump schematic [50]

2.2.1.3   Heat Storage:

Thermally driven hydrogen transport phenomenon that occurs during the absorption and desorption process in metal hydrides enables those materials to be used as reversible chemical heat storage [25, 60, 76, 80-85] systems. Several studies have demonstrated high temperature thermochemical heat storage using magnesium [81, 83] based light weight thermal storage systems. The concept was applied to prototype a process steam generator [81], which was primarily designed for storage of high grade industrial waste heat. The principle behind the thermochemical heat storage using metal hydrides consists of storing heat in the storage material from the heat source by exciting the endothermic chemical reaction and recovering heat by reversing the reaction [80]. The energy density

19

attainable in this process is very high and duration of storage can be as long as desired. For heat storage purpose Mg based light weight and high temperature storage materials are researched because of high heat storage capacity, low cost material and excellent cycling life [85].

2.2.1.4 Thermal Engine:

From the perspective of release of chemical and mechanical energy during desorption, which can also be reversed during absorption, several ideas have been proposed for integrating metal hydrides into engineering applications including heat engine. A heat engine using $LaNi_5$ as a conversion medium and a piston and cylinder for mechanical power output was prototyped and investigated [86]. Figure 2.3 shows the basic arrangement of the chemical engine proposed by Nomura *et al.* In this engine, high pressure gas is supplied to the piston cylinder in the forward stroke and hydrogen is absorbed in the low pressure container during the return stroke. Electromagnetic valves were used to synchronize pressurized gas supply to and from the storage material and the piston. The heating and cooling temperature was 80 ^{o}C and 20 ^{o}C respectively for the reactor to desorb and absorb hydrogen. Even though the theoretical conversion efficiency had been anticipated to be about 15%, 7.7% conversion efficiency was being attained experimentally.
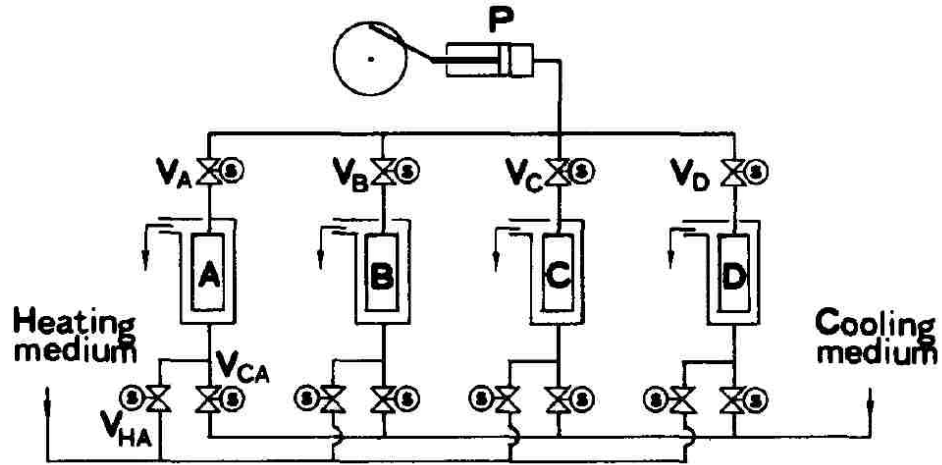
Figure 2. 3: Metal hydride integrated "chemical engine" [86]

2.2.2   Energy Systems

2.2.2.1   Battery

Metal hydride batteries [65, 87-91] have long been established as an effective and long lasting dc power source for electronic equipment's. Rechargeable versions of such batteries especially NiMH batteries [88, 89, 92, 93] are also available commercially for cameras to hybrid vehicles. Such batteries generally have positive electrode made out of nickel hydroxide, which is a very well-known electrode material for over 100 years since it has similar composition as NiCd batteries. The active material for the negative electrode is the hydrogen stored in intermetallic alloy that also serves as an electrode. Most of the batteries use AB_2 or AB_5 type metal hydride alloys as negative electrode. The reversible reaction [94] that occurs in the cell manufactured by COBASYS is given as follows:

$$MH + OH^- \leftrightarrow M + H_2O + e^- \tag{2.1}$$
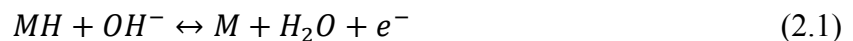
The cell diagram for those batteries is shown in Figure 2.4(a) and the combined reaction that takes place inside such cell is given as follows:

$$MH + (\beta - NiOOH.H_2O) \leftrightarrow M + Ni(OH)_2 + H_2O \tag{2.2}$$

21
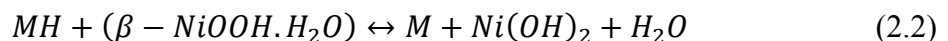
Here MH is the metal hydride, $\beta - NiOOH$ is a low conductivity p-type semiconductor when nickel valance is less than 2.25.

Because of the performance and robustness offered by the NiMH battery technology, the application realm has been extended to hybrid electric vehicles especially high power performance, cycling and operation life [90]. Most of the research related to this maturing technology is focused on characterization of negative electrode material (metal hydride) and properties enhancement methods for positive electrode [92].

2.2.2.2   Fuel Cell

Fuel cells, on the other hand, are devices that transform stored chemical energy into usable electrical energy with water and heat as byproducts. For hydrogen based fuel cells [22, 65, 67, 68, 95, 96] the chemical energy comes from hydrogen fuel stored in metal hydrides. It reacts with oxygen to create electricity by an electrochemical process. Among various types of fuel cells polymer exchange membrane (PEM) fuel cell [67, 68] is most likely a candidate to see vehicular application. Such cells are expected to replace the internal combustion engine by generating DC power to drive the electric motor of a vehicle. As shown in Figure 2.4(b), a basic PEM fuel cell contains an anode which is typically coated with catalyst that helps free electron from hydrogen molecules. These electrons flow in the external circuit to provide electricity for the load connected to the circuit. The proton exchange membrane serves as an electrolyte. Catalyst coated positive electrode (cathode) exposes hydrogen ion in the electrolyte to oxygen and as a result water molecules are formed. A single cell can produce about 0.7 volts [97] which can be multiplied by stacking a series of cells for practical purpose. One of the present challenges for this technology is to store enough hydrogen onboard so that the fuel cell

can generate enough power to drive the vehicle up to 300 miles, which is the target set by US Department of Energy. As of today, metal hydride is the only option that can store hydrogen with density greater than liquid hydrogen. So the challenge is to fabricate a new generation of metal allow that will have higher storage capacity and low temperature discharge capability. Alternatively, hybrid containment [22] technology which combines high pressure tank with metal hydride storage technology may mitigate the issue regarding onboard storage.

a)

b)
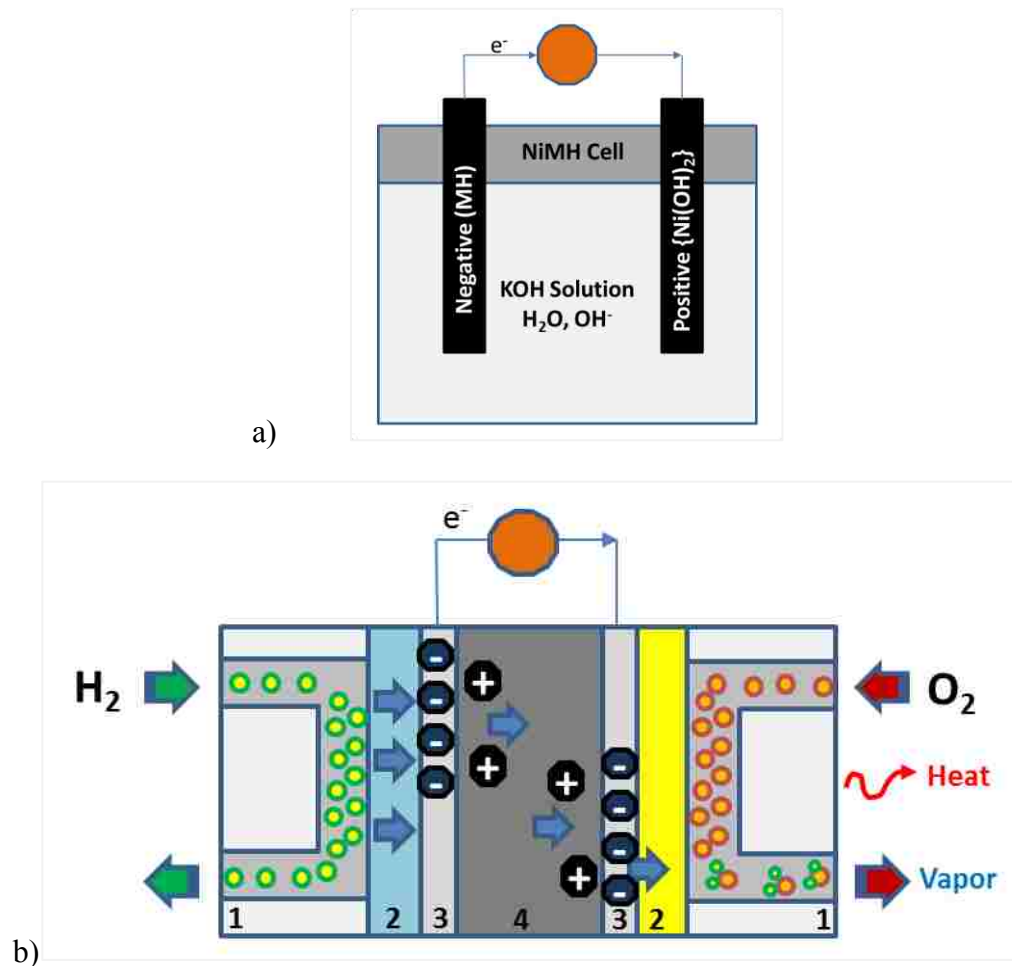
Figure 2. 4: (a) COBASYS NiMH battery cell diagram [94], (b) Proton exchange membrane (PEM) fuel cell [95]: 1-Flow field plate, 2-Gas diffusion electrode, 3-Catalyst, 4-Proton exchange membrane

2.2.3   Actuation and Sensing

2.2.3.1   Hydrogen Powered Actuator

Metal hydride integrated hydrogen powered actuators had been proposed in several studies [9, 70-73, 98-100]. The basic working principal is similar to the heat engine described above. Desorbed gas is the source of driving force for the actuator. Since the storage density of the material is very high, compact storage medium in the system desorbs tremendous amount of hydrogen at elevated temperature, which pressurize the system that may comprise of piston-cylinder assembly, cylinder with metal bellow, artificial muscles and so on. Nevertheless, the fundamental operating principal remains the same. Ken Kurosaki *et al* [70] designed and investigated an actuator with a cylindrical metal bellows as a functional part, which is powered by copper plated $LaNi_5$ storage system. They used a Peltier element to cyclically heat and cool the storage material for generating forward and reverse stroke in the actuation rod loaded with 10 kg mass. The actuation behavior of their system is shown in Figure 2.5(a), where the alternation of electric power to the Peltier element caused heating and cooling of the storage material which eventually cause desorption and absorption of hydrogen into the material. It was claimed that 10 grams of $LaNi_5$ in their actuator could easily lift 20kg load with the displacement of 80 mm. the velocities for the forward and return stroke were about 2.3 and 1.6 mm/s respectively. The efficiency of that system was calculated to be less than 1%. A similar system was developed by Vanderhoff *et al* [71] using braided pneumatic artificial muscle. The performance of the muscle was compared with different types of actuators as shown in Figure 2.5(b). The performance of such system was found to be very similar to that of the biological muscle. It was claimed that this system had a relatively good 2nd law efficiency, which is about 30% over desorption cycle.

Nevertheless, the system showed comparable work output and biological muscle like properties, which make it suitable for robotic applications.
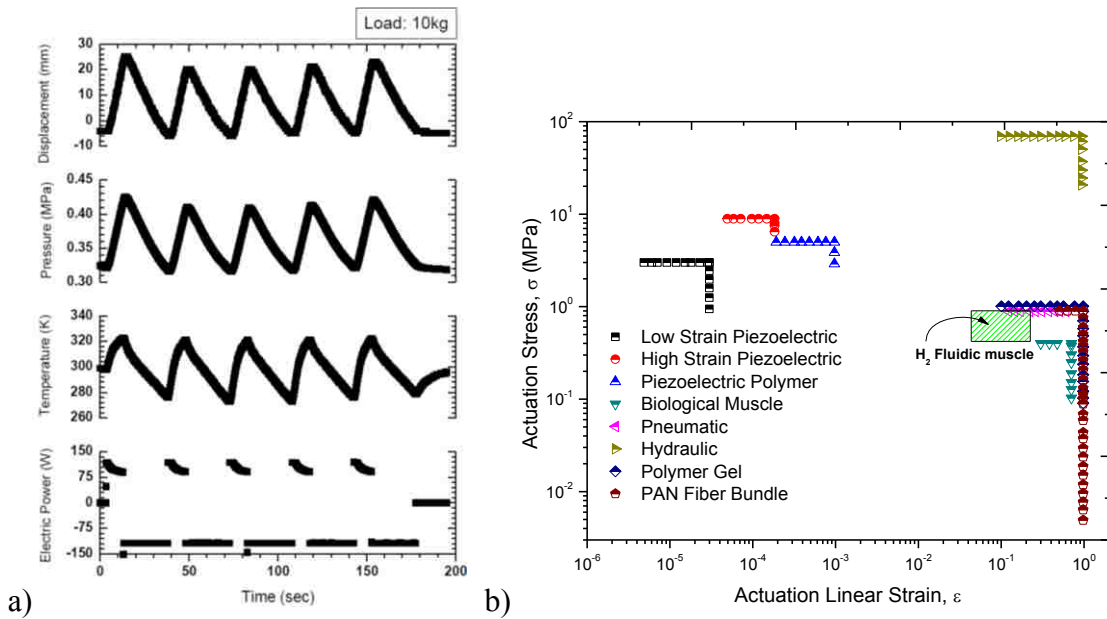
Figure 2. 5: a) Actuation characteristics of metal hydride actuator [70]
b) Actuation device comparison of stress vs. linear strain [71, 101].

2.2.3.2   Hydrogen Gas Sensor

The change in optical, electrical properties and lattice expansion of some hydrides, in presence of hydrogen, make them useful for hydrogen sensing application [102-105]. Metal hydride thin film on MEMS based micro-hotplate [102] has been demonstrated for hydrogen sensing application. A palladium coated rare earth thin metal film, in this case, changes the electric resistivity in presence of hydrogen. The rare earth thin film reacts with hydrogen after which the electric resistivity increases several orders of magnitude. Thus, such types of hydrogen sensors are highly sensitive and were reported to have less than half a second response time with 0.25% hydrogen concentration. Figure 2.6 shows how this system responds to the changing concentration of hydrogen. The response time was found to be as low as 0.44 s when the micro-hotplate was kept at 50-80 ^{o}C by

passing less than 5 mA current through the embedded heater element. The response time, however, was reported to be slower at room temperature.
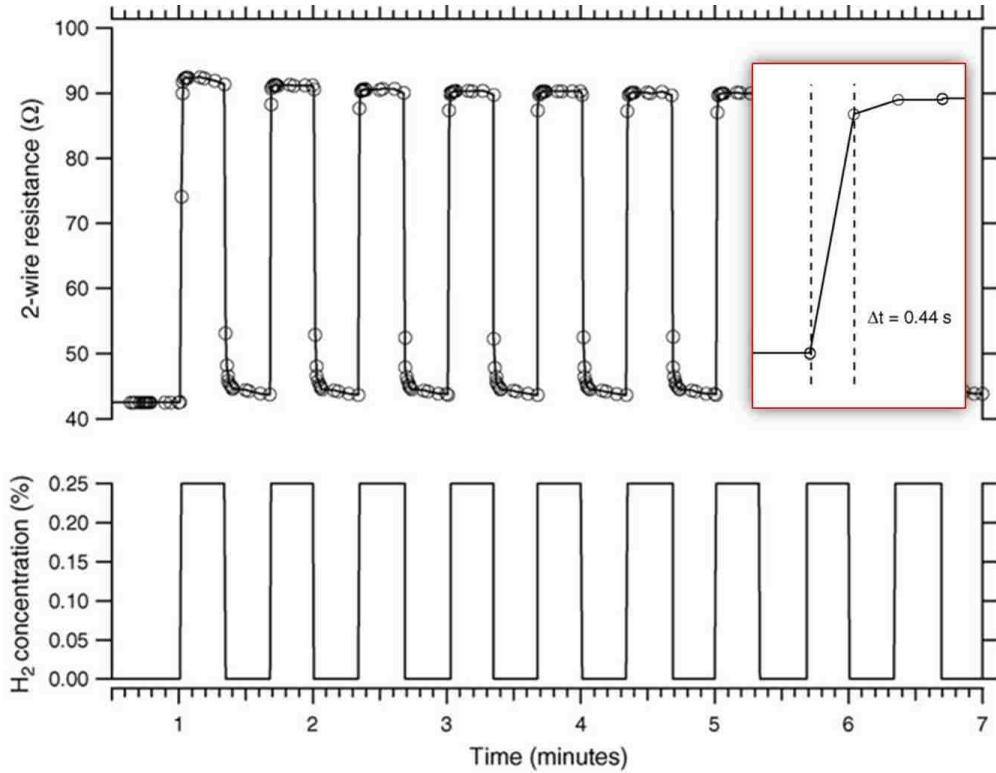
Figure 2. 6: Micro-hotplate based H$_2$ gas sensor response for repeated exposure to 0.25% H$_2$ in air with less than half second response time [102].

A fiber optic hydrogen gas sensor made with Pd-capped chemo chromic metal hydride sensing layer [103] has also been investigated for sensing application. In this study, the reflectance of Mg based hydrogen alloys were reported to reduce by a factor of 10 within a few seconds with hydrogen level of 15% or lower. Differential capacitive thin film sensor [105] has recently been proposed for hydrogen sensing application, which works based on the lattice expansion of $LaAl_{0.3}Ni_{4.7}$. It was found that the lattice expansion was proportional to the partial pressure of hydrogen over the range of 0.01-1.3 atm.

2.2.3.3 Smart Windows

Optical properties of some complex hydride were discovered to be similar to semiconductors [104], which paved the path towards the application of hydrides as antireflection coating. The concept of smart window using hydrides was first developed after the switchable optical properties of yttrium hydride and lanthanum hydride films had been discovered [106]. Transparent yttrium hydride thin film prepared by magnetron sputter deposition was found to have transparent behavior with higher partial pressure of hydrogen [107]. The crystal structure of the transparent film was reported to have fcc lattice instead of hcp in the study. The reflective/transitive nature of the coat, depending on presence or absence of hydrogen, made the hydride based coating a suitable candidate for antireflective coating for smart windows.

André Anders *et al.* [108] investigated electrochromically switched energy efficient mirror for smart window application. In this study electrochromic mirror using MnNiMg was prepared for the proof of the concept experiments, which operates by the application of small voltage that drives the electrochemical change. Nevertheless, these layers may also be switched gasochromically, which is accomplished by hydrogenation of the layer making the coat transparent and dehydrogenation of the layer making the coat reflective. Figure 2.7(a) shows the miniature insulated glass unit prepared for investigation. This study concentrated on the switching performance and durability of the system. As shown in Figure 2.7(b), the dynamic spectral reflectance was quantified as a function of wavelength. While the coat is in hydride state, reflectance is high. While the coat is dehydrated, on the other hand, the window becomes light transmitting and the reflectance drops down to below 10% for most ranges of the wavelengths. The varying transmittance

and reflectance as a function of wavelength is advantageous for over all energy saving efficacy of switchable smart windows.
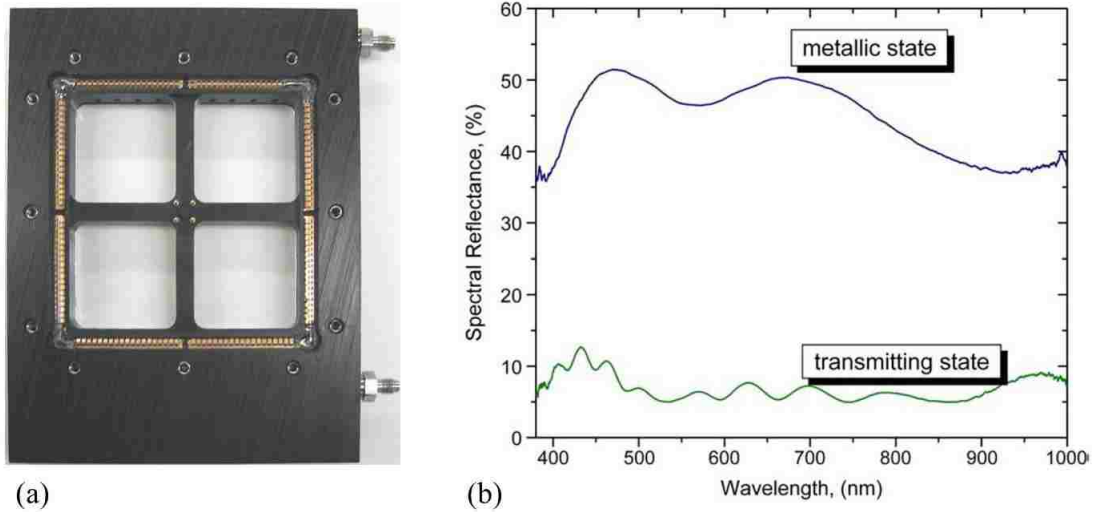
Figure 2. 7: (a) Test window, and (b) spectral reflectance and transmittance [108]

2.2.4   Hydrogen Purification

2.2.4.1   Purification

Purification of hydrogen by absorbing hydrogen in metal hydrides from a mix of gases and subsequently pressurizing the container with purified hydrogen to drive out the unwanted gases is a common technique for purification of hydrogen [63, 64, 109]. One of the earliest demonstrations of purification process was reported by Block *et al* [63], where the concept described above was applied. Later $FeTi_{0.95}Mm_{0.08}$ based hydrogen purification system [62] was reported to operate within temperature range of 25-90 ^{o}C and yielding a 99.99999 % purity of hydrogen excluding vapor content.

In a recent (2012) study, metal hydride based hydrogen purification and storage system was investigated by Shinichi Miura *et al* [2]. They incorporated carbon monoxide removal unit in the preliminary step of purification. Carbon monoxide forms a barrier

layer on the surface of metal hydride and basically kills its ability to absorb and store hydrogen. Hence, in the initial stage of purification this poisonous gas is removed by incorporating special carbon monoxide absorbent. Next, the gas mixture is introduced to metal hydride where only the hydrogen is absorbed and stored for future use. This method was referred as Carbon Monoxide Adsorption Metal Hydride Intermediate-Buffer (COA-MIB). The setup used to carry out the process is shown in Figure 2.8. In the inset of the figure the process diagram is also illustrated. Here, Carbon Monoxide Pressure Vacuum Swing Adsorption (CO-PVSA) method was used to eliminate carbon monoxide.
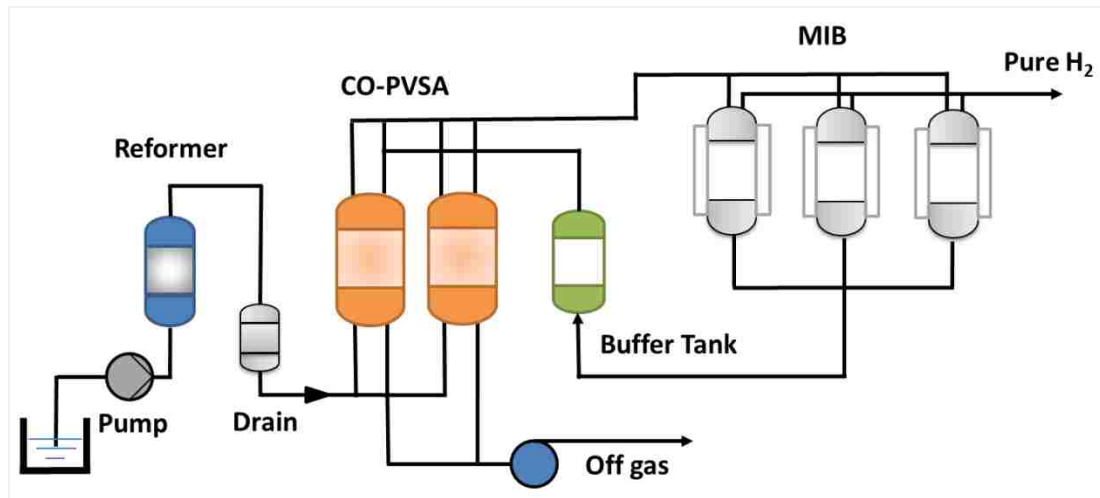
Figure 2. 8: Process flow diagram of the purification system [2]

The system utilized AB_5 type hydrogen storage material and operates from 20 to 80 °C. After 150 hours of daily start and stop operation, this 100 NL/h laboratory scale apparatus was able to attain 83% hydrogen recovery ratio defined as,

$$\text{Hydrogen recovery ratio} = \frac{\text{Amount of hydrogen absorption}}{\text{Amount of hydrogen put into the system}} * 100 \qquad (2.3)$$

Figure 2.9 shows the purity of the hydrogen and measured ppm of carbon monoxide with time for the system discussed. The switching was done every half an hour, which caused to increase the CO_2 concentration because of the fact that the residual gas was not being purged completely. Impurities other than CO_2 were not found in the final product and it was confirmed that the level of CO_2 was as high as 1% immediately after switching. Even though, the level of CO_2 drops below 1000 ppm within 15 minutes, further development may be performed on this system considering the required purity level of hydrogen in the final product prescribed by ISO for fuel cell applications.
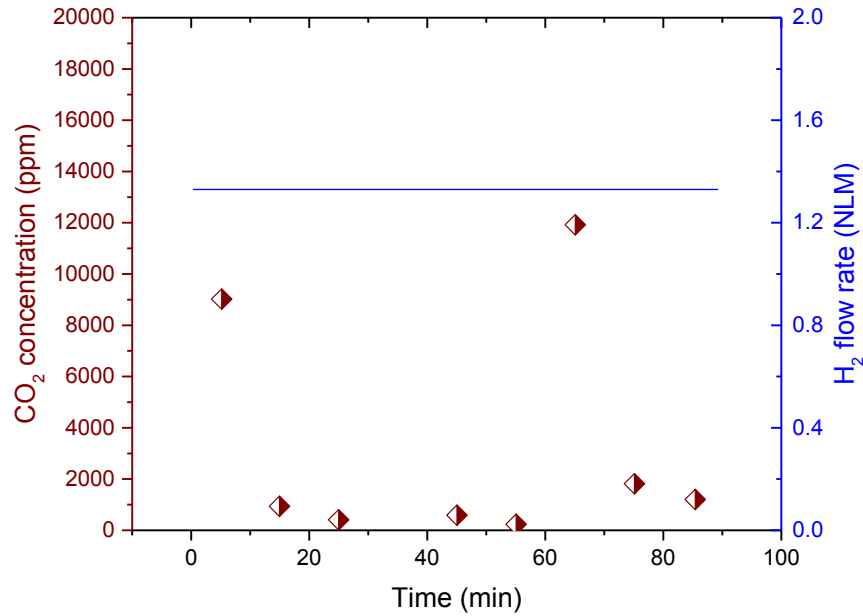
Figure 2. 9: Purity of the final product as a function of hydrogen flow rate [2]

2.2.4.2   Isotope Separation

Metals such as Palladium preferably absorb protium more than heavier deuterium and tritium from a mixture of isotopes of hydrogen. This tendency is more prominent at reduced temperature [110]. $LaNi_{4.25}Al_{0.25}$, on the other hand, absorbs tritium more at low temperatures with reversing effect (absorbing lighter deuterium and protium) at

temperature above 40 $^{\circ}$C [111]. Such properties of metal hydrides are very useful for designing isotope separation process [112-114] for industrial applications.

Ito *et al* investigated the influence of magnetic field in separation of deuterium from protium using ferromagnetic LaCo$_5$ and paramagnetic LaNi$_5$ as storage material. The dependency of equilibrium pressure of ferromagnetic hydride under magnetic field B was given as [114],

$$P_B = P_0 \exp(\frac{2B\Delta M_S}{RT})\tag{2.4}$$

Here, P is the equilibrium pressure, ΔM_S is the change in the saturation magnetization per mole of desorbed hydrogen, R is the ideal gas constant and T is the temperature. Since the equation above is dependent on the change in saturation magnetization of the storage material under the influence of applied magnetic field B, paramagnetic materials such as LaNi5 are not expected to show notable change in separation performance. Ferromagnetic materials like LaCo$_5$, however, will show improvement in equilibrium pressure under the effect of magnetic field since there will be a significant change in saturation magnetization in the material. The assumption made in this study is that the separation ability is related to equilibrium pressure difference P^D-P^H, which can be further enhanced under the influence of magnetic field for ferromagnetic hydrogen storage material.

a)

b)
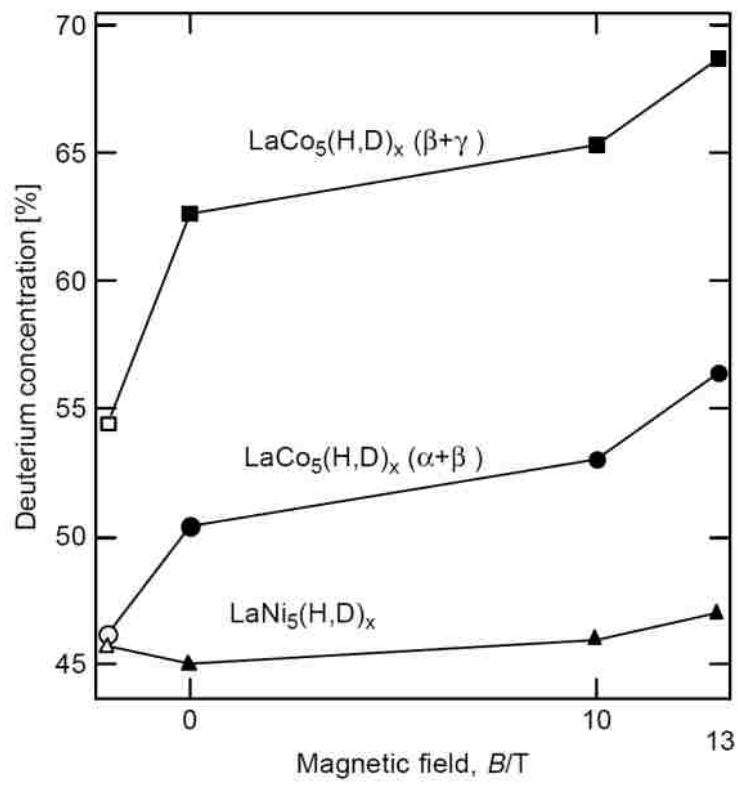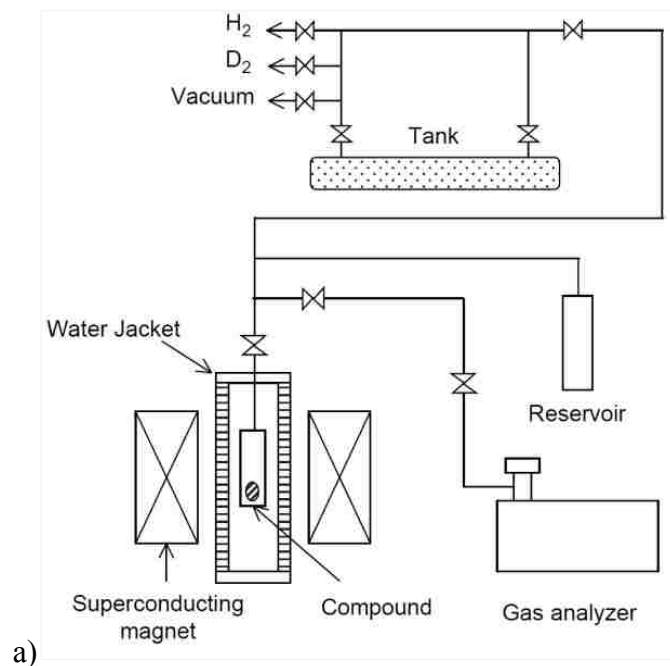
Figure 2. 10: a) schematic diagram of isotope separation setup, and b) effect of magnetic field in separation process. Adopted from Ito et al [114]

1:1 mix of protium and deuterium is introduced into the reactor containing the storage material, which is placed in the center of the cryo-cooled supper conducting magnet as shown in Figure 2.10(a). The concentration of protium/deuterium concentration was measured with a mass spectrometer. As shown in Figure 2.10(b), deuterium concentration increased with increasing magnetic field for $LaCo_5$ system. This effect is more significant for $\beta+\gamma$ region than $\alpha+\beta$ region. One of the measures for isotope separation ability of hydride is the isotope separation factor α defined as follows:

$$\alpha = \frac{(D/H)_{gas}}{(D/H)_{solid}} \tag{2.5}$$

The isotope separation ability increases as α deviates from unity. Ito *et al* reported that this separation factor can be increased about 46% under the influence of magnetic field at 13T using ferromagnetic $LaCo_5$ metal hydrides.

2.2.5   Semiconducting Hydrides

The band structures of some hydrides like AlH_3, $KMgH_3$ and others, were analyzed by Vajeeston *et al* [115] using density function theory. Several hydrides were found to have n-type and p-type electrical conductivity as seen in semiconductor materials. They also reported to have transparent and visible range of the optical spectrum. This adds a new class of semiconducting material with potential applications in "hydride electronics". In a later study [116], Karazhanov *et al* identified the features like large band gap, well dispersed bottom most conduction band, small electron/hole masses etc. as seen in the semiconductor materials. Figure 2.11 shows the band gap of metal and complex hydrides adopted from their study. Circles and triangles represent experimental and theoretical predictions respectively. Light background represents opaque, darker background represents transparency energy ranges. Darkest is the most desirable transparency range.

The issues like interface and band gap in semiconductor were argued to be solved by this new generation of hydride semiconductor. Complex hydrides such as $Be(BH_4)_2$ with slower absorption desorption kinetics and high storage capacity (20.8 wt%) was referred as a suitable candidate for semiconductor application because of its stability at high temperature. Potential applications of such semiconducting hydrides are in solar cells, which are protected from the ambient by a thin layer.
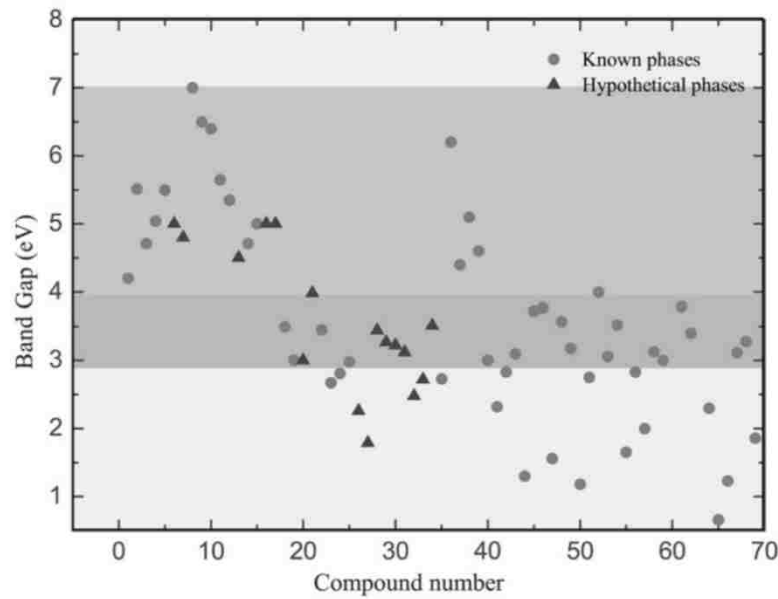
Figure 2. 11: Band gap of metal and complex hydrides adopted from Karazhanov *et al* [116]: (1–4) MgH$_2$, BeH$_2$, LiAlH$_4$, NaAlH$_4$; (5–9) KAlH$_4$, RbAlH$_4$, CsAlH$_4$, LiBH$_4$, NaBH$_4$; (10–14) KBH$_4$, RbBH$_4$, CsBH$_4$, LiGaH$_4$, NaGaH$_4$; (15–19) KGaH$_4$, RbGaH$_4$, CsGaH$_4$, Li$_3$AlH$_6$, Na$_3$AlH$_6$; (20–24) K$_3$AlH$_6$, LiMgH$_3$, NaMgH$_3$, KMgH$_3$, RbMgH$_3$; (25–29) CsMgH$_3$, LiBeH$_3$, NaBeH$_3$, KBeH$_3$, RbBeH$_3$; (30–34) SBeH$_3$, BeAlH$_5$, MgAlH$_5$, CaAlH$_5$, SrAlH$_5$; (35–39) BaAlH$_5$, MgB$_2$H$_8$, MgAl$_2$H$_8$, CaB$_2$H$_8$, CaAl$_2$H$_8$; (40–44) Ba$_6$Mg$_7$H$_{26}$, BaMgH$_4$, Ca$_{19}$Mg$_8$H$_{54}$, Ca$_4$Mg$_3$H$_{14}$, Ca$_4$Mg$_4$FeH$_{63}$; (45–49) CaMgNiH$_4$, Cs$_2$MgH$_4$, Cs$_3$MgH$_5$, K$_2$MgH$_4$, LiMg$_2$RuH$_6$; (50–54) Mg$_2$RuH$_4$, Mg$_3$ReH$_7$, Rb$_2$MgH$_4$, Rb$_3$MgH$_5$, Rb$_4$Mg$_3$H$_{10}$; (55–59) SrMg$_2$FeH$_8$, SrMgH$_4$, SrMgNiH$_4$, Yb$_4$Mg$_3$H$_{14}$, Sr$_2$Mg$_3$H$_{10}$; (60–65) LiH, NaH, KH, RbH, CsH, CuH; (66–69) BaLiH$_3$, CaCaH$_3$, RbCaH$_3$, SrLiH$_3$; (70–72) α-AlH$_3$, β-AlH$_3$, γ-AlH$_3$.

2.2.6 Biomedical Application

Metal hydride integrated actuators [100, 117] and artificial muscles [71, 98, 100, 117] for application in biomimetic systems have been proposed and investigated by many researchers. These applications involving metal hydride are basically related to biomimetic devices that are powered by hydrogen stored in metal hydride. For biomedical applications, the hydride material is usually not used directly in living biological systems. Materials such as titanium can form hydride and whose powdered state can be compacted and used *in vivo* since such material is biocompatible. The process for powdering the material is, however, expensive and can be replaced by hydrogenation and dehydrogenation process, which eventually transform the agglomerates into powder after multiple cycles of sorption. This procedure is referred as hydride-dehydride (HDH) method. The sorption cycles with titanium in HDH method were adopted by Barreiro *et al* [118] to manufacture powders with particle sizes of 37 and 125 micron. These powders were further sintered into desired shape in order for osseointegration in the tibia bone of wistar rat.

Cylindrical Ti implants prepared from these powders were implanted inside the tibia bones of wistar rats. The study showed uneventful healing with normal pattern of bone repair without inflammatory reaction. The histological analysis of this study was performed using microscopic analysis of the behavior of bone tissues in contact of the metal. Almost the entire surface area of the bone that was exposed to the metal was found to have close contact for both the cases indicating a progressive integration of the implant material into the bone.

This investigation indicates biocompatibility of titanium prepared by HDH process followed by compaction using high pressure sintering. The process is economic and no difference was observed for compaction and sintering behavior for materials prepared by HDH process as compared to the commercially available titanium powders. In a nutshell, this study demonstrated indirect application of metal hydride in living biological system.

2.2.7   Recent Development in Nuclear Engineering

Application of metal hydride in nuclear engineering was being proposed as neutron absorber back in 1973 by R. V. Houten [119]. Boron carbide (B_4C) is typically used as neutron absorber, which generates helium gas and has a short life. Reported in 2012, Konashi *et al* [120] envisioned a new material that would increase transmutation rate without generating helium gas for environmentally benign nuclear application. In the latter study, hydride materials were proposed and investigated for application in nuclear reactor cores.

Based on the fact that hydrogen atoms in hydride can efficiently moderate fast neutrons, Konashi *et al* suggested that hafnium hydride can be used in reactor core, which can absorb three times more neutrons per atom than B_4C. Also, it does not generate helium gas in the process as shown in Figure 2.12. After performing the irradiation test on Hf hydride neutron absorber, the capsule was investigated using X-ray computed tomography. The capsule was found intact and no swelling was found in the disk which is highly desired for mechanical integrity of the system. Nuclear power plants also generate a high level of radioactive long lived minor actinides (MAs) whose transmutation is achieved by irradiation. This study also suggested actinide hydride fuels containing ^{237}Np, ^{241}Am and ^{243}Am as a transmutation target of long lived nuclear wastes.
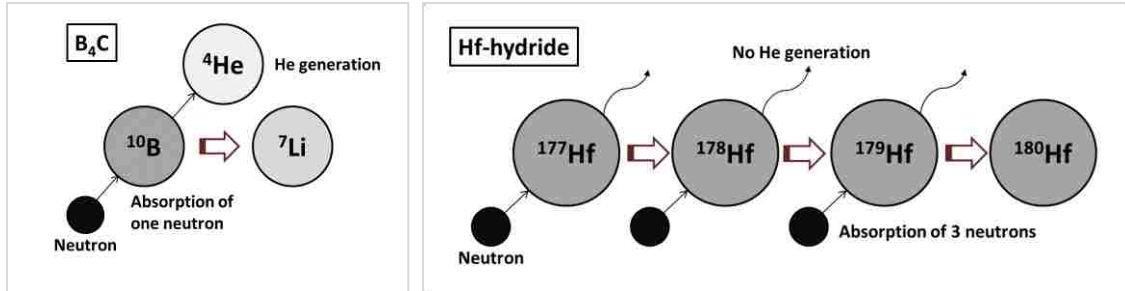
Figure 2. 12: Neutron absorption in B4C and Hf-hydride, [120]

2.3   Alternative Fuel Perspective

The title of highest energy density by weight (143 MJ/kg) and, unfortunately, the lowest energy density by volume (0.0108 MJ/L) belongs to hydrogen [24]. Yet, it is considered to be the replacement of depleting fossil fuel because of the environmentally friendly combustion product it generates and the carbon free natural resources from which it can be extracted. US Department of Energy (DOE) has been sourcing a comprehensive hydrogen research program for about a decade now to design innovative materials and develop techniques that would increase the storage energy density. The programs are focused on production, delivery, storage, application in fuel cell, manufacturing R&D, safety codes, education and so on. Metal hydride, chemical storage, hydrogen sorption, and also high strength light weight and low cost tanks are the key focus areas for extensively researched to attain high density storage capacity for onboard vehicular applications and off board transportation, delivery and storage. Ongoing research and development is focused on attaining onboard hydrogen storage target for vehicular application as listed in Table 2.1. The targeted onboard storage capacity should enable a vehicle to be driven over 300 miles with a single fill and within the constraints of weight, volume and efficiency. Among the other issues 1,500 cycles of lifetime,

duration of refueling, and cost have to be addressed for hydrides to be a viable alternative fuel storage technique in automotive sector.

Surprisingly there are no hydrides that fulfill the targets set by DOE for onboard hydrogen storage for light vehicular application at the moment. This issue remains unsolved and poses as the most significant hurdle for proliferation of hydrogen as an alternate fuel. Apart from designing new materials, researchers are continually looking into new avenues to solve the gravimetric energy density issue of hydrogen storage system. One such material under investigation is graphene. Theoretically, 8% and 8.3% gravimetric density can be attained using nanostructured graphene and chemisorption in graphene [21], respectively, which are even larger than the ultimate target set by DOE. Even if the target for gravimetric density is met, the challenge will still persist in terms of faster sorption kinetics and cycle management.

Table 2. 1: Onboard hydrogen storage targets for light duty vehicles set by DOE [26]

Storage Parameters	2017 Target	Ultimate Target
Gravimetric Capacity [kgH$_2$/kg]	5.5%	7.5%
Volumetric Capacity [gH$_2$/L]	40	70
Cycle Life	1500	1500
Fill Duration for 5 kg H$_2$ [min]	3.3	2.5
Minimum Delivery Pressure at 85°C [atm]	4	3

2.4 Summary

Various properties/features of the wide varieties of hydride have been explored for a broad range of applications besides the storage purpose by a large number of research groups all around the world since the discovery. A brief summary of the working principles and features of the application area was being explained in this chapter. The

feature of hydrides and applications that have been developed, proposed or researched based on those features are tabulated in Table 2.2.

Table 2. 2: Hydride features and corresponding applications

Applications Areas	Hydride Features Utilized	Engineering Systems
Thermal systems	- High storage capacity - Reversible reaction during sorption process involving heat	Compressor, refrigeration, heat storage, thermal engine
Energy Systems	- Hydrogen storage - Hydrogen supply at moderate pressure from certain hydrides	Battery, fuel cells
Actuation and Sensing	- Reversible high pressure hydrogen supply - Temperature variation in presence of gas - Ability of certain hydrides to switch between transparency to opaqueness in presence or absence of hydrogen	Actuators, gas sensors, smart windows
Process	- Reacting with hydrogen and forming hydride when exposed to a mixture of gases - Absorption preference of certain metals to certain isotopes of hydrogen, eg. Palladium preferably absorbs protium than heavier deuterium	H_2 purification, isotope separation
Semiconductors	- Electrical conductivity of several hydrides similar to n-type and p-type conductivities of semiconductors	Semiconducting hydrides for "hydride electronics"
Biomedical	- Powder formation by repeated hydrogenation and de-hydrogenation - Biocompatibility of such process	Pre-processing of implant material preparation
Nuclear	- High transmutation capability without generating helium gas	Neutron moderator, transmutation

CHAPTER 3: Storage Material and Reactor

The reactor houses the hydride materials that absorbs and desorbs hydrogen reversibly to drive the system. Thermal conductivity of the storage material plays an important role in hydrogen storage process since the reversible reaction is regulated mainly by removal and application of thermal energy. These materials, when pelletized and exposed to cyclic absorption and desorption of hydrogen process, morph into powdered state and become very poor conductors of heat. This eventually reduce the response time and consequently reduce the efficiency of the system. Thus, improving thermal conductivity of the storage material can play the key role in improving the system's response and consequently reduce the energy requirement for driving the cycles of operation. To improve thermal conductivity of the storage material is to copper coat the particles, which was proved [121] to be effective since copper is highly conductive of heat. Among other techniques, compaction of the storage material in aluminum matrix [122] using high pressure sintering process was also reported to be highly effective in increasing thermal conductivity of $LaNi_5$ storage material. Using the second method 8-23 $W/m \cdot K$ of thermal conductivity can be attained. In this study, $LaNi_5$ particles are microencapsulated with copper initially and later compacted into cylindrical pellets using press and die at a predetermined pressure. The method for pellet formation that were adapted in this study helped improve the following aspects:

- Thermal conductivity of the hydrogen storage system
- Uniform sorption within the material and maximum utilization of the storage material due the cylindrical shape with central channel for flow of H_2
- Reduce dust and, hence, loss of material after a extended period of operation

3.1   Copper Encapsulation

Procedure for copper encapsulation of hydrogen storage material comprises of mixing particles in copper enriched solution. Initially copper sulfate crystal is completely dissolved into a solution of sulfuric acid and distilled water by vigorous magnetic stirring. The stirring process continues until copper sulfate completely dissolves in the solvent at room temperature. Then a known amount of $LaNi_5$ powder is added to the solution and vigorously stirred for about 40 seconds. After this phase, particles are mostly encapsulated by thin layer of copper. Copper coated powder is then rinsed with ethyl alcohol and deionized water twice in a row. In the final step, the powder is filtered and allowed to dry in room temperature overnight. The finished product is mostly encapsulated with copper which transforms the hue of dark green particles into tan coat of copper as shown in insets of Figure 3.1. The scale shown in the inset images are 500 microns whereas the SEM images show scales of 200 microns.
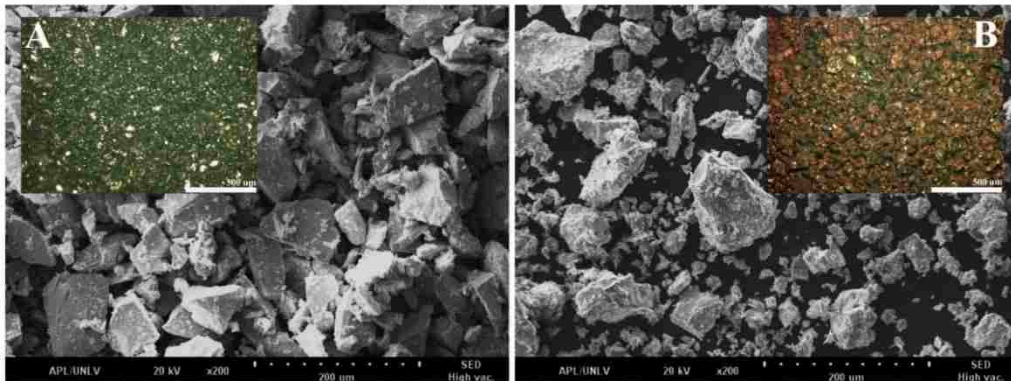
Figure 3. 1: Uncoated (A) and copper coated (B) LaNi5 hydrogen storage material

Figure 3.2(A) and (B) shows metallic particles before and after the process of copper encapsulation using copper rich chemical solution. For cross sectional view of the coating, the coated particles were attached to a transparent polymeric disc using epoxy as shown in Figure 3.2(C). After curing the particles were fine polished using alumina

particles, which is a standard procedure used in the metallurgical lab for observing cross-section of micro particle. Figure 3.2(D) shows the SEM image of the coated particle depicting a coated copper layer on the LaNi$_5$ particle. The thickness of the coated layer is approximately 1-2 micron thick as visualized in the SEM image. Note that there are signs of delamination observed in the SEM images, as shown in Figure 3.3, which usually occurs during the curing process of the epoxy. The shrinkage of epoxy usually causes delamination of coated layer, which can be observed throughout the SEM images at different magnifications. This phenomenon is relevant to the samples prepared for SEM analysis only and should not be present in the actual material prepared for hydrogen storage reactor.
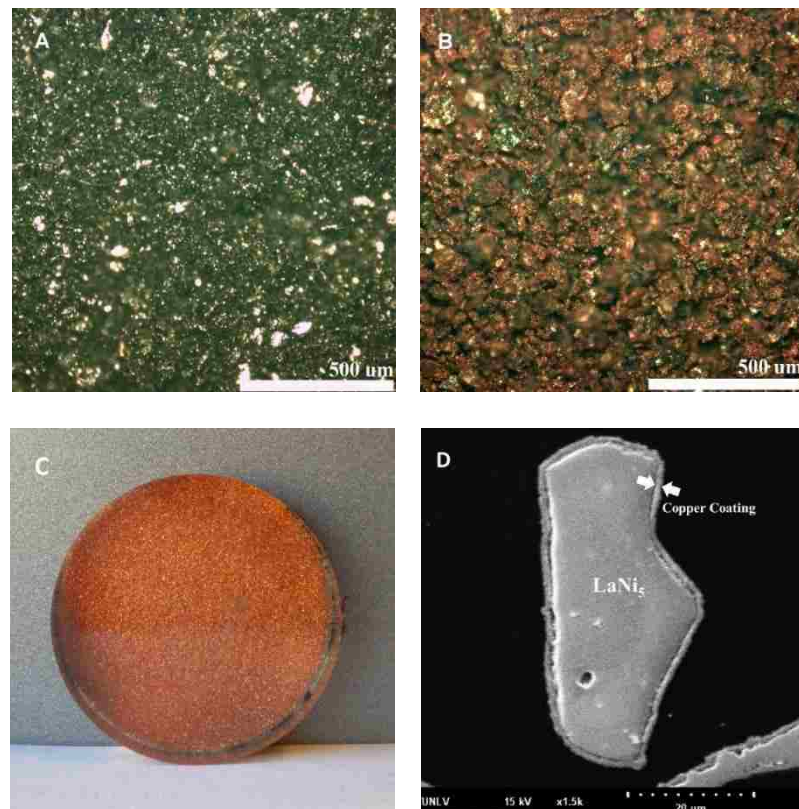
Figure 3. 2: Metal hydride powder (A) before, (B) after copper encapsulation process; (C) sample prepared for SEM analysis, and (D) LaNi5 particle with copper coated layer at 1500X magnification

(a)

(b)
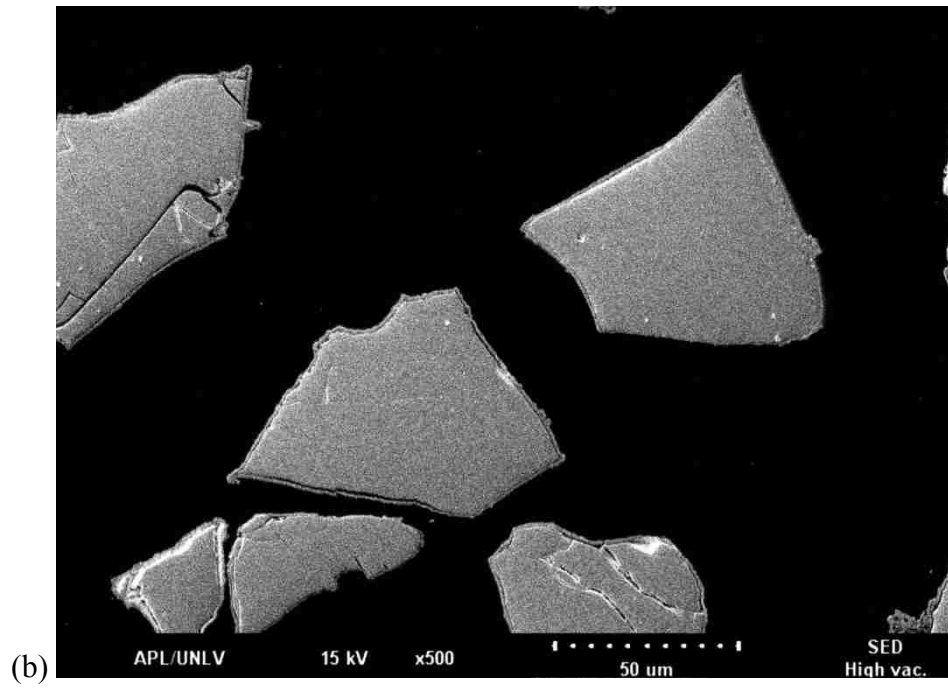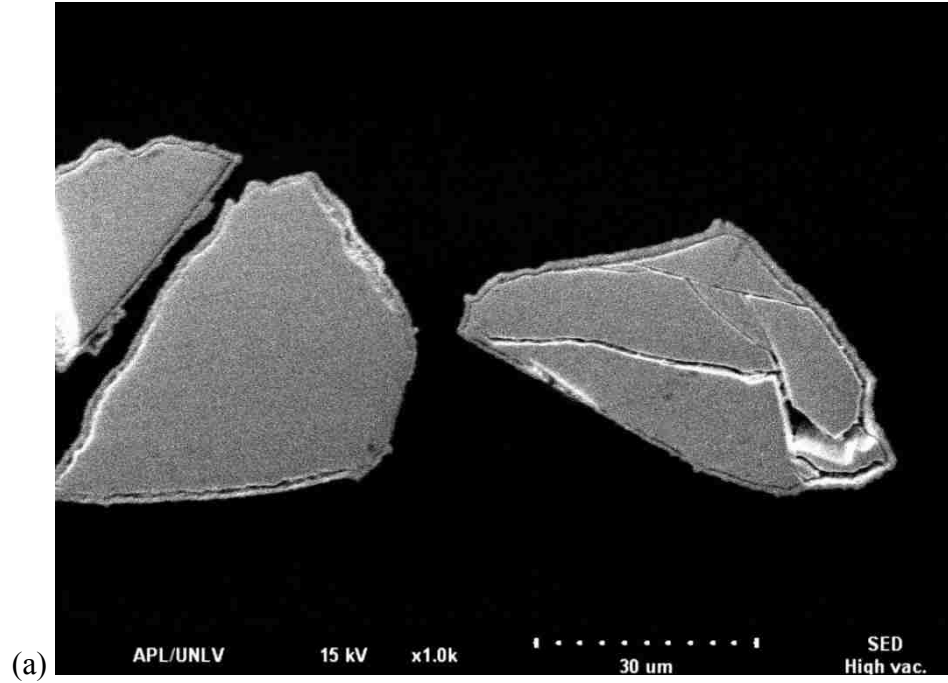
Figure 3. 3: SEM images of coated particles showing signs of delamination at (a) 1000X magnification and (b) 500X magnification

3.2 Pellet Formation

Metal hydride compacts were prepared using the die as shown in Figure 3.4(a). Each LaNi$_5$ pellet, as shown in Figure 3.4(b), contains 5 g of Cu coated particles and 0.5 g of tin (Sn) binder which was compressed at a pressure of 17.24MPa (2,500 psig) to maximize thermal conductivity of the metal hydride while maintaining an optimum porosity as suggested by the experimental results [121] reported previously. In case of Ca$_{0.6}$Mm$_{0.4}$Ni$_5$ and Ca$_{0.2}$Mm$_{0.8}$Ni$_5$, pellets are usually made using 3 g of Cu encapsulated metal particles with only 0.3 g of Sn binder. The mixture was then compressed at 20.68MPa (3,000 psig) to form pellets.

a)   b)

Figure 3. 4: (a) Die and (b) metal hydride pellets prepared for H$_2$ storage

Compaction of copper coated particles into pellets would also enhance thermal conductivity of the compacts by improving physical contact among the coated particles by eliminating void contents. After the compaction process the particles are tightly packed into cylindrical hollow pellets as shown in Figure 3.4(b). The scale shown the image is in inches. The hollow channel in the center facilitates the flow of hydrogen with

negligible flow resistance during the sorption process. Finally, all those compacts were placed inside a cylindrical reactor with a circular aluminum screen inserted through the core as shown in Figure 3.5(a). The screen ensures that the hollow channel remains intact after repeated cycles of hydrogen sorption process. The pellets are activated by pressurizing them with hydrogen and subsequently exposing them to vacuum. This activation process is repeated for several cycles till the temperature rise during absorption shows identical behavior at every cycle. What essentially happens during activation is that hydrogen atoms are forced to become part of the lattice during the pressure driven absorption process, and subsequently they are forced to leave the lattice by the application of vacuum. After several cycles of such activity, the material are considered activated as they show signs of absorption and desorption with ease. The reactor and associated pipe fittings are shown in Figure 3.5(b) before assembly.
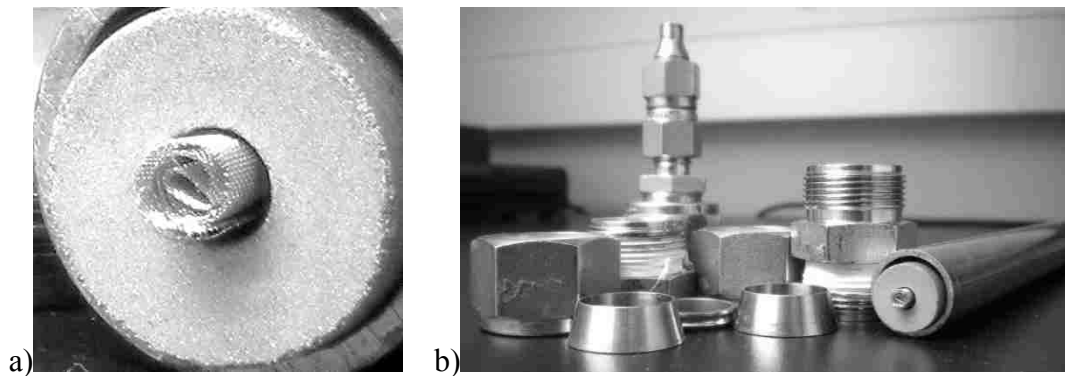
Figure 3. 5: (a) Aluminum screen passing through the central hole of the pellets, and (b) tube fittings and pellets stacked inside a cylindrical reactor for hydrogen storage

Thermal conductivity of metal hydride pellets were measured using a comparative method in an earlier study [121]. The samples were placed in between two copper cylinders whose conductivity is well established. Copper was preferably used as reference material not only for its high conductive nature but also for the strength which

allows various compaction pressures during measurement. To ensure one dimensional heat flow a constant temperature heat sink was placed on the top, which allows implementing one dimensional heat transfer calculation using Fourier's law. Thermal conductivity of the copper coated metallic particle was found to be in the range of 3-6 W/m-K[121].

3.3 Reactor Design Guide [123]

To ensure safety of the pressure vessel used in the design ASME Boiler and Pressure Vessel Code can be implemented in the design. The cylindrical shaped pellets are considered in the design for homogeneous storage of hydrogen in the radial direction, provided that the gas will be supplied through the core. It not only ensures uniform absorption throughout the material but also maximum usage of the storage materials, which are often very expensive. Square pellets, for example, would have unsaturated areas in the corners since the gas would have to travel extra path to saturate the corner materials. In case of circular pellets, uniform saturation is obvious and thus reduced amount of material is guaranteed for a given cycle time and pressure. Besides, housing the pellets in circular tubes would also reduce cost of manufacturing the reactors.

Designing a reactor may start from identifying the pressure requirement of the application. An application, for example, may require P_{max} pressure, which may be assumed to be the maximum design pressure for the reactor. The very first step in design is to identify the amount of storage material need that would store enough hydrogen to generate such pressure at the end of desorption cycle. To estimate the storage material required for such design, the amount of hydrogen that would generate such pressure at room temperature, needs to be quantified using Equation 2.1.

46

$$m_{H_2} = \frac{M_{H_2} V P_{max}}{RT} \tag{2.1}$$

Where m_{H2}, M_{H2}, R, T, and P_{max} are the desorbed hydrogen mass, molar mass of hydrogen gas, ideal gas constant, temperature, and pressure, respectively. Once the amount of hydrogen is determined, the amount of storage material can be determined from the molar mass. To store 1.01g of hydrogen atoms, 432 grams of LaNi$_5$is needed. The calculated amount of material requirement can then be translated to the number of pellets and subsequently the length of the reactor required to store that many pellets in it. For selecting high pressure cylinder geometry ASME Pressure vessel design guide can be followed considering homogeneous stress distribution on the vessel body. Depending on the ratio of the outer to inner diameters R ($= r_o/r_i$) of the cylindrical vessel, a calculation guide based on ASME pressure vessel design guide for ductile vessels is provided as in Equations 2.2 ~ 2.4. For thin-wall vessels, where R is less than 1.1, the maximum allowable working pressure (MAWP) is calculated by

$$P = \frac{S_a E t}{r_i} \quad \text{or} \quad \frac{\sigma_u E t}{SF_u r_i} \tag{2.2}$$

For medium-wall vessels, where R is between 1.1 and 1.5,

$$P = \frac{S_a E t}{r_i + 0.6t} \quad \text{or} \quad \frac{\sigma_u E t}{SF_u (r_i + 0.6t)} \tag{2.3}$$

For thick-wall vessels, where R is between 1.5 and 2.0,

$$P = S_a \frac{(r_o^2 - r_i^2)}{(r_o^2 + r_i^2)} \quad \text{or} \quad \frac{\sigma_u (r_o^2 - r_i^2)}{SF_u (r_o^2 + r_i^2)} \tag{2.4}$$

Where S_a, E, t, SF_u, and σ_u represent the allowable stress of the material, joint efficiency factor (usually 1), safety factor based on ultimate strength of the material, and ultimate strength of material, respectively.

As an illustration of the design procedure, Figure 3.6 shows the drawing of a storage vessel design with (a) dimensions and (b) three-dimensional view. The storage volume of the design is approximately 100 cm^3. Because the value of R is 1.67 (50mm/30mm), the maximum allowable working pressure given by Equation 2.4 is found to be 7272.7 psi when stainless steel (S_a = 20,000 psi) is used as the material. This design satisfies the vessel design guide.
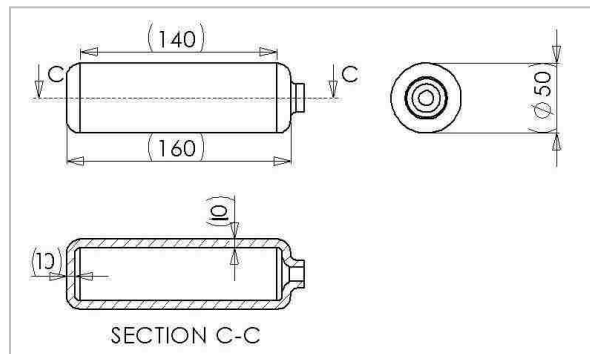
Figure 3. 6: CAD drawings for ductile pressure vessel calculation illustration [123]

This chapter outlined the procedure followed for copper encapsulation of the hydrogen storage material and design of reactor based on the ASME pressure vessel design guide. Even though the pressure vessel were not used to house the pellets for actuator setup, the concept was used to verify the safe operation of low cost stainless steel tubes that were used to house the pellets and construct the reactor. During the procurement of the reactor housing, plumbing, valves and so on, it was made sure that the operating pressure rating of those materials are larger than the maximum pressure attainable at desorption.

CHAPTER 4: H₂ Sorption Simulation and Experimental Validation

Simulation of hydrogen absorption and desorption processes in metal hydride pellets using axisymmetric domain was performed followed by carefully designed validation experiments with identical boundary conditions. Porous AB_5 type metal hydride pellets made of copper coated $LaNi_5$ particle was used as storage material for validation experiment. The mathematical model for simulation was described by considering mass conservation of hydrogen-absorbed metal alloy, Darcy flow in the porous medium, and heat generation and absorption by exothermic and endothermic reactions during the absorption and desorption process, respectively. The boundary conditions used in the simulation are similar to the conditions maintained later on in the experimental validation processes. Copper encapsulated $LaNi_5$ was pelletized and stacked inside a tubular reactor for the study of the sorption behavior. The reactor temperature history data were obtained from the reactor wall during the sorption processes. Despite the fact that there are a number of simulation efforts reported by several researchers, only a few validation data derived experimentally were being reported in literatures. The research presented in this article attempts to abridge that gap and complement the modeling efforts involving AB_5 type metal hydrides with experimentally deduced insights for the purpose of model validation. In a nutshell, this study will:

- Provide insight into the H₂ sorption behavior

- Understand influence of the controllable thermo-physical properties of the hydrides

- Provide ground work for future modeling of MH integrated systems

- Establish a validated modeling framework for hydride based applications

4.1 Background

Hydrogen sorption behavior in metal hydrides is given high emphasis in designing metal hydride integrated systems such as biomimetic artificial muscle [100], actuators [70, 71, 98, 99], refrigerator and cooling systems [54] etc. The sorption kinetics usually influences the appropriate material selection in the system design for reliability and operation safety. It further helps engineers optimize system design for maximizing efficiency by minimizing the cost of energy. Thus, proper understanding of sorption mechanism helps design better systems integrating intermetallic compounds in engineering systems, devices and sensors.

The extremely complicated hydriding and dehydriding mechanism of metal hydride have been modeled by several researchers using nonlinear partial differential equations as well as relatively simple thermodynamic relations [10]. On top of the intricate nature of the process, the process itself is affected by the type of material, supply pressure and temperature, porosity, thermal conductivity, diffusivity etc. Nevertheless, absorption and desorption models proposed by A. Jemni [77] are very comprehensive and provided an elaborated basis for further formulation [124]. In some studies, the problem was modeled as one dimensional [6, 45, 74-76] where as some others considered it as two dimensional [77, 78, 125, 126] problem. In recent studies, however, multi-dimensional models have been presented with simulation results for application oriented problems in heat pump [41, 48, 49] design, hydrogen purification [64], fuel cell [69], storage [127-129] and so on. The fundamentals behind the sorption phenomena described in formulating the process are very similar in all those studies. For validation of most of these numerical models, the authors mostly relied on the data published decades ago for a specific

material. There is certainly a scarcity of experimental data available in literatures regarding the sorption mechanism in most types of metal hydrides.

In this chapter a 2-dimensional axial symmetric model is presented for describing the absorption and desorption processes that take place in porous metal hydride compacts of cylindrical shape that conforms the actual setup used in the experiments. First, a series of equations governing the heat and mass transfer process as well as the sorption mechanism would be discussed. These equations were implemented in the simulation of the two dimensional axially symmetric model describing actual hydrogen storage reactor used in the validation experiments. The experimental results were obtained using identical boundary conditions, as used in prior simulations, and compared for validation of the mathematical model. This study focused on simulation and model validation of AB_5 type metal hydrides, for which $LaNi_5$ was used in the experimental procedure.

4.2   Mathematical Model and Simulation

The mathematical sorption model for porous metal hydride compacts takes into account mass conservation of hydrogen-absorbed metal alloy, Darcy flow in the porous medium, heat generation by exothermic reaction during absorption and heat absorbed by endothermic reaction during desorption. The following assumptions were made for the flow and transport process in porous medium:

- Constant thermo-physical properties

- Complete absorption and extraction of hydrogen

- Negligible viscous dissipation and compression work

- No heat transfer between the metallic pellets and hydrogen gas

- No radiation heat transfer
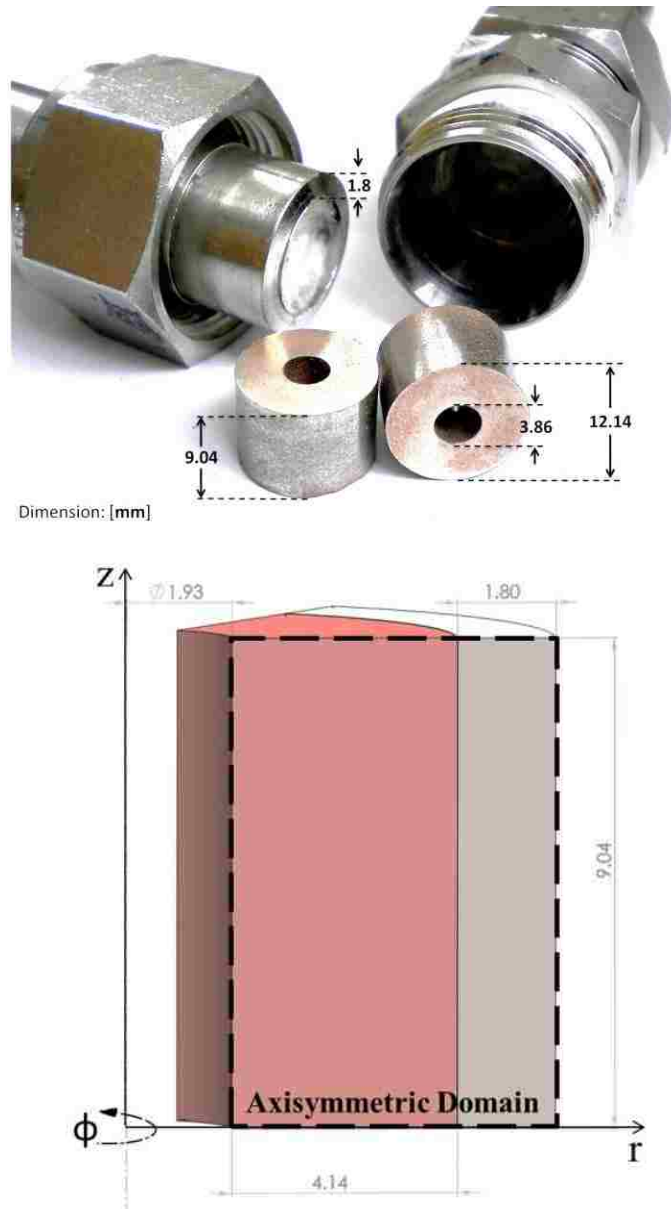
Figure 4. 1: Two dimensional axisymmetric domain for simulation

Assuming that the result would not change in the φ-direction, the sorption mechanism in porous compacts can be described by axially symmetric model in the r-z space (3D) as shown in Figure 4.1. Since the reactor consists of a column of porous metallic pellets, a single pellet would be sufficient to simulate using symmetric boundary conditions on the bottom and upper surfaces.

4.2.1 Governing Equations:

The mass conservation of the hydrogen-absorbed metal hydride during hydriding process can be addressed by considering diffusion of hydrogen into the metal hydride compacts,

$$\frac{\partial c}{\partial t} = \nabla \cdot (\mathbf{D}\nabla \mathbf{c}) + \mathbf{R} \tag{4.1}$$

Where c is the concentration of the hydrogen absorbed into metal hydride and the reaction rate R is the rate, at which the hydrogen gas is absorbed (positive) or desorbed (negative) in metal hydride with unit of mol/m^3-s. Therefore, the mass rate of hydrogen into the pellets can be written as

$$\dot{\mathbf{m}} = \mathbf{M}_{H_2}\mathbf{c} \tag{4.2}$$

The change of the concentration Δc is proportional to the change of the density of H_2-absoring metal hydride $\Delta \rho_s$. Thus, Equation 4.1 can be rewritten as

$$\frac{\partial \rho_s}{\partial t} = \nabla \cdot (\mathbf{D}\nabla \rho_s) + \dot{\mathbf{m}} \tag{4.3}$$

The diffusivity of hydrogen in LaNi$_5$ was studied by Majer *et al* [130] who concluded that diffusivity D can be represented by the Arrhenius law,

$$\mathbf{D} = \mathbf{D_0} \exp(-\frac{H_0}{k_b T}) \tag{4.4}$$

While the density of the solid phase is solved from the Equation 4.3, the pressure field in the reactor can be solved by considering the hydrogen flow in the porous metal hydride compact using Darcy flow equation,

$$\epsilon \frac{\partial \rho_g}{\partial t} = \frac{\kappa}{\mu} \nabla(\rho_g \nabla p) - (1-\epsilon)\dot{m} \qquad (4.5)$$

The hydrogen gas density (ρ_g) can be found using Equation 4.6 where the compressibility factor, Z is considered for modeling hydrogen as a real gas. The compressibility factor used in the simulation was deduced based on the experimental pressure and temperature data from the reactor. Z can be assumed to be unity for implementation of ideal gas law. An assumption that the gas temperature T_g stays constant at the room temperature is made for lowering computational load. Since it was assumed that the hydrogen gas density is a function of only the gas pressure p, Equation 4.5 can be reformatted as Equation 4.7.

$$\rho_g = \frac{M_{H_2} p}{ZRT_g} \qquad (4.6)$$

$$\frac{\partial p}{\partial t} = \frac{\kappa}{\epsilon \mu} \nabla(p \nabla p) - \frac{1-\epsilon}{\epsilon} \frac{ZRT_g}{M_{H_2}} \dot{m} \qquad (4.7)$$

Temperature distributions in the porous metal hydride compact and the reactor wall are identified with the energy conservation equations shown in Equation 4.8 and Equation 4.9, respectively.

$$\rho_0 c_{p_s} \frac{\partial T}{\partial t} = k_s \nabla^2 T + \dot{m}(1-\epsilon)\Delta H \qquad (4.8)$$

$$\rho_{ss} c_{p_{ss}} \frac{\partial T}{\partial t} = k_{ss} \nabla^2 T \qquad (4.9)$$

Note that the initial density ρ_0 is taken for simplification in computation. This assumption is reasonable because the actual density of metal hydride compact varies in a range of ρ_0 and ρ_{sat}, resulting in a maximum change of 1.4%. The enthalpy of formation

ΔH acts as the source of heat generation during absorption and heat sink during desorption.

The mass source ($\dot{m}$) terms during the absorption [77] and desorption [126] can be written as the following two equations,

$$\text{Absorption: } \dot{m} = C_a \exp\left(-\frac{E_a}{RT}\right) \ln\left(\frac{p}{p_{eq}}\right)(\rho_{sat} - \rho_0) \tag{4.10}$$

$$\text{Desorption: } \dot{m} = C_d \exp\left(-\frac{E_d}{RT}\right)\left(\frac{p - p_{eq}}{p_{eq}}\right)(1 - \rho_{sat} + \rho_0) \tag{4.11}$$

Finally, the P-C-T state equation proposed by Dhaou *et al* [124] was implemented to evaluate the equilibrium pressure during absorption and desorption. Here, constants A and B were empirically determined, and the equilibrium pressure p_{eq} in equation is in the unit of atm.

$$p_{eq} = \exp\left(A - \frac{B}{T}\right) \tag{4.12}$$

4.2.2 Compressibility Factor

The hydrogen gas density in Darcy flow equation was derived by assuming ideal gas law that solved for the hydrogen density term in the equation. The compressibility factor of hydrogen can vary significantly in certain situations and thus ideal gas assumption may not prove to be a valid assumption for simulation purpose. Figure 4.2 in the following shows experimentally obtained pressure dependent compressibility factor for hydrogen at several constant temperatures from the data base of Engineering Equation Solver (EES) software. The factor shows a dramatic swing at extreme low temperatures like 35 K. On the contrary, the change in compressibility factor with pressure is linear

with miniscule slope at temperatures closed to room temperature or above. The compressibility factor for hydrogen at 15°C ranges from 1.001 to 1.092 for a pressure range of 101 kPa to 15 MPa. This is indicative of the fact that ideal gas assumption would be a reasonable approximation for modeling hydrogen sorption behavior in LaNi$_5$ hydride since such AB$_5$ types operate at moderate temperature and pressure. Table 4.1 shows the approximate pressure and temperate for hydrogen sorption process and corresponding compressibility factors. It is evident that only during the desorption process, the compressibility factor may reach a value of 1.024 which is about 2.4% deviation from the ideal case (Z=1). The validation experiments conducted in this study, however, were within the maximum pressure limit of 4.57 MPa at which the Z value is 1.024.

To identify the appropriate compressibility factor, experimental absorption and desorption temperatures and corresponding pressures were used as shown in Figure 4.3. Since the pressure and temperature during absorption are constants the compressibility factor related to absorption is a constant, which is 1.008 as shown in Figure 4.3(a). Desorption pressure increases with the reactor temperature and thus the compressibility factor is not a constant as can be seen in Figure 4.3(b). At the end of desorption process this Z value reaches 1.024 which can be used for simulation of desorption process. The summary of the applicable compressibility factor (Z) is listed in Table 4.1.
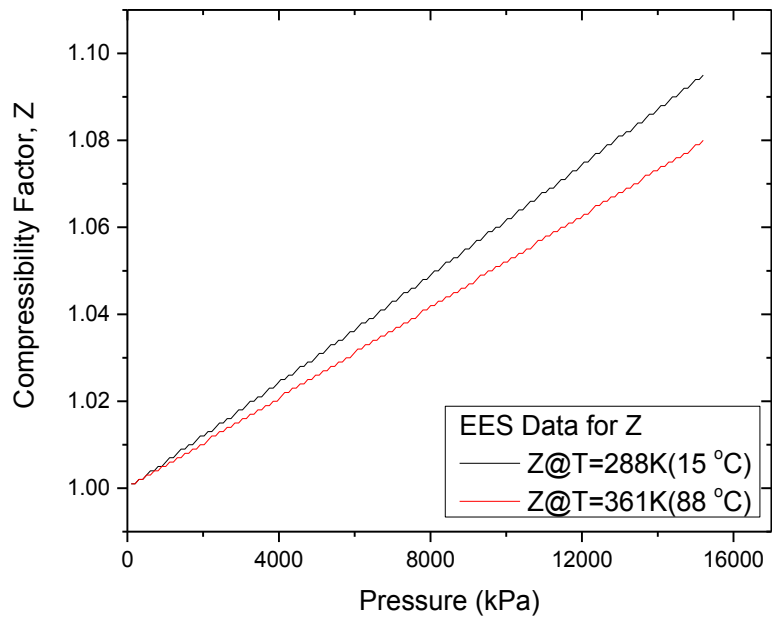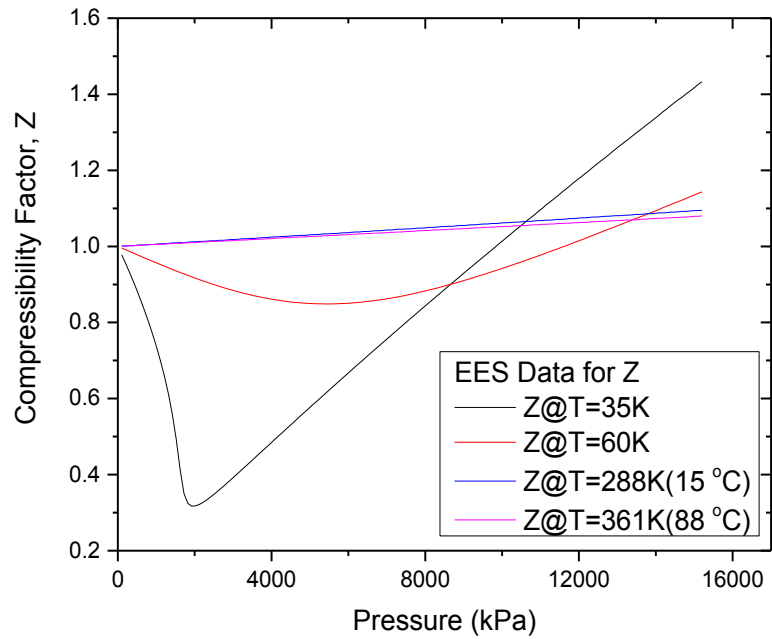
Figure 4. 2: Compressibility factor (Z) for hydrogen gas
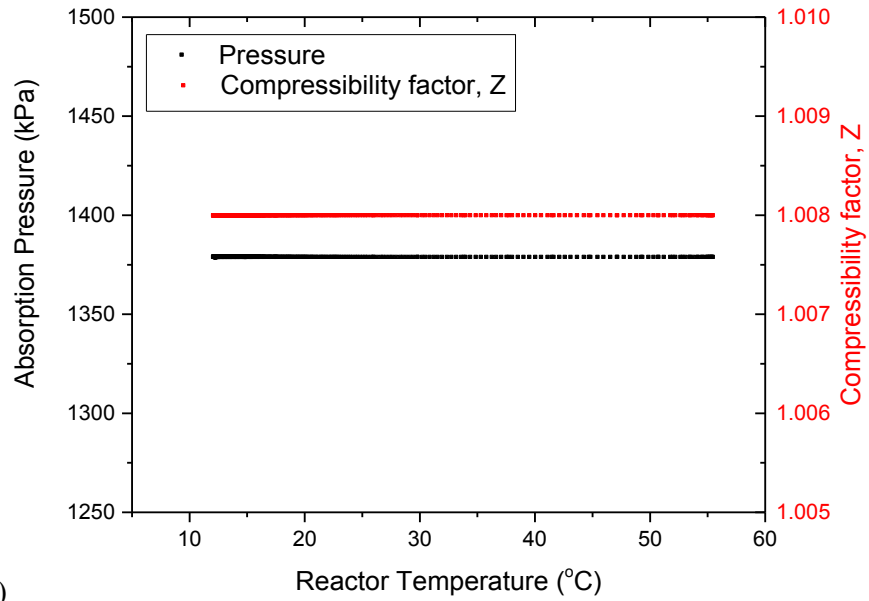
(a)
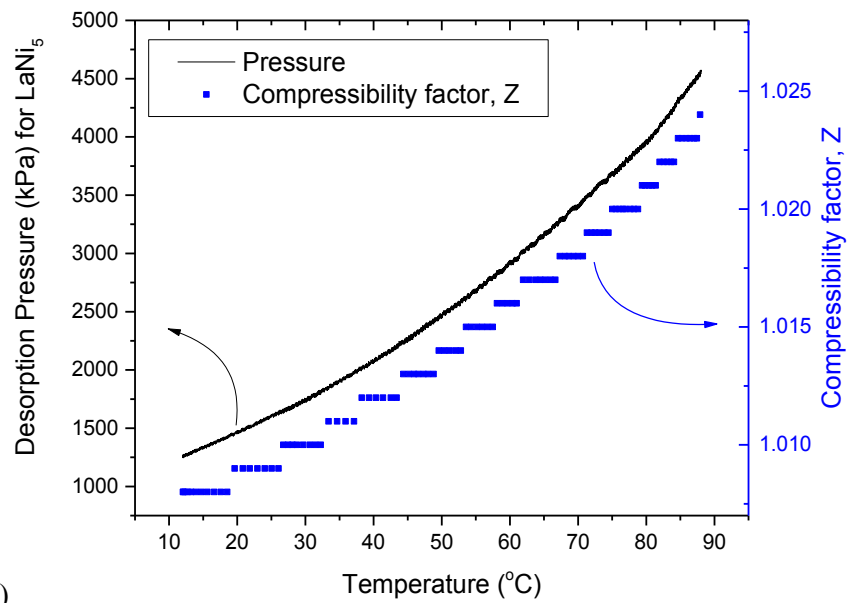
(b)

Figure 4. 3: compressibility factor, Z as a function of pressure and temperature – (a) Absorption (b) Desorption

Table 4. 1 Applicable compressibility factor during sorption process

Application involving LaNi₅		Temperature	Pressure	Z	% Deviation from ideal case(Z=1)
H₂ Storage	Absorption	15 °C	1378 kPa (200 psi)	**1.008**	0.8 %
	Desorption	88 °C	4572 kPa (663 psi)	**1.024**	2.4 %

4.2.3 Initial and Boundary Conditions

The pressure, temperature and density were assumed to be in equilibrium initially, which can be expressed as following:

For absorption: at t=0, $T_s = T_g = T_{ss} = T_a$; $\rho_s = \rho_o$; $P_g = P_a$

For desorption: at t=0, $T_s = T_g = T_{ss} = T_d$; $\rho_s = \rho_{sat}$; $P_g = P_d$

The reactor wall was assumed to be exposed to a pool of ethylene glycol (liquid coolant) with constant temperature during the sorption processes. The boundary conditions relevant to such arrangement are written as follows:

At r = r₁: $P_g = P_a$ (for absorption) or $P_g = P_d$(for desorption); $\frac{\partial T_g}{\partial r} = 0$;

At r = r₂: $\frac{\partial P_g}{\partial r} = 0$; $k_s \frac{\partial T_s}{\partial r} = k_{ss} \frac{\partial T_{ss}}{\partial r}$

At r = r₃: $-k_{ss}\frac{\partial T_{ss}}{\partial r} = h(T_{ss} - T_\infty)$

At Z=0 and Z=L: $\frac{\partial P_g}{\partial r} = 0; \frac{\partial T_g}{\partial r} = 0; \frac{\partial T_s}{\partial r} = 0$;

4.2.4 Meshing Geometry

The entire geometry was meshed using triangular elements as shown in Figure 4.4. The element quality is shown on the scale of the plot in greyscale with white being the best and black being the worst. The minimum, maximum and the average element quality for the mesh were found to be 0.8842, 0.9997 and 0.9742, respectively.
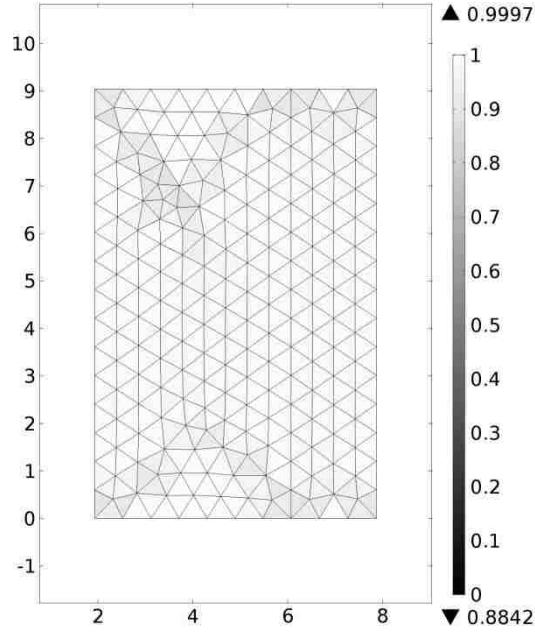
Figure 4. 4: Mesh Quality information

4.3   Simulation Results

In summarizing the results obtained from the numerical simulation, surface average pellet temperature was calculated using surface integral from the axisymmetric model in COMSOL. The surface considered for averaging is the two dimensional axisymmetric plane that was initially constructed for simulation. The reaction fraction, as defined by the following Equation 4.13, was also calculated using surface integral of the axisymmetric surface. The reaction fraction, X is defined by the hydrogen to metal atom ratio at a given instance to that at saturated state. In calculating temperature at different radial distances, line average temperature was computed from the numerical solution.

$$\text{Reaction Fraction, } X = \frac{\left(\frac{H}{M}\right)}{\left(\frac{H}{M}\right)_{sat}} \tag{4.13}$$

60

4.3.1 Temperature History

Surface average temperature of the pellet during the processes is shown in Figure 4.5. From the temperature history of the pellet, the peak temperature for absorption is reached at 27.4 seconds whereas for desorption it is reached at 18.8 seconds. It takes about 353.4 seconds during absorption to reach a temperature that is within 1% of the initial temperature at which the process initiated. Time duration for completing the desorption process is faster provided that the process initiates at an elevated temperature. In such condition, system temperature reaches within 1% of the initial temperature in 152 seconds from initiation of the process.

Since the reaction is intense in the inner core from where hydrogen is flowing into the pellets during desorption, temperature at the core would be highest with gradual decrease towards the outer edge. During desorption, reaction would also be intense at the core since hydrogen would be leaving the material and flowing out of the reactor through the core. This would cause a sharp temperature drop at the beginning of the process. This sudden drop in temperature would be less intense at the outer surface of the reactor since the reactor would be exposed to the pool of heated liquid ethylene glycol that maintains a constant elevated temperature suitable for desorption to take place. Line average temperatures at different radial distances are shown in Figure 4.6. For absorption the lowest temperature is at the reactor wall since the reactor is kept cooled to take away the heat of reaction during absorption reaction. As for desorption the reactor wall temperature is the highest. Overall, absorption and desorption process show opposite trends in every aspect as expected.
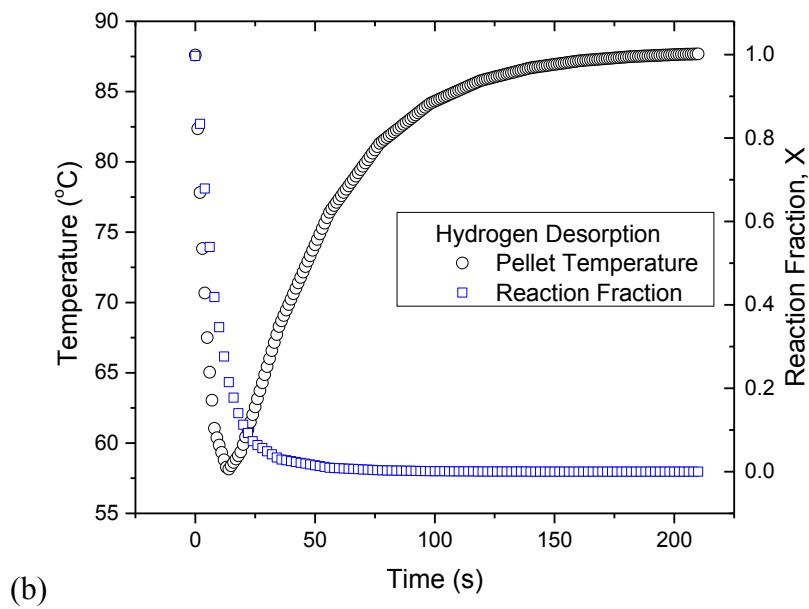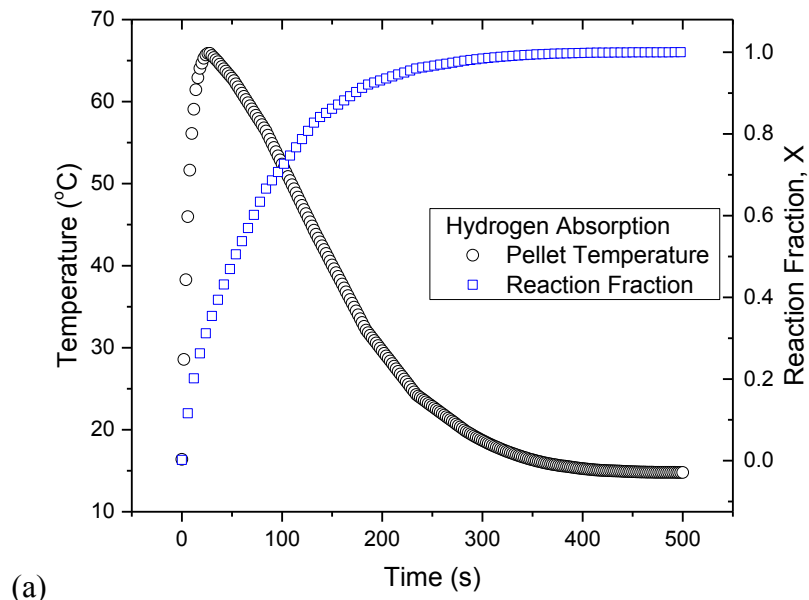
Figure 4. 5: Surface average temperature response and reaction fraction of the pellet during (a) absorption and (b) desorption simulation results
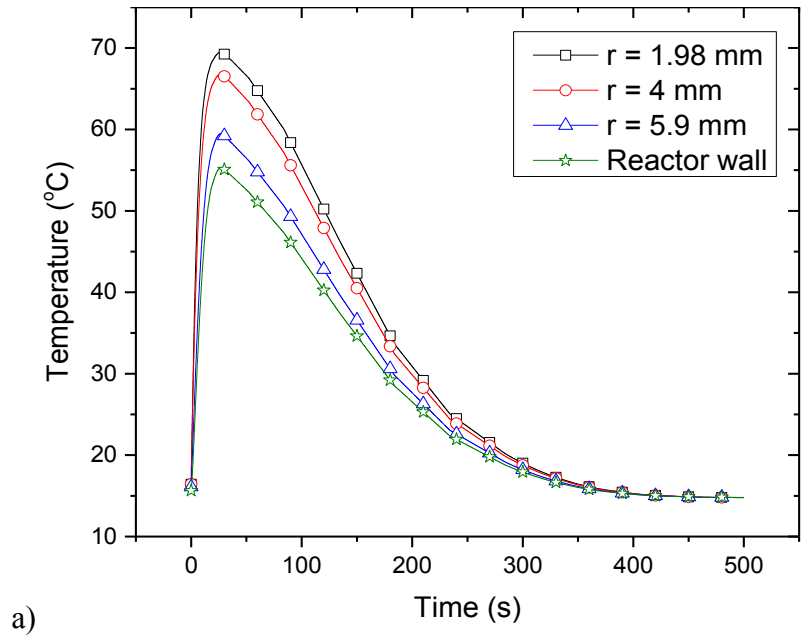
a)
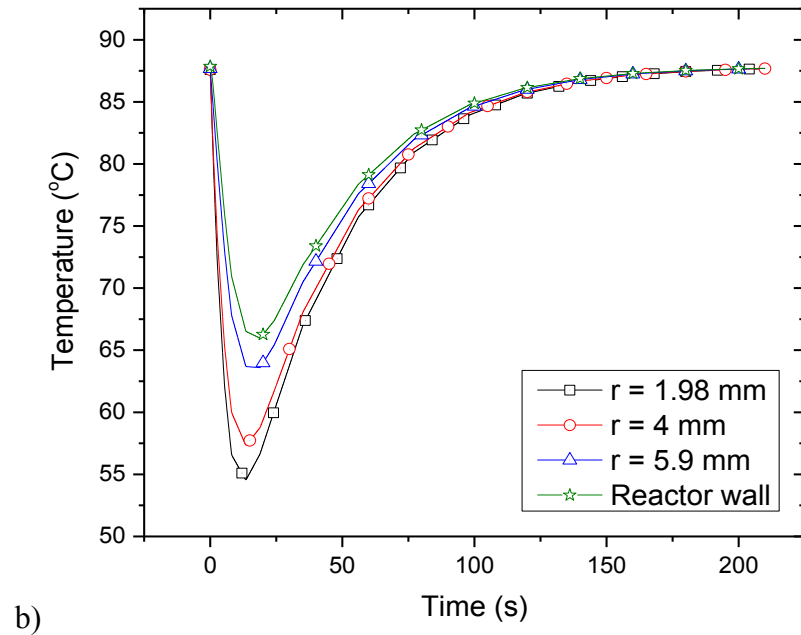
b)

Figure 4. 6: Simulated line average temperature history at different radial distances

The temperature history of the simulation domain in three dimensional view is illustrated in Figure 4.7. The system is kept cold using the coolant to expedite the

absorption process and thus the pellet and reactor starts with a temperature around 15°C. The exothermic reaction generates heat as time progresses with the supply of hydrogen into the system, which causes a gradual increase of temperature within in the system. The process reaches the peak at approximately 27.4 seconds as this state can be distinguished with the color scheme representing the upper limit of the scale shown in Figure 4.7.
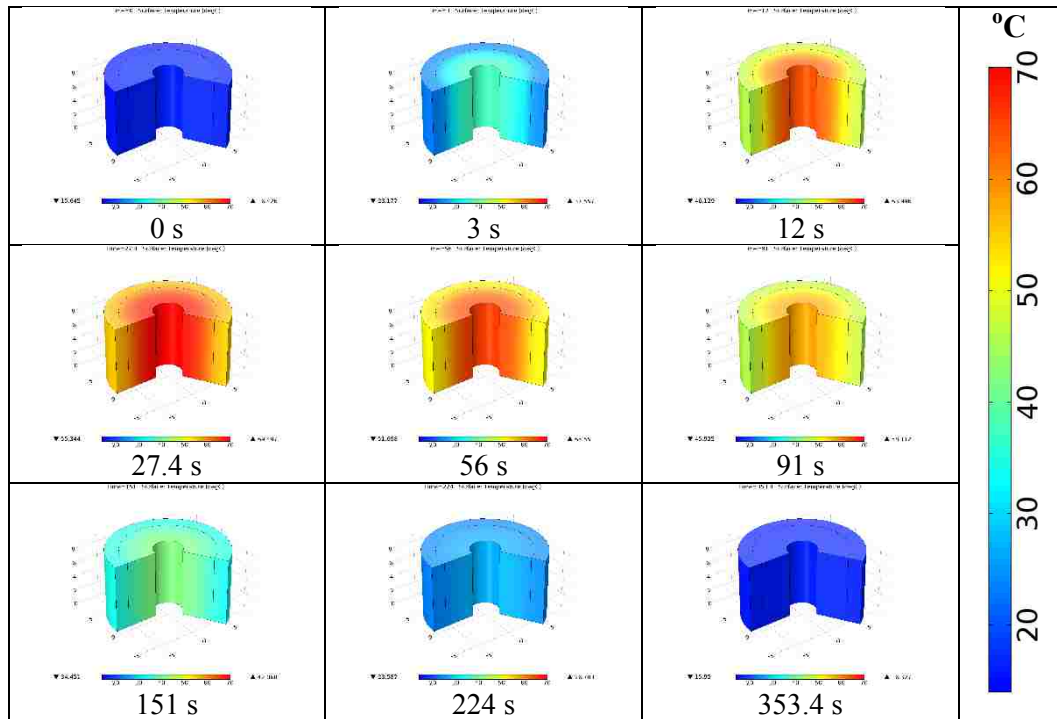
Figure 4. 7: Simulated system temperature evolution during absorption

A similar but opposite trend can be observed while hydrogen desorption process occurs within the reactor as shown in Figure 4.8. The simulation process begins with temperature being at elevated level for which the system remains at upper end of the temperature scale in the figure. The reaction starts to occur immediately and system temperature starts to decrease as soon as the reaction starts. Since the core area is the only way out for hydrogen to exit the system, it remains at the coldest state at any given temperature as the endothermic reaction is most intense at that area. The nadir (lowest)

temperature is reached at approximately 18.8 seconds. From that point onward, the reaction slows down as most of the hydrogen is desorbed and the system temperature slowly reaches the elevated temperature level of the heated bath. The process takes about 152 seconds to desorb and rebound to initial temperature state.
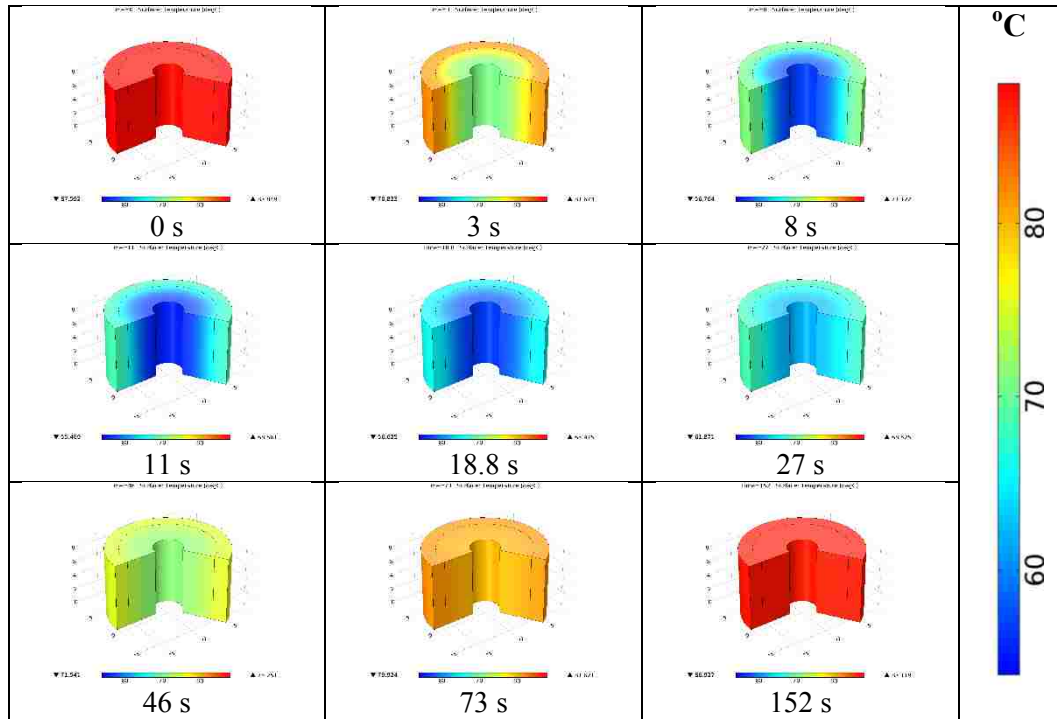
Figure 4. 8: Simulated system temperature evolution during desorption

4.3.2   Influence of physical properties

Thermal conductivity and porosity are the two parameters that may vary depending on the coating and compaction process of the storage material, which finally morphed into pellets. Thermal conductivity is sensitive to chemical process duration during which copper encapsulation of the storage material is performed. Porosity of the pellets depends on the compaction pressure at which pellets are formed. The influences of these two parameters on sorption process were studied in a parametric study.

Improved thermal conductivity of the pellets would ensure better heat transmission rate to the pellets, which eventually translates to faster reaction rate and hence swifter actuation. Both copper encapsulation and compaction to pellets process improve overall thermal conductivity of the pellets. The powdered material, after repeated hydriding and dehydriding process, may have significantly low thermal conductivity whereas the coated pellets have conductivity ranging from 2.17 to 6.63 W/m.K [121] as concluded in a previous study. Figure 4.9 shows the overall effect of varying thermal conductivity in heat transfer process while the exothermic absorption reaction is taking place. An interesting effect was observed in the heat transport process in the plot of the reactor wall temperature from the numerical solution. While absorption process is in progress, the wall temperature is dominated by heat of reaction during certain duration from the beginning of the process. After a while, as the reaction slows down with storage material reaching saturation, the external cooling effect tends to out weight the internal heat generation by reaction. This trend was identified from the plot in Figure 4.9(a) where the effect of varying thermal conductivity of the pellets on thermal state of the reactor wall is illustrated. For highly conductive hydride the heat of reaction is transported to the cooling media faster. On the other hand, when reaction slows down, the heat generated during the reaction process is extracted from the reactor faster because of better thermal conductivity of the pellets. Thus, an intersecting zone among the reactor wall temperature history lines, as seen more clearly in Figure 4.9(b), is observed from the results of parametric study using thermal conductivity as the varying parameter. On the left side of that zone heat of reaction dominates the system temperature and on the right, cooling effect of the bath dominates the heat transport process.

66
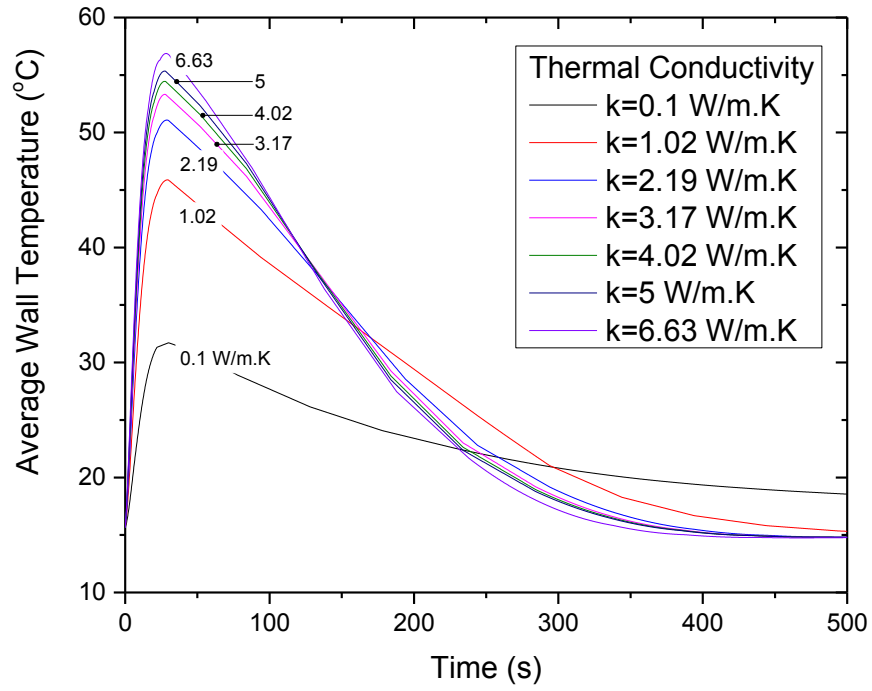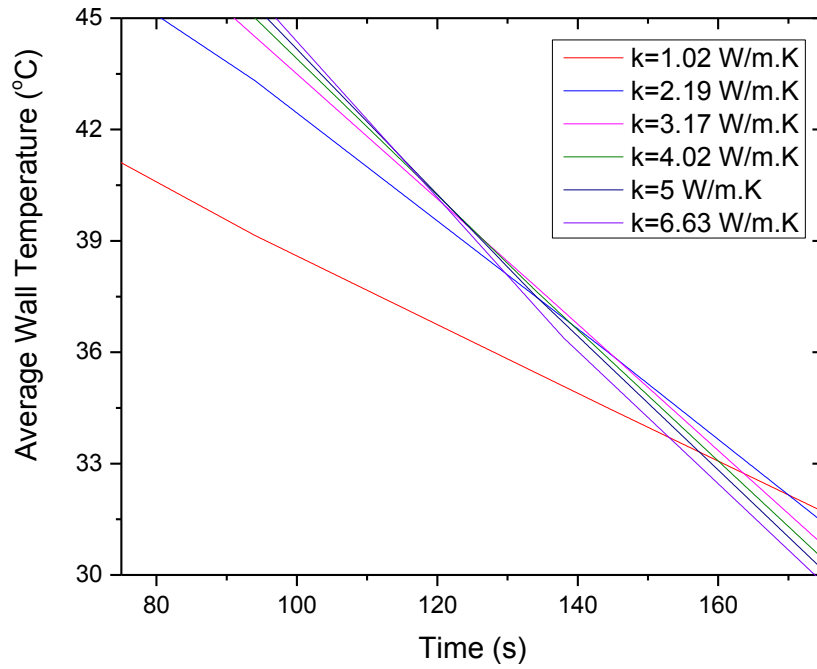
Figure 4. 9: (a) Effect of thermal conductivity with transition zone marked in red rectangular area, and (b) magnified image of the transition zone
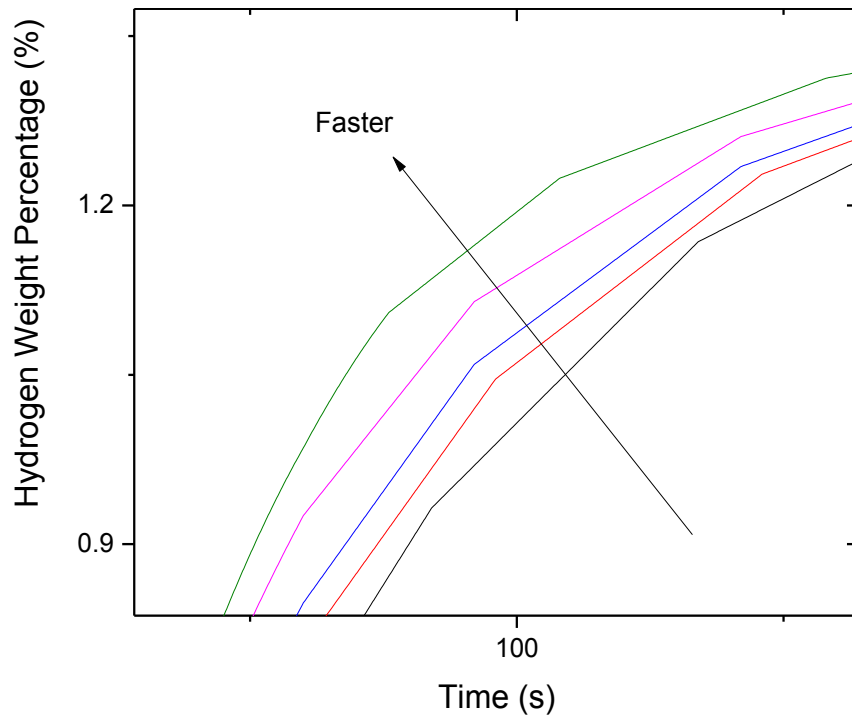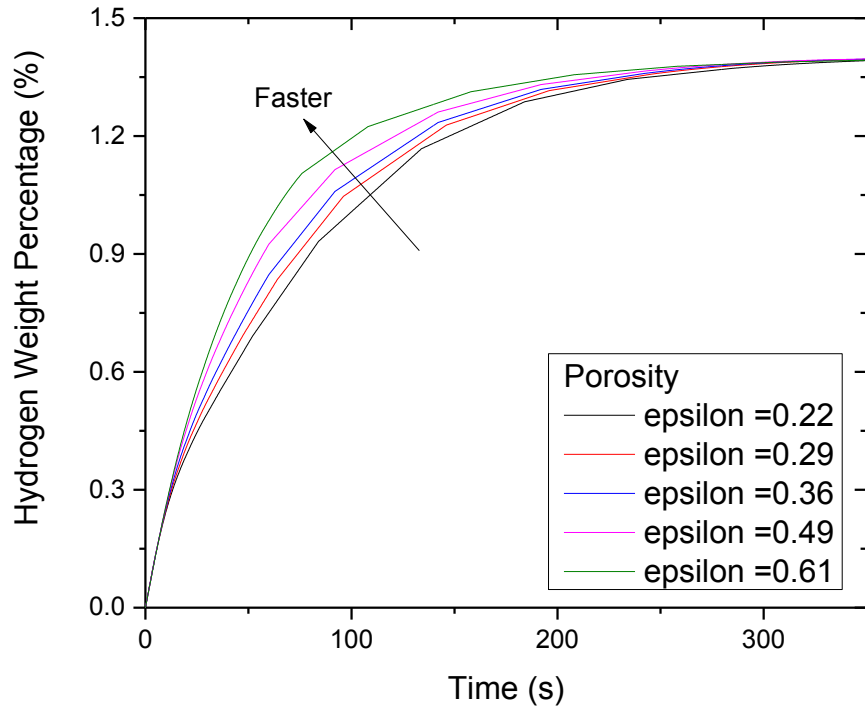
Figure 4. 10: (a) Effect of porosity on hydrogen concentration during absorption and (b) magnified portion of the selected area

The void fraction or porosity simply represents the void spaces in the pellets since they are formed by compaction of particles with mesh size of 100. For same amount of material, the porosity of the pellets would vary depending on the compaction pressure applied to form the compacts. Assuming that other properties remain same, increasing porosity would   actually increase permeability of hydrogen through the porous space. Thus, the particles will easily come into contact with the hydrogen gas during the sorption process, which would eventually accelerate the reaction process and help reach saturation relatively fast. As shown in Figure 4.10, with increasing porosity hydrogen concentration in the hydride increases at relatively faster rate during the reaction process.

4.4   Experimental Validation

4.4.1   Setup Preparation

LaNi$_5$ metallic particles selected for the experiment were obtained from Japan Metals & Chemical Co. Ltd. Copper encapsulated particles were compacted into cylindrical pellets using a press and die at a predetermined pressure. Metal hydride compacts were then prepared using the die as shown in Figure 4.11. Each LaNi$_5$ pellet contains 5 g of Cu coated particles and 0.5 g of tin (Sn) binder which was compressed at a pressure of 2,500 psig to maximize thermal conductivity of the metal hydride while maintaining an optimum porosity as suggested by the experimental results [121] reported previously. In the end, all the pellets were stacked inside a single reactor and subsequently passed through activation process that involves exposure of the storage material to pressurized hydrogen for 30 minutes and subsequently extraction of hydrogen using vacuum. This process was repeated until the reactor temperature response during absorption showed consistent behavior during the repeated cycles.
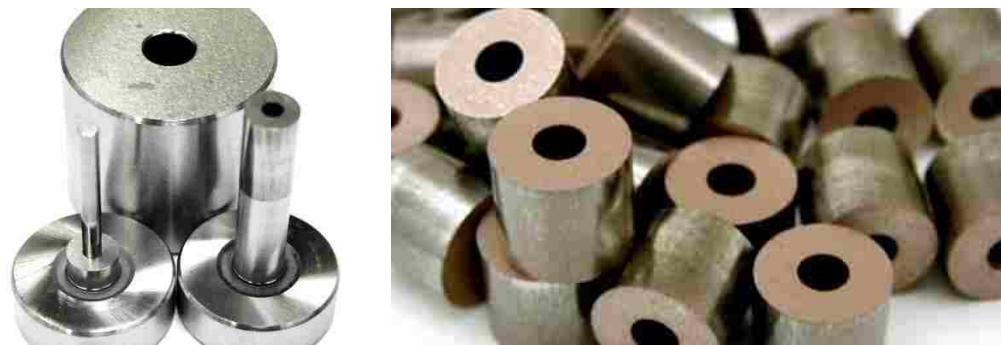
Figure 4. 11: Die and metal hydride compacts

4.4.2 Setup

The experimental setup was prepared for identification of the thermal response characteristics of the reactor during the absorption and desorption of hydrogen using LaNi$_5$ hydrogen storage material. The setup consists of a tubular reactor that houses the pellets, a jacketed beaker used as constant temperature bath, and a high capacity chiller for maintaining constant temperature during the reaction process. The reactor was placed inside the temperature controlled bath, entirely submerged, during the reaction process so that desired temperature could be maintained throughout the process. The temperature of the reactor surface was monitored using K type thermocouples and the water bath temperature was monitored using a RTD obtained from Omega Engineering Inc. Figure 4.12 (a) shows the CAD image of the reactor containing pellets inside and Figure 4.12 (b) shows the actual experimental setup used for acquiring the temperature history data from reactor wall during the sorption process. The reactor has a gate valve on the top for regulating gas flow. The valve also enables pausing desorption process while the temperature of the bath gradually increases to a predetermined level.
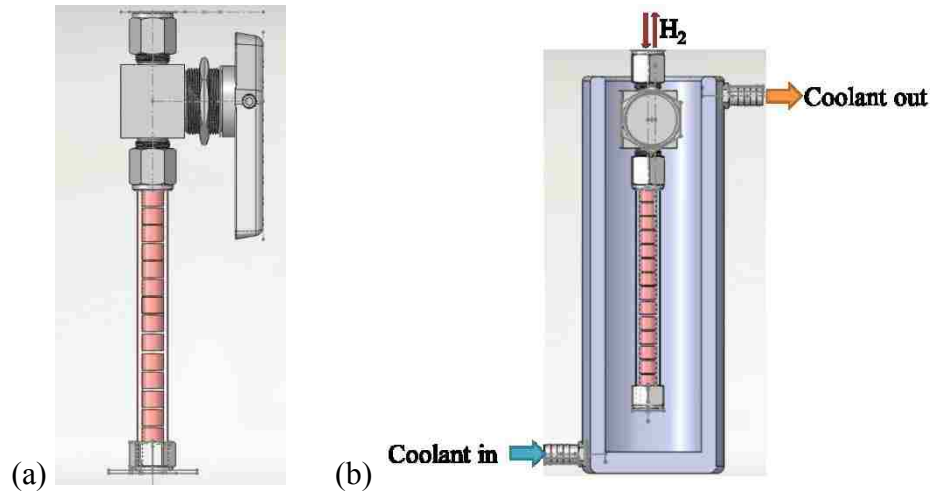
**Figure 4. 12: (a) CAD image of the reactor and
(b) Jacketed beaker housing the reactor**

4.4.3   Validation

Since the sorption process is either exothermic or endothermic during hydrogen absorption and desorption respectively, reactor temperature history data is the most suitable parameter to validate the model outcomes. For absorption the supply pressure during the experimental absorption process was maintained at the same level as the pressure boundary condition applied in the simulation. Initially the reactor was exposed to vacuum and the reactor was submerged into the pool of cooling liquid whose temperature, approximately at 15°C, was maintained by a high capacity chiller. When the temperature was stable, hydrogen was supplied, at 200 psig, to the reactor for the exothermic absorption process took place. It abruptly increased the temperature of the reactor. Reactor wall temperature was recorded since the initiation of the process and this temperature history was matched with the simulation results for model verification. The experimental and simulation results for reactor wall temperature history is shown in the Figure 4.13 for absorption.
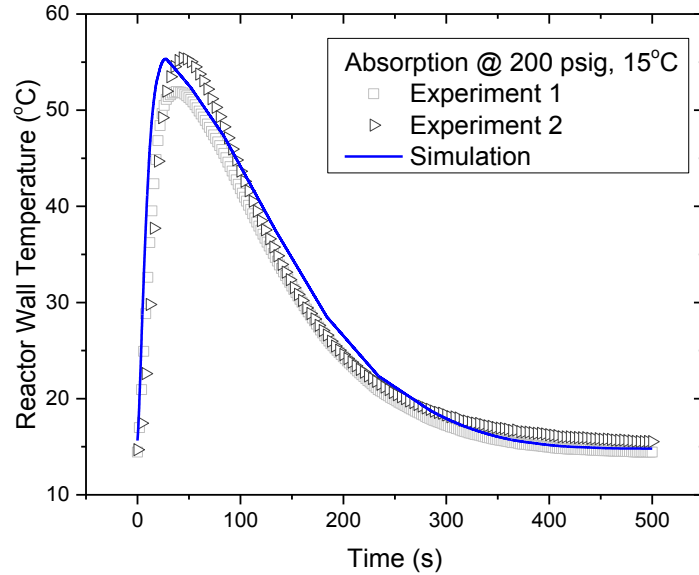
Figure 4. 13: Experimental and simulated temperature history of the reactor wall during absorption

The temperature response data obtained during the absorption process matches reasonably well with the numerical solution as shown in Figure 4.13. The peak temperature of 55.33 ^{o}C was found from the numerical solution whereas the experimental results indicate that the peak is at about 55.43 ^{o}C. Still, there is shift in phase observed in terms of time required to attain the peak temperature. The simulated peak temperature was reached at around 27.4 seconds whereas experimental data shows that the peak was reached after 44 seconds after the initiation of the process. The reaction rate applied in the simulation might be faster than the actual rate, which might have contributed the time lag in reaching the peak during the experiment. Both numerical solution and experimental data, however, shows good agreement overall.

For desorption, the liquid water bath temperature was set at the elevated initial temperature, 88°C, used in the simulation. Usually hydrides are unstable at elevated temperature and initiate desorption of hydrogen as soon as heat is supplied. The closed

gate valve, as in the experimental case, would maintain hydrogen pressure in the hollow spaces inside the reactor with increasing temperature. This would allow the interstitial hydrogen atoms to remain in the lattice as long as the gas pressure is maintained in the hollow spaces and the valve is kept closed to do so, even with the rising temperature. So, after the initial absorption process, the reactor gate valve was shut off and was totally isolated from the ambient. At that instance, the storage material was saturated with hydrogen and the void space inside the reactor was still pressurized with the supplied hydrogen that couldn't get absorbed simply because of saturation condition. Thus, even at elevated temperature, hydrogen filled storage material inside the reactor should be at complete pause and hence, desorption would not initiate simply because the hydrogen atoms were trapped in the interstitial spaces of hydrides. This concept was implemented for identical boundary conditions as implemented for the simulation of hydrogen desorption from metal hydride. Figure 4.14 shows the experimental and simulated temperature history for desorption of hydrogen from metal hydride reactor.

The desorption process comprises of exposure of the storage material to heat, which causes immediate initiation of hydrogen extraction from the lattice of the storage particle. This endothermic reaction causes a sudden drop of the system temperature as seen in Figure 4.14. Numerical solution of the model equations indicate that the nadir temperature during desorption process would be about 66 $^{\circ}$C reached within 18.8 seconds from the initiation of the process. Experimental results initially shows very similar trend in reaching the nadir temperature. 66.7 $^{\circ}$C was recorded at 12.5 seconds from the initiation of the process. Overall there is a subtle difference in the time history of the nadir temperature but the trend is very similar. Desorption process suddenly pressurize

73

the system which may cause hydrogen to push back into the particle if corresponding equivalent pressure at such temperature favors absorption. Since the pressure inside the system is not regulated (unlike absorption process), the irregular pressure buildup inside the system may have caused the irregularities in the experimental data. Both experimental and numerical results, however, shows similar trend and reach saturation approximately within 200 seconds.
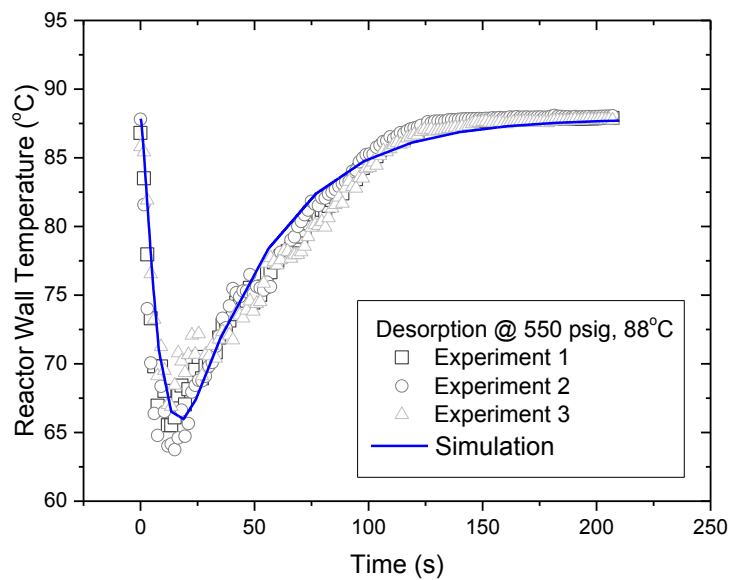
**Figure 4. 14: Experimental and simulated temperature history
of the reactor wall during desorption**

The randomness in desorption experimental data is attributed to the fact that, desorption pressure was not well regulated since desorbed hydrogen gas could freely exit the reactor with steady temperature rise. During absorption experiments, both pressure and temperature were maintained constant using a hydrogen gas reservoir and high capacity chiller, respectively. Hence, the fluctuations in experimental data weren't visible in hydrogen absorption experiments. Overall, the model was able to capture the sorption process reasonably well as reflected in the graphs.

CHAPTER 5: H₂ Powered Soft Robotic Actuator

A thermo-kinetically driven, hydrogen powered soft robotic actuator integrating metal hydride hydrogen storage technology for compact, noiseless and smooth actuation, is presented in this chapter. To test the plausibility of a thermally driven actuator, a conventional piston type actuator was integrated with $LaNi_5$ based hydrogen storage system. Copper encapsulation followed by compaction of particles into pellets, were adopted to improve thermal conductivity of the storage system and minimize thermal energy requirement to drive the system. The operation of the actuator was thoroughly investigated for arrays of operating temperature ranges. Thermally driven operation procedure was implemented for smooth and noiseless actuation over the entire operating range. The actuator also produced smooth and consistent strokes for repeated cycles of operation. The actuator exhibited performance similar to biological muscles at certain operating temperature range. The performance of such actuator, however, can be tuned to conform that of hydraulic actuators by design modification and proper selection of the storage material. The data used in this and subsequent segment of dissertation is representative data. Repeated experimental data is shown in Appendix - C and D.

5.1   Overview

Since the discovery of hydrogen absorbing alloys, a wide range of applications involving such materials have been developed. Metal hydride integrated systems such as thermally driven metal hydride compressor [3, 7, 10], heat pump [28, 38-40, 45, 47-53, 131], refrigerator and air conditioning system [41, 50], heat transformer [8, 60] etc. have been developed and reported in scientific research communications. The technology has also been implemented in purifying hydrogen [2] in semiconductor industry where high

purity hydrogen is needed for certain processes. Hydrogen powered Ni-MH batteries have already found its application in consumer electronics and are commercially available in retails. Fuel cells [27, 65] using metal hydride to store hydrogen are also in use in commercial forklifts because of the high storage capacity that the material offers, which enables compact, efficient and powerful cell design.

Hydrogen can be stored and extracted reversibly to and from metal hydride through the removal of heat for absorption and supply of heat for desorption. The exothermic absorption and endothermic desorption processes can be described by Equation 5.1 in the following where M, H and ΔH in the equation represents metal, hydrogen and enthalpy of reaction respectively. The enthalpy change during the process permits a number of applications such as the ones mentioned earlier. Moreover, the process is reversible with negligible hysteresis for most of the materials that are of design interest for engineering systems and devices.

$$\mathbf{M + H_2 \leftrightarrow MH \pm \Delta H} \tag{5.1}$$

Storing hydrogen in inter molecular spaces of metal hydrides enables safe storage of the gas at a density greater than the storage densities achieved by conventional methods [14, 17, 20]. Compact storage volume with ultra-high density of hydrogen and noise less operation using metal hydride have opened up doors for its application in robotics and industrial automation. Hydrogen powered actuator made of cylinder with metal bellows [99] as a functional part was being investigated. Copper plated hydrogen absorbing $LaNi_5$ was used for storage of hydrogen which was reversibly heated and cooled by Peltier element in that study. A special type of metal hydride was also used for storage and supply of hydrogen to power a similar type of actuator [5]. Both studies focused on the

76

performance of the actuator using different temperature, pressure and external loads. Hydrogen powered braided artificial pneumatic muscle [71] was also being investigated for compact, noiseless and smooth operation. This actuator claimed to have very high second law efficiency as well as very high force to weight ratio. Biomimetic Mckibben actuator combined with metal hydride was also being reported [72] with comprehensive simulation strategy for actuation purpose. It is evident from these studies that the coupling of actuator with metal hydride offers compactness, high force to mass ratios and noiseless soft actuation similar to biological muscles. Solar or surplus heat driven metal hydride integrated actuator [73] has also been investigated with findings supporting the operation of the actuator without any energy consumption from sources such as electric or fossil fuel. The concept of powering up actuators with hydrogen stored in metal hydride has been getting attention because of its unique characteristics such as biomimeticity, compact design, high force to mass ratio, and environmentally benign frictionless operation.

In this study a spring loaded piston type actuator is presented, which is powered by hydrogen stored in LaNi$_5$ storage system. The schematic diagram of the concept of hydrogen powered soft robotic actuator is shown in Figure 5.1. The basic building blocks comprise of a metal hydride hydrogen storage reactor, hydrogen gas filter, gate valve, pressure transducer and an actuator with spring mounted actuation rod. A resistive heating element is used to supply the heat of reaction to the metal hydride, which drives the desorption process. The reactor is heated and cooled alternatively using electric heater and natural convection process for desorption and absorption of gas in the storage reactor, respectively. While the reactor is being heated, the desorbed gas causes to pressurize the

actuator initiating a forward stroke. The cooling of the reactor causes to retract the actuation rod while the gas is being reabsorbed into the metal hydride. This backward stroke is assisted by the spring force as well as the absorption of gas into the hydride structure by cooling of the reactor, causing a combined effect of complete retraction of the actuation rod. Hence, the operation of the system comprises of controlling the reactor temperature only. Once the desired displacement is attained, the power supply to the heating element is shut off, which causes the reactor temperature to decrease gradually. During that time the actuator retracts to the initial position and hydrogen in the actuator cylinder gets reabsorbed into the metal hydride hydrogen storage unit completing a full cycle. This cycle can be repeated as per requirement and the operating temperature range can be set in accordance with the desired stroke length. An elaboration of such system's operating procedure and performance is illustrated throughout this paper.
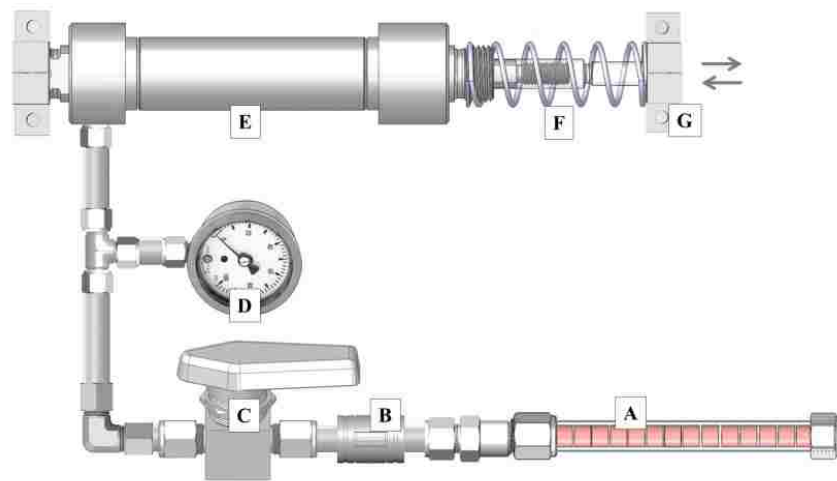
Figure 5. 1: Schematic diagram of hydrogen powered actuator: (A) H2 reactor (B) hydrogen filter (C) gate valve (D) pressure gauge (E) piston type actuator (F) spring loaded actuation rod (G) mount/hinge

5.2   Experimental Setup

5.2.1   Hydrogen Storage

A reactor housed the storage materials that absorbs and desorbs hydrogen reversibly to drive the system. Pellets were prepared by compressing copper encapsulated particles in a stainless steel die shown in Figure 5.2(A). After the compaction process the particles are tightly packed into cylindrical hollow pellets as shown in Figure 5.2(B). The hollow channel in the center facilitates the flow of hydrogen with negligible flow resistance during the sorption process. Finally, all those compacts are placed inside a cylindrical reactor, as shown in Figure 5.2(C), with a circular aluminum screen through the central hollow channel. All the pellets were activated by pressurizing them with hydrogen and subsequently exposing them to vacuum. This activation process is repeated for several cycles till the temperature rise during absorption shows identical behavior at every cycle.
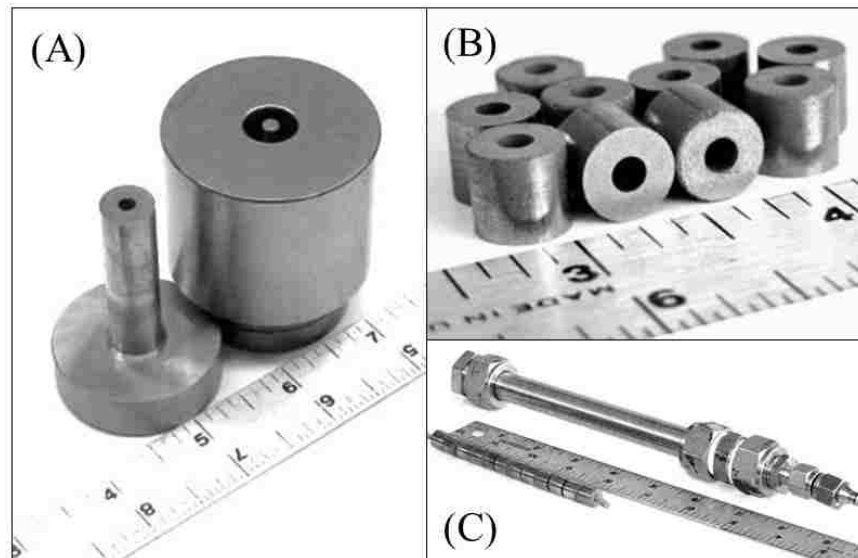
Figure 5. 2: (A) Die, (B) compacted LaNi5 pellets and (C) reactor containing pellets

5.2.2 Actuator Assembly

The setup has three major components: hydrogen storage reactor covered with heating element, a gas filter that blocks dust or any powdered material generated from the storage particle, and a piston type actuator whose actuation rod is loaded with a spring. The overall experimental setup is shown in Figure 5.3. The hydrogen storage reactor (A) contains LaNi$_5$ pellets and is covered with flexible heater that heats the reactor during desorption process. The heat generated by the heater is regulated by a percentage controller (B) that supplies power to the heater at a preset percentage of the rated power. The reactor surface temperature is monitored using a J type thermo couple attached to the surface of the reactor. When power is turned ON, the temperature of the reactor rises to a predetermined level. Once that temperature is reached the switch is turned off and the reactor is allowed to cool by means of natural convection. When the temperature of the reactor rises, desorbed hydrogen flows through the gas filter (C) to the cylindrical actuator (G). The gate valves (D & E) are considered in the design to regulate hydrogen flow during loading of the reactor. Valve (E) isolates the actuator portion from the gas reservoir tank and eliminates the possibility of exposing the actuator to a pressure level that exceeds the pressure rating (250 psi) of the actuator. The pressure during the operation is monitored using a pressure transducer (F) with a maximum pressure rating of 300 psi. When desorbed hydrogen in the cylinder (G) creates necessary pressure to move the piston, the actuation rod (H) starts to move forward. The motion of the actuator rod is resisted by the spring which simplifies the quantification of force generated during actuation and substitutes the application of load on the actuation rod. The displacement generated in the actuator is recorded using LVDT (I) whose output remains linear for a

total stroke length of approximately 28 mm which is also the stroke length of the actuator. Voltage output of the displacement transducer is processed using a digital signal conditioner (J). The DC power supply (K) is used to supply power to the pressure transducer. All the signals from thermocouple, pressure transducer and displacement transducer (LVDT) are acquired using Personal DAQ56 (L) manufactured by IOtech.
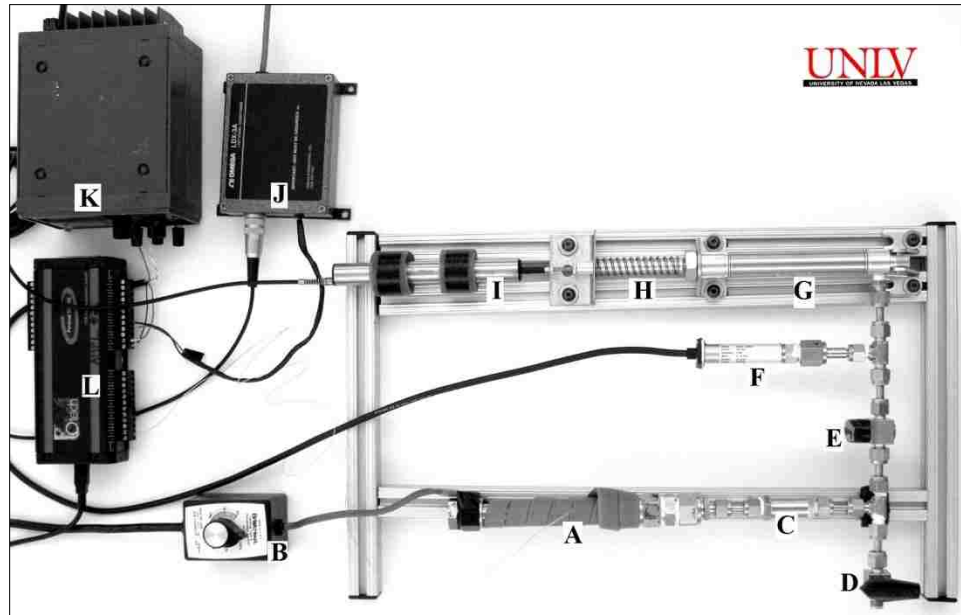
Figure 5. 3: Experimental setup showing (A) Reactor, (B) Percentage controller, (C) Filter, (D) & (E) Gate valves, (F) Pressure transducer, (G) Piston-Cylinder actuator, (H) Spring loaded actuation rod, (I) LVDT, (J) Signal conditioner, (K) DC power supply, (L) Data acquisition

5.2.3 Displacement Transducer

The displacement of the actuation rod is recorded every half second using a LVDT which generates output in AC voltage. LDX-3A signal conditioner from Omega Engineering Inc. is used to convert the AC signals of LVDT to computer readable DC signals. With a precision caliper actual displacements are measured within the limits wherein the outputs are linearly dependent on measured displacements. The graph in

Figure 5.4 shows the linear region in hollow squares and initiation of nonlinearity in solid circles. The linear region can be best fitted with Equation 5.2, which is used to convert transducer voltage output to meaningful displacements in millimeter. Here x is the voltage output of the displacement transducer and y is the actual displacement calculated using that correlation. All the measurements in this investigation are taken within the linear region of LVDT output.

$$y = -1.7482x + 14.952 \tag{5.2}$$
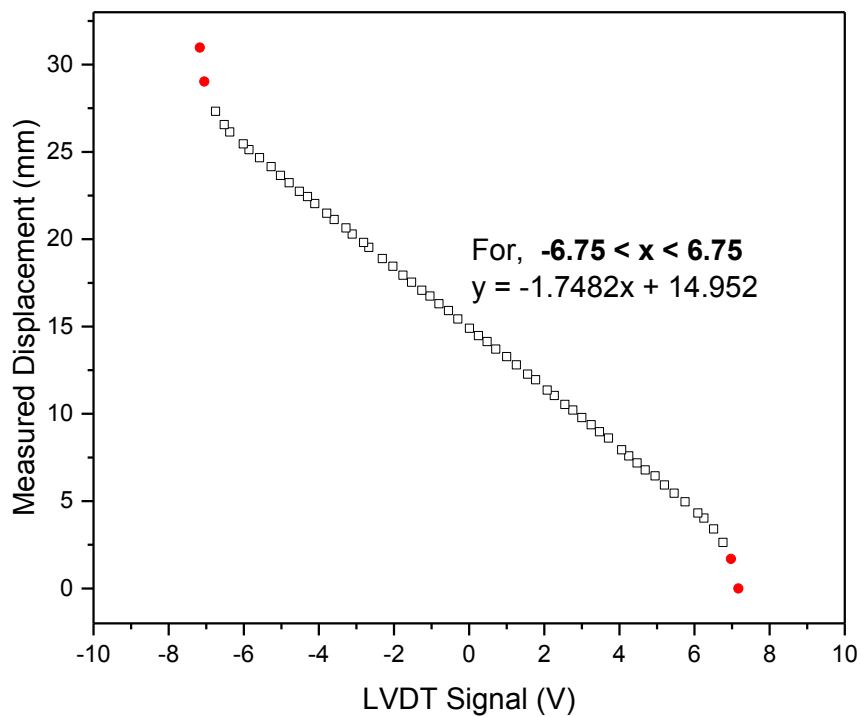
Figure 5. 4: Linear dependence of the LVDT output signal to actual displacements.

5.3 Results

5.3.1 Hydrogen Storage

The very first step to initiate the experiment is to expose the system to vacuum in order to extract air inside the system. Then hydrogen is stored in the reactor which is used as the prime source during operation of the actuator. Hydrogenation reaction that forms hydride phase is an exothermic process that gives up heat and increase the reactor temperature as soon as hydrogen is introduced to the reactor. Figure 5.5 shows the temperature response of the reactor filled with $LaNi_5$ pellets during the initial loading at about 100 psi supply pressure. As soon as hydrogen is introduces into the system temperature shoots up to a peak in about 35 seconds. During this period the reaction rate is very high and most of the material is hydrogenated. Then the reaction rate slows down and reaches saturation, which can be realized from the short plateau. The temperature of the reactor at some point shows a drastic decline, which is the indication of the end of loading process. Once the reactor is saturated with hydrogen, no further reaction takes place and there is a gradual declining in temperature observed while the reactor cools down to the ambient temperature. At this point supply of hydrogen is turned off by closing the gate valves of the reservoir and the setup. It takes about 52 seconds to fill the reactor which is kept at room temperature of about 23^oC. The highest temperature of the reactor during the loading process is recorded to be about 67^oC which roughly indicates the limiting operating temperature during operation. A temperature above this limit can also be applied which would expand desorbed hydrogen gas rather drive the desorption process. Thus, the experiments are performed at different ranges within this limiting temperature.
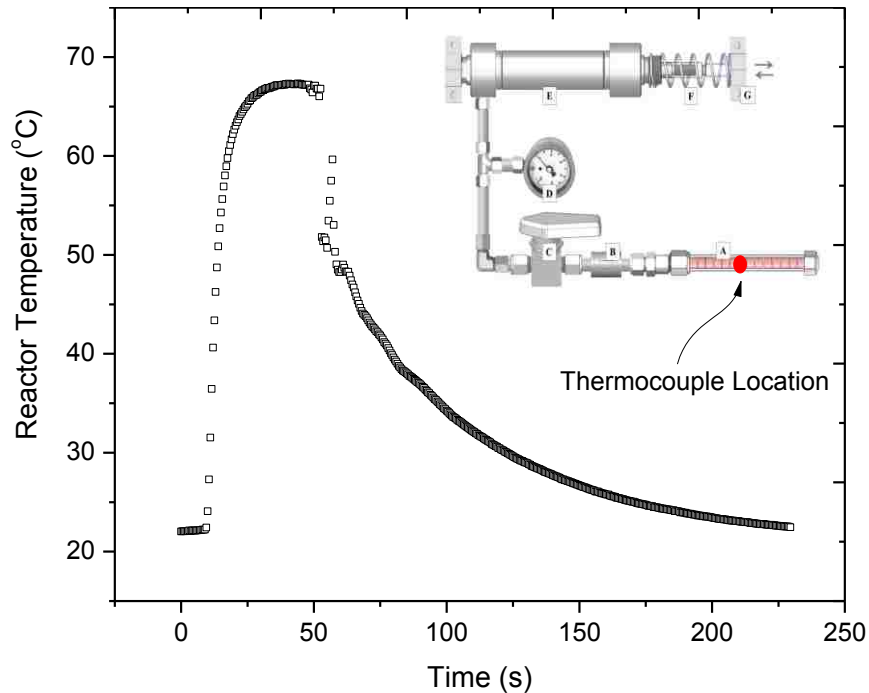
Figure 5. 5: Temperature response of the reactor during absorption of hydrogen

5.3.2 Operating Temperature

The actuation setup under investigation is designed to operate by controlling the reactor temperature only. Once the upper limit of the operating temperature is deduced from the temperature response of the reactor during the loading of hydrogen, several arbitrary operating ranges can be determined within that envelop. Five different operating temperature ranges that would be used throughout the study are shown in Figure 5.6(A). When the percentage controller is turned on the temperature of the reactor gradually increases towards the upper limit. The power supply is shut off as soon as the limit is reached. Time required to reach the limiting temperature varies depending on the targeted upper limit of the operating range. It takes about 280 seconds to reach a temperature of about 60°C, 140 seconds to reach 40°C, 80 seconds to reach 30°C and so on. Cooling of reactor is done by natural convection inside the air cooled laboratory space.

(A)

(B)
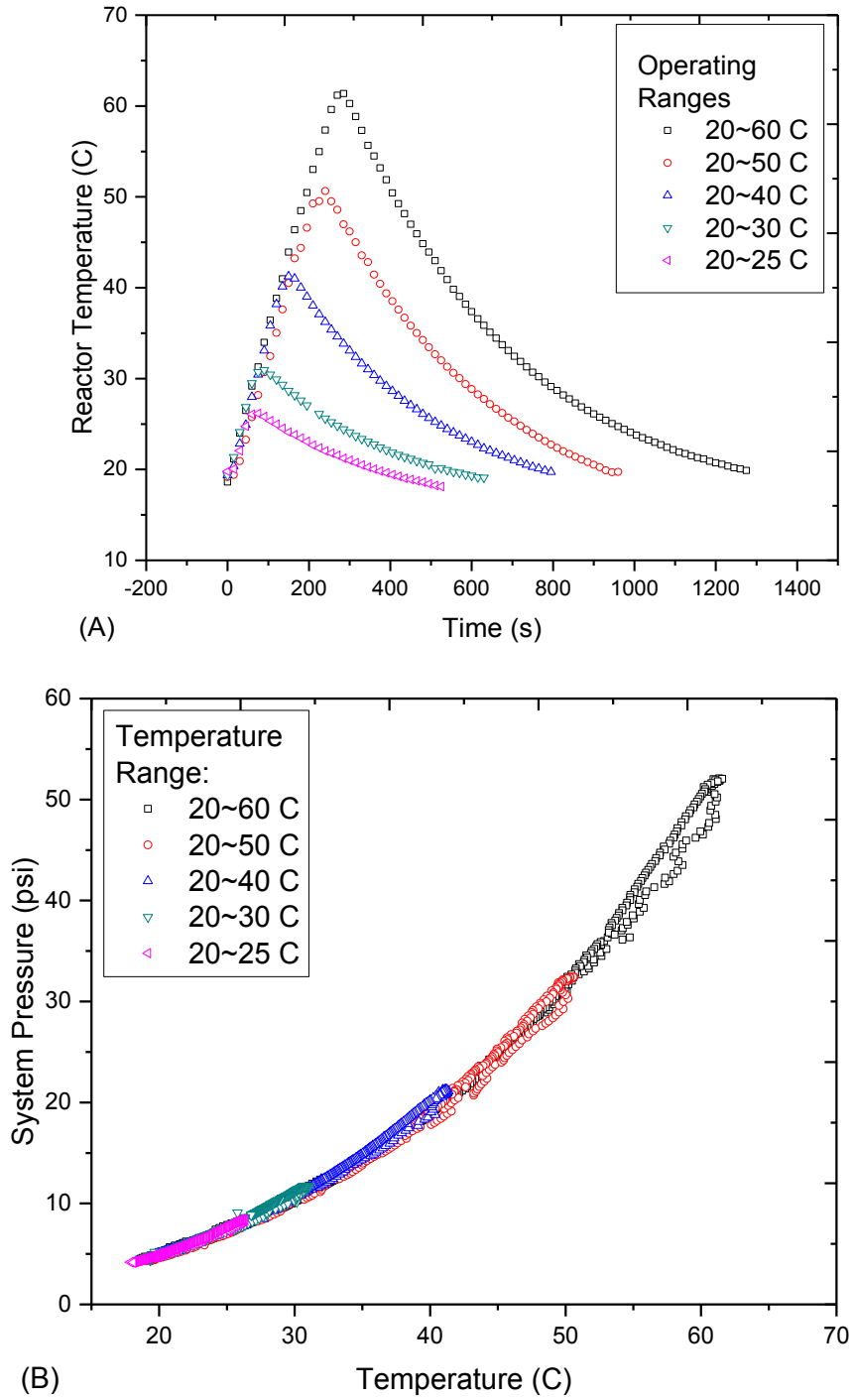
Figure 5. 6: Reactor operating temperature ranges (A) and corresponding system pressure (B) for actuation

5.3.3 System Pressure

Rise in reactor temperature causes the stored hydrogen in $LaNi_5$ to desorb. Dehydrogenation process is endothermic and the heat needed to sustain the process is to be supplied from external heat source. A part of the heat supplied is utilized to desorb hydrogen and the rest is lost in the ambient. Nevertheless, as the temperature increases hydrogen starts to desorb and flows into the actuator, which builds up pressure inside the cylinder. Figure 5.6 (B) shows the variation of system pressure with the changing operating temperature maintained at the reactor wall. From the figure it can be realized that desorption pressure rise is mostly smooth with negligible fluctuations with the increase in temperature. Return stroke, on the other hand, of the actuator is performed by natural convective cooling the reactor while system pressure response is observed to be erratic. During this return stroke hydrogen gets re-absorbed into the storage material and this process is dominated by three factors: temperature, spring force and friction between piston and cylinder. The reactor is cooled during the return stroke to promote absorption since absorption is an exothermic process. The heat of reaction during this stroke needs to be removed in order to ensure smooth actuation and to ensure re-absorption of hydrogen into the storage system. The spring force generates additional pressure on hydrogen to pressurize the gas atoms back into the lattice of $LaNi_5$, which may also cause disruption in the smooth absorption in the storage material. Friction between piston and cylinder wall also disrupts the gradual and smooth reduction of system pressure to some extent during the return stroke. Thus, even though the temperature is reduced gradually, system pressure tends to exhibit deviant behavior during the return stroke. The fluctuation in

system pressure during the return stroke appears to be noticeable at higher operating temperature ranges than at lower ranges within 40°C.

5.3.4 Actuation

The output of the system is measured in terms of stroke generated by the actuator, which is measured using displacement transducer. Pressurized hydrogen inside the cylinder is the driving force for actuation. Since the increase in system pressure is smooth with increasing reactor temperature, displacement was observed to be smooth during the forward strokes for all five operating ranges shown in Figure 5.7. System pressure was observed to be irregular during the return or compression stroke, which might have influenced by a number of factors discussed earlier. During this stroke the displacements generated by the actuator also appears to be irregular for most operating ranges. For all of the cases presented, once the peak temperature is reached, system pressure reaches the peak and starts to decline from that point onward. But for the displacement curve, the highest level of displacements sustain at that level for a while till the spring force overcome the net force due to friction and pressure inside the system. Evidently, the return stroke is not as smooth as the forward stroke due to pressure fluctuations observed with declining temperature. Nevertheless, the displacement curves show hysteresis in the strokes, which can be attributed to the friction associated with piston and cylinder and the hysteresis that exists in between the absorption and desorption processes.
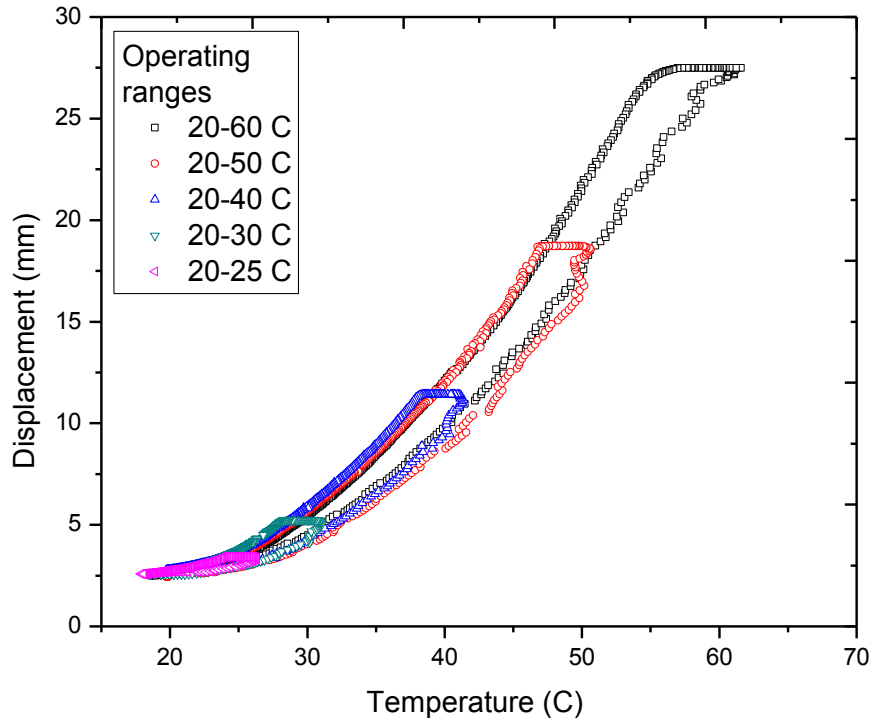
Figure 5. 7: Strokes generated at different operating temperature ranges

5.3.5 Effect of Temperature Ranges

System pressure was found to be aberrant during the return stroke, especially for the cases with higher upper limits of the operating ranges shown in Figure 5.6. At lower temperature ranges the pressure fluctuation was negligible and the actuation was comparatively smooth. A closer look at two such intermediate temperature ranges, such as 25-35°C and 25-45°C, were also exercised. Figure 5.8 shows a comparison of system behavior at the two intermediate operating ranges. The variation of temperature with time was mostly smooth and so was the system pressure. One may note that the displacement data at the transition from forward to return stroke does not display a flat plateau as observed for the first case. After reaching the initial peak the actuation rod pulls back and then goes back up again before it starts to pull back gradually. This transitional behavior

is almost negligible since it occurs within a fraction of a millimeter but it may become significant when higher displacement is attained by applying very high temperature ranges. This tendency may have root cause to the dynamic behavior of the sorption process associated with the storage material. Heat generated during absorption increases the temperature of the reactor, which may also trigger desorption process in the heated zone within the reactor by providing the heat of reaction. The system may always find dynamic balancing of the sorption process whose direction is always dominated by the external influences that are driving the process. This transient behavior can only be seen during the stroke reversal. Another important point to note that the fluctuations in displacement are realized when it is observed from the temperature frame of reference. When time is the frame of reference, those fluctuations in system pressure and displacement diminish, which refers to smooth operation of the system over time.
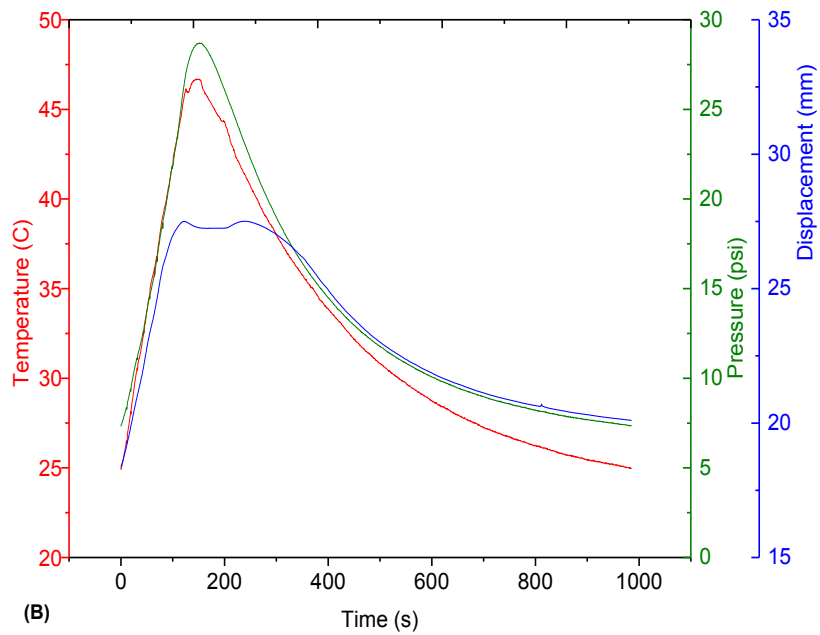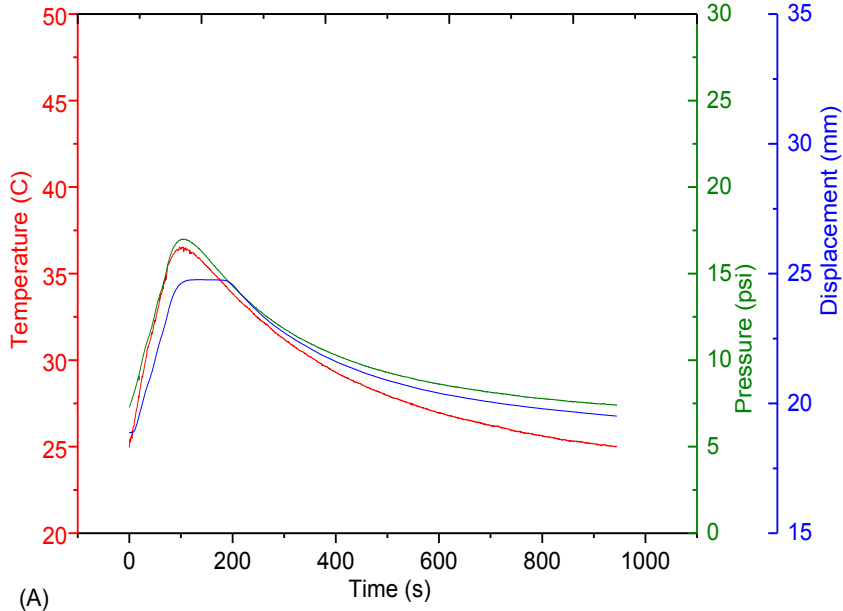
Figure 5. 8: Actuation during operating temperature of (A) 25~35 ^{o}C; (B) 25~45 ^{o}C

5.3.6 Periodic Operation

The actuator presented in this study can also be operated in periodic operation with smooth and consistent performance. Figure 5.9 shows repeated forward and reverse strokes generated in the actuator for a temperature range of approximately 25 to 40°C.

Average electric power input to the heater per cycle is recorded to be about 15.65 watts, a part of which converts to heat used in raising the temperature of the reactor. The percentage controller which supplies power to the heater, turns on and off automatically at some random intervals programmed by the manufacturer. So the duration for which the switch is on does not reflect the actual duration over which power is actually supplied. Hence, once the targeted upper temperature limit of the operating range is reached, power supply is switched off. The entire period over which the operating switch is on is shown relative to the other system parameters in the following figure. While the switch is on temperature rises gradually and so does the pressure of the system. Displacement generated in the actuation rod tends to follow the pressure curve with a flat peak during the reversal of the stroke. Overall the actuation is observed to be smooth even for repeated cycles from time frame of reference.
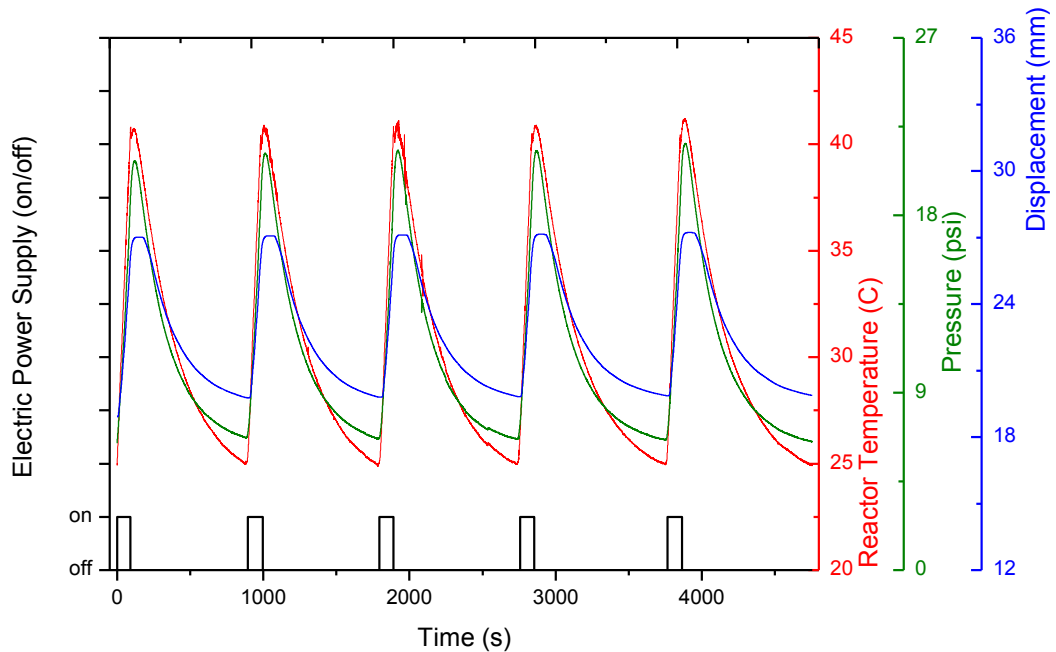
Figure 5. 9: Periodic operation of Metal Hydride integrated actuator system

5.4   Comparison

The actuator under investigation is compared with wide range of actuators from previous studies [101], shown in Figure 5.10, in terms of system stress and strain. The stress for this system is defined as the pressure generated inside the system during desorption of hydrogen. The strain for the current system is defined as the ratio of displacement generated by the system to the maximum possible linear stroke which can be generated by the actuator. Since the system operating temperature range can be varied, the performance region may actually vary in accordance with the applied operating temperature. In the figure the white rectangular area represents the operating temperature range of 25-40°C. Increasing the upper limit of the operating range dramatically increases the application region in the map shown. The patterned rectangular area represents the entire operating region when 20-60°C operating temperature is applied to the current system. It is evident that the system proposed can mimic biological muscle in terms of stress and strain generated in the system by regulating temperature. Nevertheless, the application region of this system is not necessarily limited by the area shown in the graph. Based on the requirement and by eliminating unnecessary volume in the system, application stress region can be extended as high as the region covered by hydraulic actuators. High pressure hydrides such as $Ca_{0.6}Mm_{0.4}Ni_5$ can be used to store hydrogen for the actuator. The stress produced by the system can exceed the current version of the actuator that uses $LaNi_5$. Actuator stress can be as high as 24 MPa [132] if such high pressure hydride is used. Also, the displacement generated in this system is not limited by the stretching or bending limits of materials, which is the case for most other actuators in focus. Hence, the actuator presented can be more reliable and economic from the

perspective of longer term operation. Like any other mechanical system, this may need

some periodic maintenance which can obviously be offset by the lower initial cost and

consistent performance.
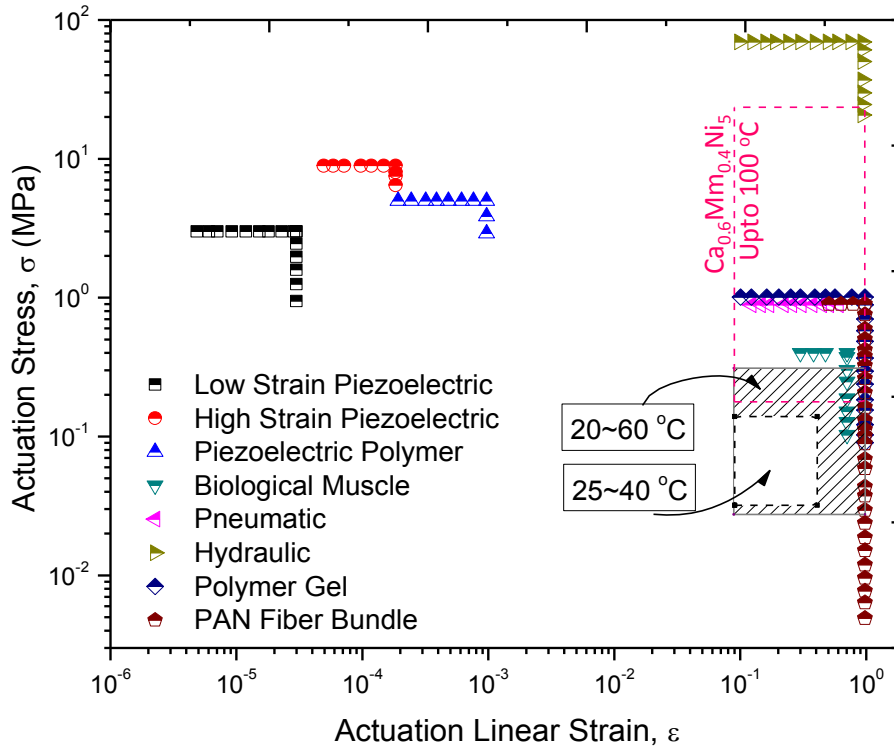
Figure 5. 10: Other actuator devices [101] vs. device under investigation. The white rectangular and the patterned rectangular area represents 25~40 $^{\circ}$C and 20~60 $^{\circ}$C operating region.

CHAPTER 6: Actuator Performance & Uncertainty Analysis

By analyzing the all possible energy inputs and work outputs of the system, a series of mathematical models are presented to account for all system inputs and outputs in this chapter. The objective of this chapter is to quantify the thermodynamic efficiency of the system along with the propagated uncertainty in the results. The model consists of a number of preliminary measurements, which are subjected to error or inaccuracies outlined by the manufacturers of measuring probes and devices. The values of physical properties used in the model are well established but some estimation were made in cases like convective heat transfer coefficient of the laboratory space to account for heat loss. Hence, all the parameters have a certain degree of experimental inaccuracies, which would propagate to the final result of calculated efficiency of the system. To account for the inaccuracy in the final results, a distribution propagation method was used in developing a MATLAB script for uncertainty quantification. This chapter describes the formulation of efficiency for the system and quantification of associated uncertainty using a statistical method known as Monte Carlo experiments.

6.1 System Inputs and Outputs

Metal hydride integrated actuator system is driven solely by heat input, which transform into displacement work done by the actuator and compression work done by the spring. While the reactor is heated, desorbed hydrogen causes displacement in the actuation rod, which may seem to be the only source of work done by this system. At the end of the desorption cycle, when the heat supplied to the reactor shuts off, the spring mounted on the actuation rod pushes the gas back to the reactor. Hence, over a complete cycle of desorption and re-absorption of hydrogen into the metal hydride reactor, work

done by the system can be estimated by accounting for the displacement work and spring work over a complete cycle. The input to the system is basically heat. A part of the heat input is lost through the insulation while the other part flows into the reactor to drive the desorption process. Thus, the efficiency of the system is formulated using Equation 6.1 through 6.6, which account for displacement work (W_d) and spring energy (W_{sp}) of the actuator as system outputs; and reaction enthalpy (Q_{reac}) and heat loss (Q_{loss}) as system inputs. The ratio of output to input quantifies the efficiency of the system as shown in equation 6.1.

$$\eta = \frac{W_d + W_{sp}}{Q_{reac} + Q_{loss}}$$

(6.1)

The work done by the system has two segments, which are mechanical work by displacement of the actuation rod and compression work done by the spring to reabsorb hydrogen gas after the end of the desorption process. Work done by the actuator during desorption cycle (W_d) was calculated using the pressure and volume change during the actuation process using the following modified state equation. Here, pressure (P) and volume (V) are both time dependent quantities, which were acquired experimentally as a function of time. System pressure was recorded directly using a pressure transducer every half seconds. The displacement of the actuation rod was recorded using a LVDT, which was multiplied with the cross-sectional area of the piston to quantify the cylinder volume. The actuator displacement was also recorded every half seconds using a personal data acquisition system.   So, the state equation was modified to account for the time dependent pressure and velocity data and calculate the work done by the system as shown in the Equation 6.2.

$$W_d = \int_{state\ 0}^{state\ 1} Pdv = \int_{t0}^{t1} p(t)\frac{dV(t)}{dt}dt \qquad (6.2)$$

Then end of the heating/desorption cycle demarcates the beginning of the absorption cycle. The stored spring energy is then applied on the previously desorbed hydrogen gas in the system, which pushes them back into the storage martial through an exothermic reaction. Hence, the system also performs compressing hydrogen at the end of desorption or actuation process which can be considered to be the work done by the system and quantified by the spring energy gain at the end of desorption process. Equation 6.3 was used to quantify the compression work, W_{sp}, performed on the hydrogen to absorb them back into the storage material. The spring constant, K, was specified by the manufacturer, which is 31 [lbs/inch] or 5.43 [N/mm], and the displacement x was recorded by the displacement transducer. During the return stroke a small portion of the spring energy is also spent to overcome the friction associated with the piston and cylinder. The lost energy over a complete cycle is the system hysteresis.

$$W_{sp} = \frac{1}{2}kx^2 \qquad (6.3)$$

The heat input to the system has two parts: heat of reaction (Q_r) and heat lost (Q_{loss}) in the ambient. The heat of reaction can be quantified by calculating the amount of hydrogen desorbed in moles, using gas law, and multiplying that by the reaction enthalpy (ΔH) in kJ/mole as shown in Equation 6.4. Where, P, V, Z (1.008), R and T are pressure, volume, compressibility factor, gas constant and temperature respectively; 0 ad 1 represents the initial and final states of the process.

$$Q_r = \Delta H \frac{P_1 V_1 - P_0 V_0}{ZRT} \qquad (6.4)$$

A part of the heat input is lost in the atmosphere even though the reactor was instated during the desorption process. Equation 6.5 was used to quantify the heat loss through the insulation of the reactor. The ambient temperature T_o is constant and the inner surface temperature of the industrial pipe insulation was recorded using thermocouple throughout the cycle. To calculate the thermal conductance term (UA), Equation 6.6 was employed where it was assumed that contact resistance is very small and hence negligible. The details on the parameters used in calculating heat loss is listen in Table 6.1.

$$\dot{Q}_{loss} = UA(T_i - T_o) \tag{6.5}$$

$$\frac{1}{UA} = \frac{1}{2\pi L}\left[\frac{ln\left(\frac{r_o}{r_i}\right)}{k_{insl}} + \frac{1}{r_o h_{rm}}\right] \tag{6.6}$$
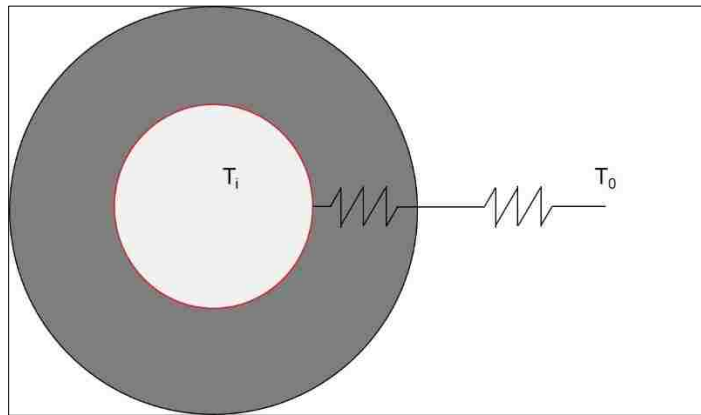
Figure 6. 1: Thermal circuit to estimate heat loss

Table 6. 1: Parameters used for Heat loss calculation

Parameters	Value	Unit
Length of the reactor, L	0.1778	[m]
Outer to Inner radius ration, r_o/ r_i	2.1429	[-]
Outer radius of the insulation, r_o	0.0238	[m]
Conductivity of polyethylene foam insulation, K_{insl}	0.25	[W/(m.K)]
Natural convection heat transfer coefficient, h_{rm}	5	[W/(m^2.K)]

The displacement work performed by the actuation rod was calculated directly from the experimental pressure vs volume data shown in Figure 6.2. The graph shows all such data at different operating temperature ranges. The end of desorption phase or forward stroke is marked on the graph. For each temperature range the area underneath the forward stroke curve represents the displacement work done by the actuation rod. The procedure described in the previous section has been applied to determine the area underneath the forward and return stroke curve using Equation 6.2. The areas underneath the curves in Figure 6.3 represent the work done by the actuator in Joules during desorption (left column) and absorption (right column) cycles at different operating temperatures. The Difference between desorption and absorption work is the amount of hysteresis that the system have for corresponding temperature range. Nevertheless, the potential energy gained by the spring at the end of the forward stroke would be spent partly to overcome friction and mostly to recompress hydrogen back to hydride phase. Hence, the spring work was calculated using Equation 6.3 that quantifies spring energy based on the maximum displacement achieved by the spring at the end of desorption cycle. The actuator is basically a thermally driven actuation system, which requires heat as the only input source. The supplied heat is the source for reaction enthalpy since hydrogen desorption is an exothermic reaction. Even though the reactor was well insulated with standard pipe insulation, a tiny fraction of the heat will always be lost since there is no such material known as perfect insulator. Table 6.2 summarizes the quantified performance parameters of the actuator.
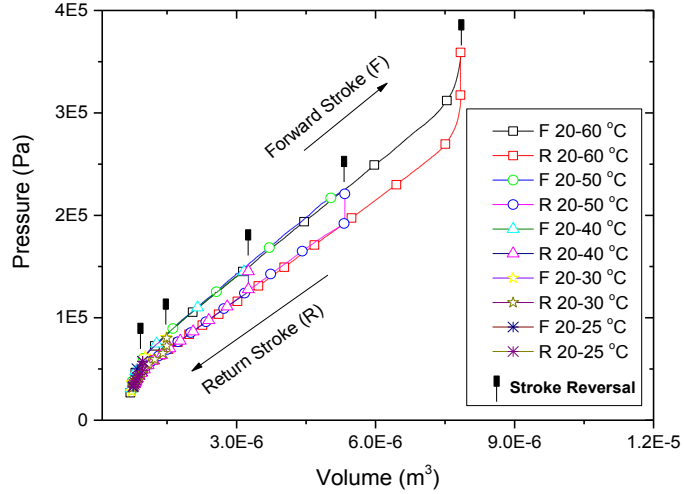
Figure 6. 2: Experimental data for pressure and volume change in the actuator
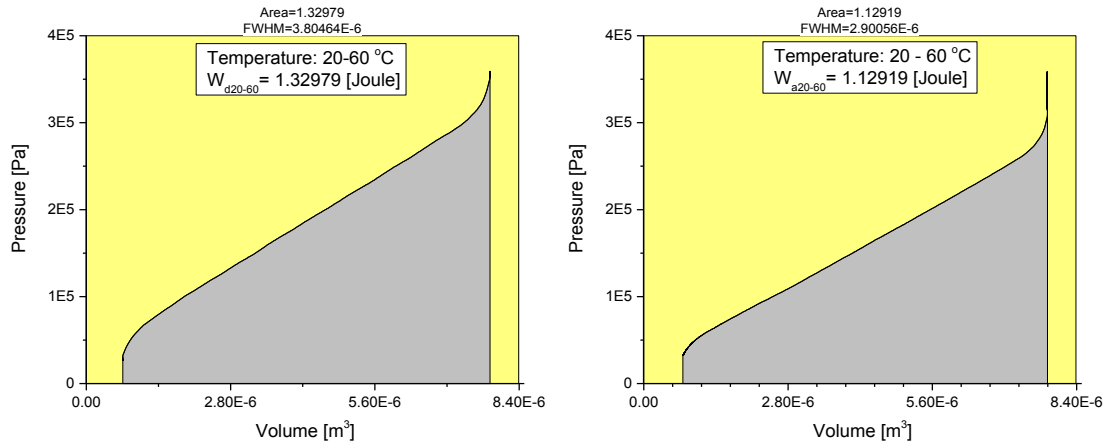
Figure 6. 3: Work done during desorption (left) and absorption (right) at 20-60 °C
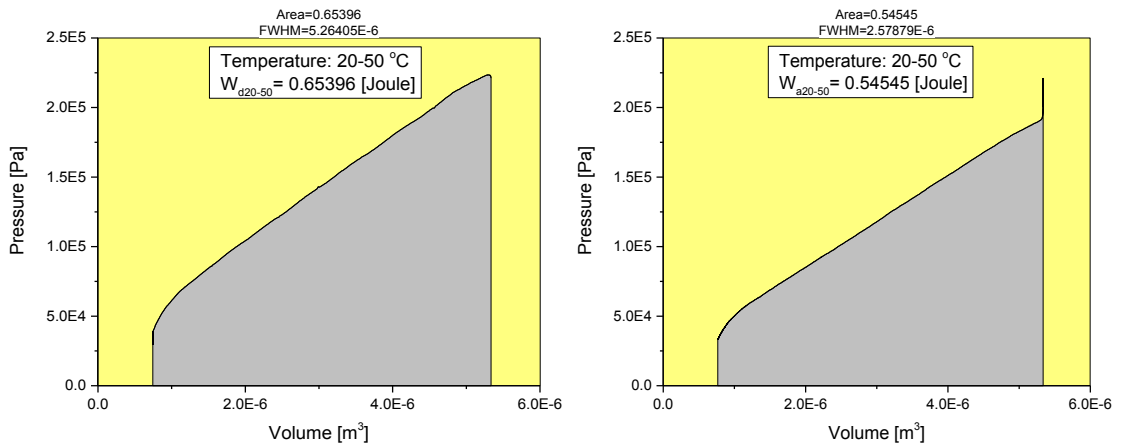
Figure 6. 4: Work done during desorption (left) and absorption (right) at 20-50 °C
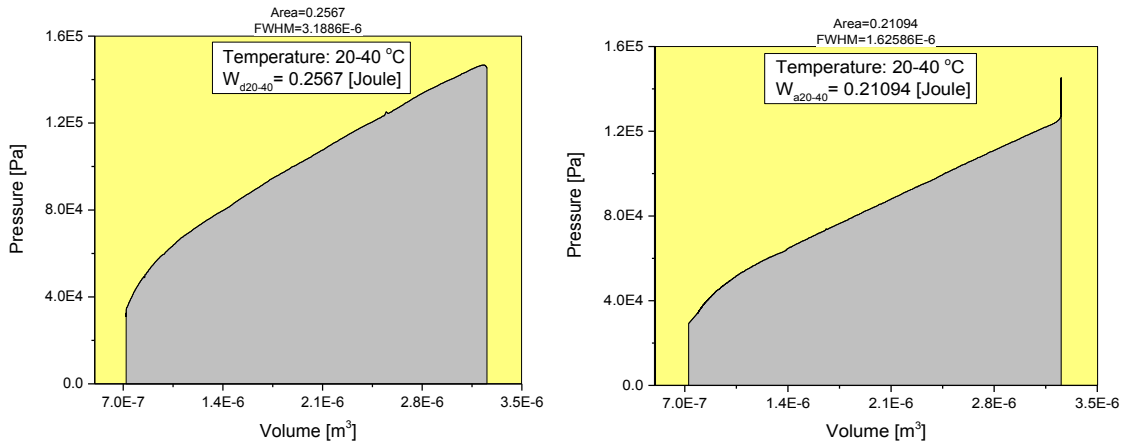
Figure 6. 5: Work done during desorption (left) and absorption (right) at 20-40 ^oC
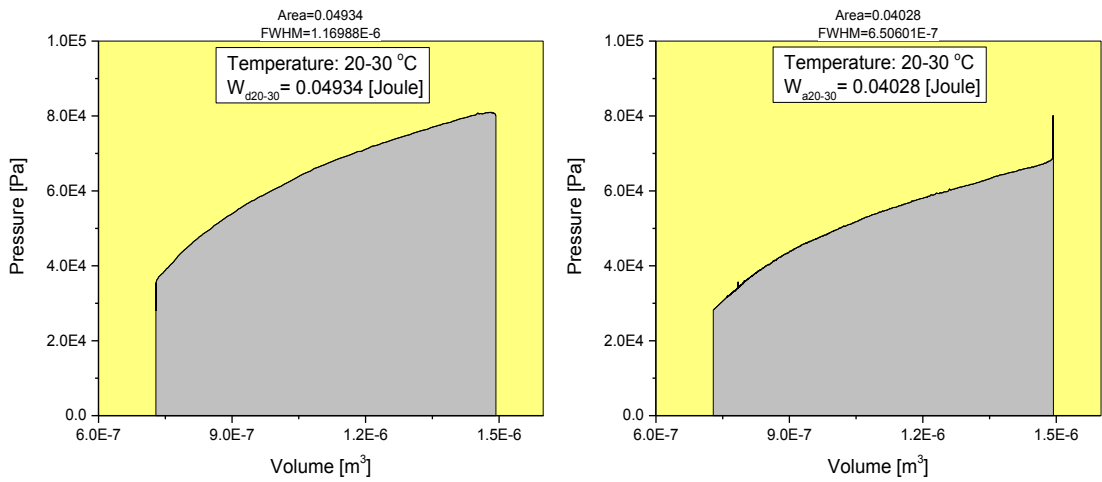
Figure 6. 6: Work done during desorption (left) and absorption (right) at 20-30 ^oC
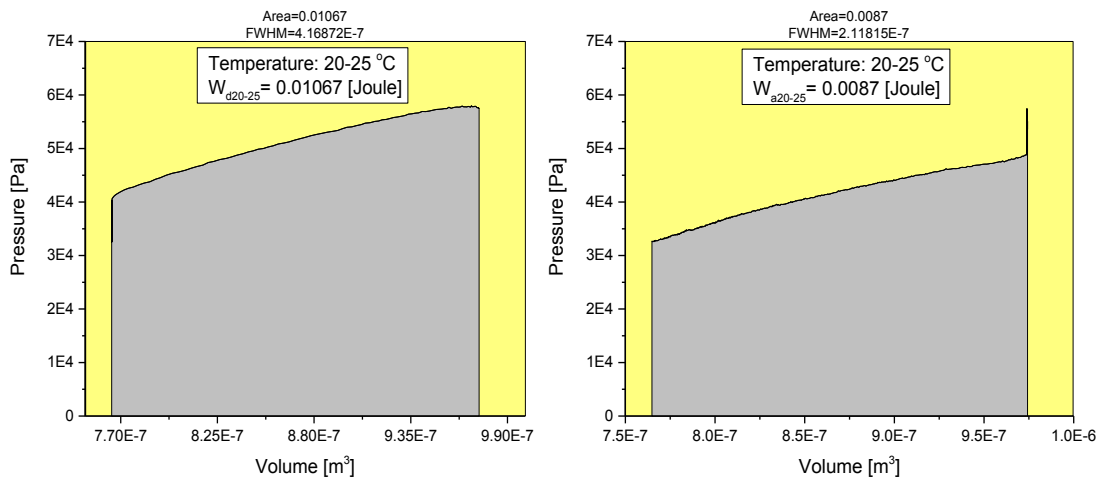
Figure 6. 7: Work done during desorption (left) and absorption (right) at 20-25 ^oC

100

Table 6. 2: System input-output summary

Temp. °C	Enthalpy (J)	Heat Loss (J)	Displacement Work, W_d (J)	Spring Energy (J)	Absorption Work, W_a (J)	Actuator Hysteresis (J)
20-60	27.2440	0.9059	1.3298	2.0511	1.1292	0.2006
20-50	11.3061	0.7150	0.6540	0.9518	0.5455	0.1085
20-40	4.4070	0.4842	0.2567	0.3541	0.2109	0.0458
20-30	0.9701	0.2442	0.0493	0.0745	0.0403	0.0091
20-25	0.3048	0.1261	0.0107	0.0317	0.0087	0.0020

6.2   System Performance

For a thermally driven metal hydride actuator, heat is the only input that drives the system. The work done by the system would comprises of the displacement work (PdV during the forward stroke). The work done (PdV at return stroke) during the return stroke is defined as the absorption work, which is a fraction of spring energy. The difference between work done during forward stroke (displacement work) and return stroke (absorption work) is the hysteresis of the system.   Heat input to the system comprises of the heat of reaction and heat loss. Figure 6.4 shows relative percentage of the system energy in pie chart for different temperature ranges. For lower temperature ranges the relative heat loss is very high since a significant portion of the energy is spent to raise the temperature of the system while an insignificant portion of useful work is actually done. With the increasing operating temperature, relative heat loss decreases as significant portion of the heat is spent to actually perfor the displacement work done by the actuator. Nevertheless, the relative amount of displacement work and spring energy shows the highest relative percentage at operating temperature of 20-50 °C, which is the indication of this range being the most efficient operating range.

The hysteresis of the actuator as a fraction of total system output is shown in Figure 6.5. Even though actuator shows very low hysteresis at lower operating temperature rage such as 20 to 25 ^{o}C, it increases abruptly with further increase to 20 to 30 ^{o}C. The maximum hysteresis was observed at 20-40 ^{o}C, which gradually decreased to about 6 % at the higher temperature range. Nevertheless, the actuator is expected to perform best for ranges within 40, 50 or 60 ^{o}C within which the hysteresis is within 6 to 8 % of the output of the system.

One important aspect of the actuator is its ability of generate strain with the applied stress. For a piston-cylinder type actuator, the strain is defined as the ration of displacement generated to the maximum possible displacement. The stress of the actuator is the pressure inside the cylinder that is causing the displacement. Figure 6.6 shows the stress strain behavior of the actuator at different temperature ranges. The overall behavior is observed to be linear, which is highly desirable from practical point of view as linear actuators need simpler control schemes for automation.
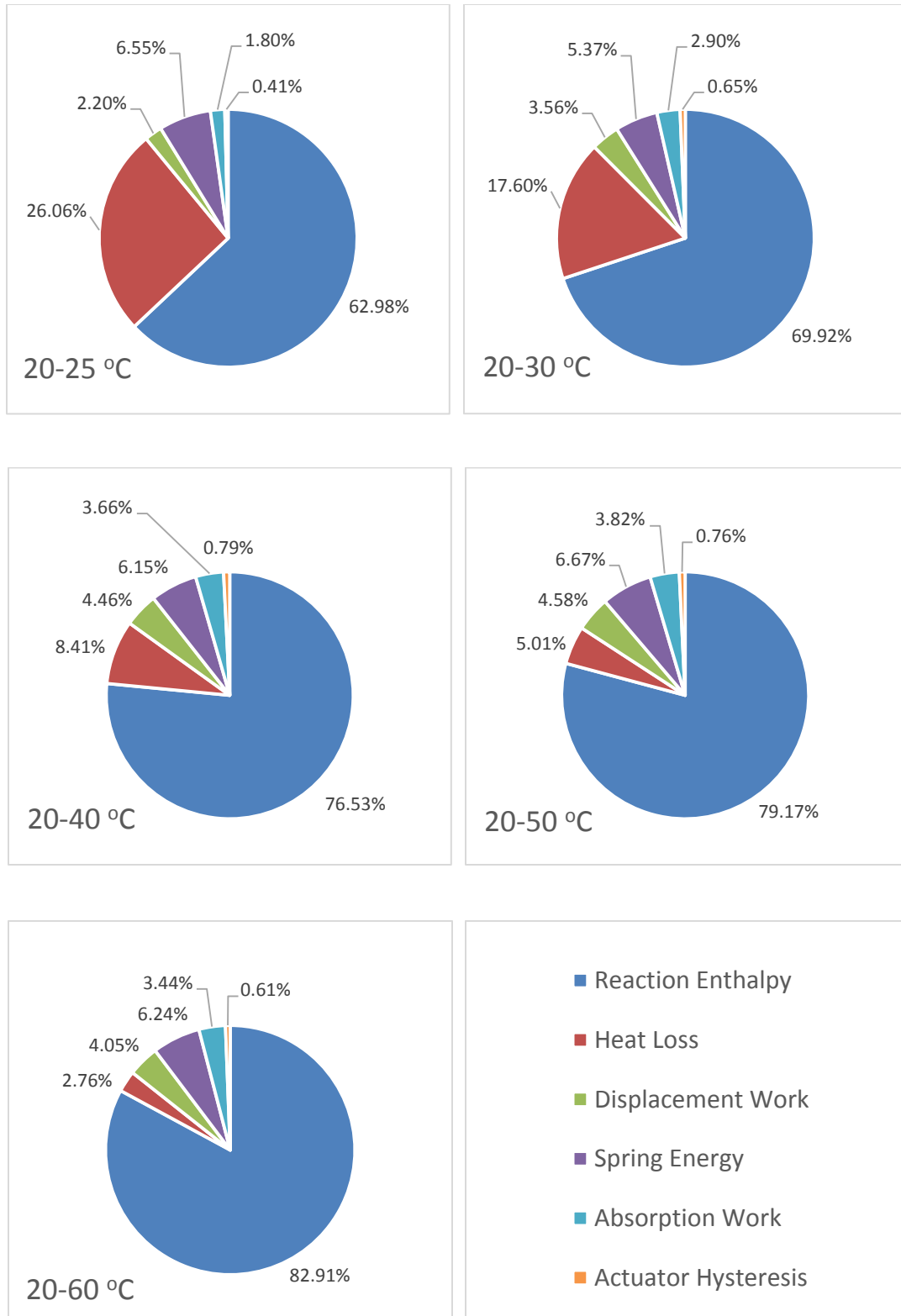
Figure 6. 8: Relative energy distribution
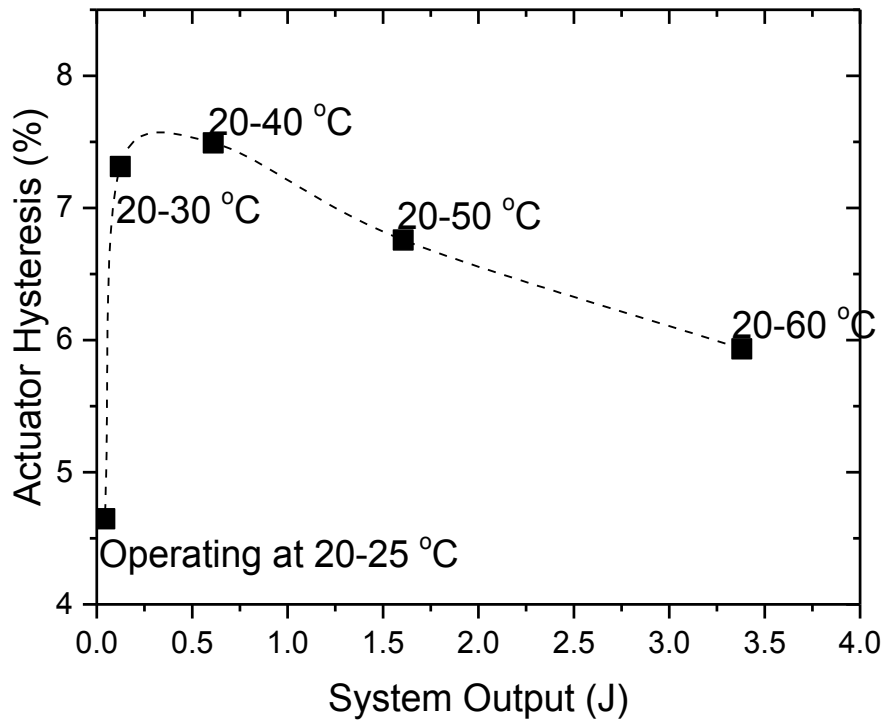
Figure 6. 9: Actuator hysteresis as a function of total system output
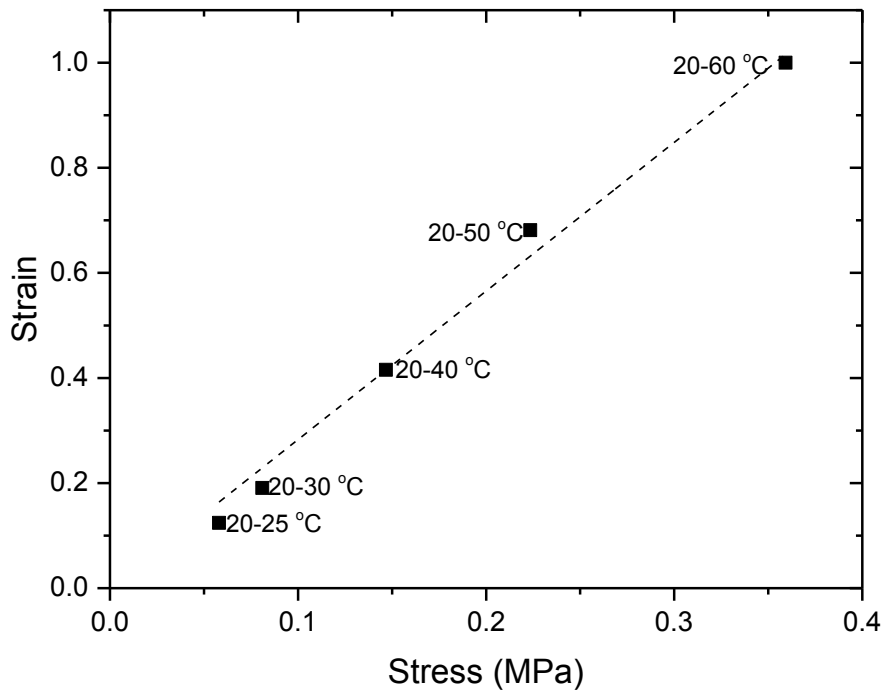
Figure 6. 10: Actuator stress-strain behavior

6.3   Uncertainty Analysis - Monte Carlo Experiment

In reporting experimental results, error and uncertainty play a vital role in determining the reliability of the results. To calculate system efficiency, a number of experimentally obtained inputs were used, which were subjected to inaccuracies due to the inaccuracies associated with the measuring probes as prescribed by the manufacturers. Errors of the primary measurements that propagate to the final result, have to be determined in order to determine the reliability of the final results and conclusion deduced from it. In this section Monte Carlo method/experiment will be discussed and implemented for determining the relative uncertainty associated with the calculated efficiency of the thermally driven metal hydride actuator.

Measurand (a quantity intended to be measured) or Result (y) as a function of input sources $(x_1, x_2, x_3...x_n)$ can be written as $y = f(x_1, x_2, x_3.... x_n)$. The uncertainly associated with the measurand originates in the measured input sources (x) in the primary investigation. Law of propagation of uncertainty (LPU) relies on the previously determined uncertainty associated with the measurement and uses that information to calculate the uncertainty that may propagate in the result. This approach accounts for the maximum deviations in the primary measurements and calculate the deviation in the final result using root of the sum of the squares (RSS) method. This method does not reflect actual or realistic uncertainty associated with the final result since all the extreme limits of the primary measurements never occur simultaneously. Hence, in such process a certain amount of information is always lost and the uncertainty in the final result is over inflated and unrealistic, which increases cost of fabrication or manufacturing of the system for practical reasons.

Monte Carlo (MC) method for uncertainty quantification, propagates entire distribution of the source data to calculate measurand (efficiency, in this case). Hence, from the distribution of the measurand, more reliable and complete information regarding uncertainty associated with the measurand can be determined. The estimation of a measurand in Monte Carlo method requires a certain number trials to be performed. This minimum number of trials (M) is given as

$$M > \frac{10^4}{1-p} \qquad (6.7)$$

For 95% confidence interval p=0.95 and M>200,000. Thus, minimum of 200,000 trials need to be performed with appropriate input distributions to estimate the result. The simulation is performed in five steps:

- Identification of measurand (efficiency, in this case) and input quantities (displacement work, spring energy, reaction enthalpy, heat loss).
- Formation of model equation (Equation 6.1)
- Appropriate probability density function for reconstructing randomized source data within the limits. In this case normally distributed random numbers for each input quantities were generated within the limits, using MATLAB script.
- Apply Monte Carlo experiment/method using the custom script developed for determining efficiency and associated uncertainties of the metal hydride actuator.
- Tabulate results for 95% confidence interval (CI) in accordance with ISO/IEC Guide 98-3: Guide to the expression of uncertainty in measurement (GUM), with the following information:

- o Result

- o Standard Deviation

- o Low End Point for 95% CI

- o High End Point for 95% CI

6.4 Efficiency and Uncertainty

In quantifying efficiency of the actuator, Monte Carlo method was applied. Instead of generating distribution for every single primary measurement involved, the variables were reduced to four major categories as seen in Equation 6.1. The extreme bounds of this four individual quantities (W_d, W_{sp}, Q_{reac} and Q_{loss}) were determined using Law of uncertainty propagation formula as known as root of sum of squares (RSS). Since this method accounts for the extreme limits of errors of each individual sources, the extreme bounds for all four major categories can be determined using RSS method. Using the expected values and extreme bounds for all four quantities in the Equation 6.1, random numbers can be generated using Gaussian/normal distribution using MATLAB script. These distributions are then propagated through the model for efficiency (Equation 6.1) using the Monte Carlo method, which generates a normally distributed results for quantification of efficiency. From the resulting frequency distribution of efficiency mean, standard deviation can be easily determined and relative uncertainty can be calculated. Figure 6.7 shows frequency distribution plot for the four parameters of Equation 6.1, which were propagated through the efficiency model and resulting distribution of efficiency for the metal hydride actuator is shown in Figure 6.8. From the resultant distribution the average efficiency was found to be 0.1316 or 13.36% with standard

deviation of 0.0017, which can be translated to relative uncertainty of 2.4735% as summarized in Table 6.3.
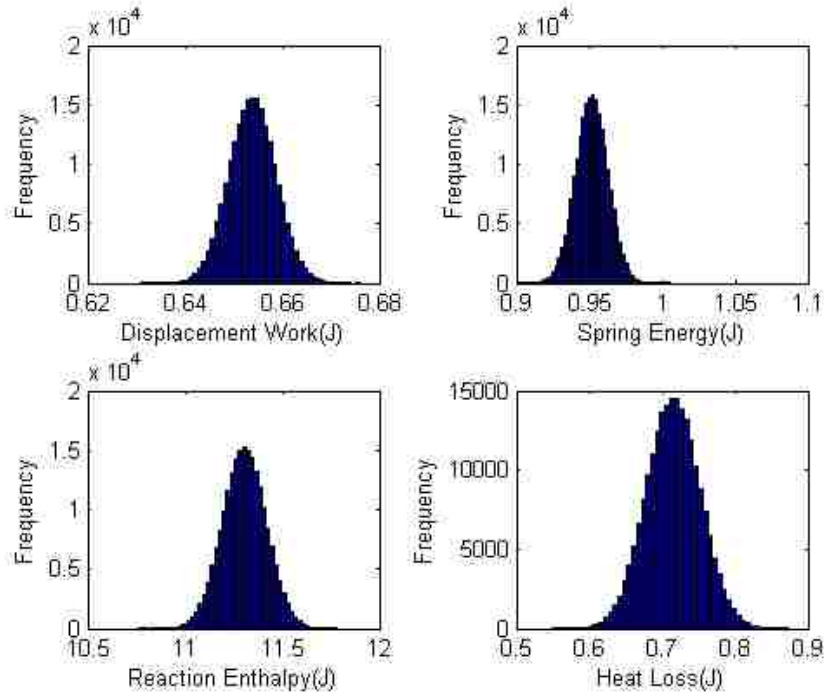

Figure 6. 11: Frequency distribution of four major parameters for quantifying efficiency for operating temperature of 20-50 ^{o}C
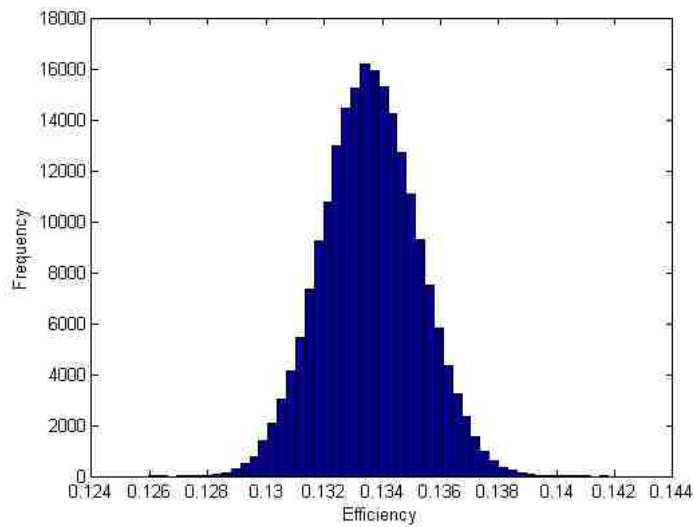
Figure 6. 12: Frequency distribution of absolute efficiency for operating temperature of 20-50 ^{o}C using Monte Carlo experiment

Table 6. 3: MC experiment for operating temperature of 20-50 ^{o}C

Efficiency (absolute)	Standard Deviation	Low End Point for 95% CI	High End Point for 95% CI	Efficiency %	Relative Uncertainty %
0.1336	0.0017	0.1265	0.1418	13.36	2.4735

Monte Carlo experiment was applied for all five temperature ranges. System efficiencies along with associated uncertainties were determined using this method. The Script developed to apply Monte Carlo method is attached in Appendix A. The frequency distribution graphs of the input quantities and resultant efficiencies are also attached in Appendix B along with tables summarizing results and relevant statistics. In conclusion, all the efficiencies and associated relative uncertainties are summarized in Table 6.4.

Table 6. 4: Efficiency and uncertainty using Monte Carlo experiment

Operating Temperature Range ^{o}C	Efficiency %	Relative Uncertainty %
20-60	12.01	2.4721
20-50	13.36	2.4735
20-40	12.49	2.5385
20-30	10.2	3.0232
20-25	9.84	3.7894

The bar graphs in Figure 6.9 shows the overall efficiency of the system for each operating temperate range. The system is obviously less efficient while operating at low temperature ranges due to relatively higher percentage of heat loss and lower percentage of useful work output. At a temperature range of 20-50 ^{o}C, this system operates most efficiently while attaining the maximum relative percentage of displacement work done by the system with minimum relative amount of heat loss. Analyzing performance of this metal hydride actuator, it can be concluded that the system performs best at 20-50 ^{o}C

with a maximum displacement of 20 mm. At lower temperature ranges, heat loss is dominant with insignificant amount of useful work done by the system. At the highest temperature range 20-60 $^{\circ}$C, relatively larger portion of the input energy is spent for desorbing more hydrogen from the storage that generates increased system pressure. But at this point, the maximum limit of the stroke is reached and thus a lower relative percentage of displacement work is done. This leads to a reduction in overall system efficiency.

The efficiency of metal hydride actuator was found to be in the range of approximately 9 to 14% with relative uncertainty of about 2.4 to 3.8% using Monte Carlo experiment. Figure 6.10 shows the efficiency of the system as a function of the maximum displacement and strain attainable at corresponding temperature ranges. As mentioned earlier, strain for this actuator is defined as the ratio of displacement to the stroke length of the actuator, which is the highest displacement attainable. From the plot it can be concluded that the system performs most efficiently around a maximum temperature of 50 $^{\circ}$C, generating 0.7 strain approximately.
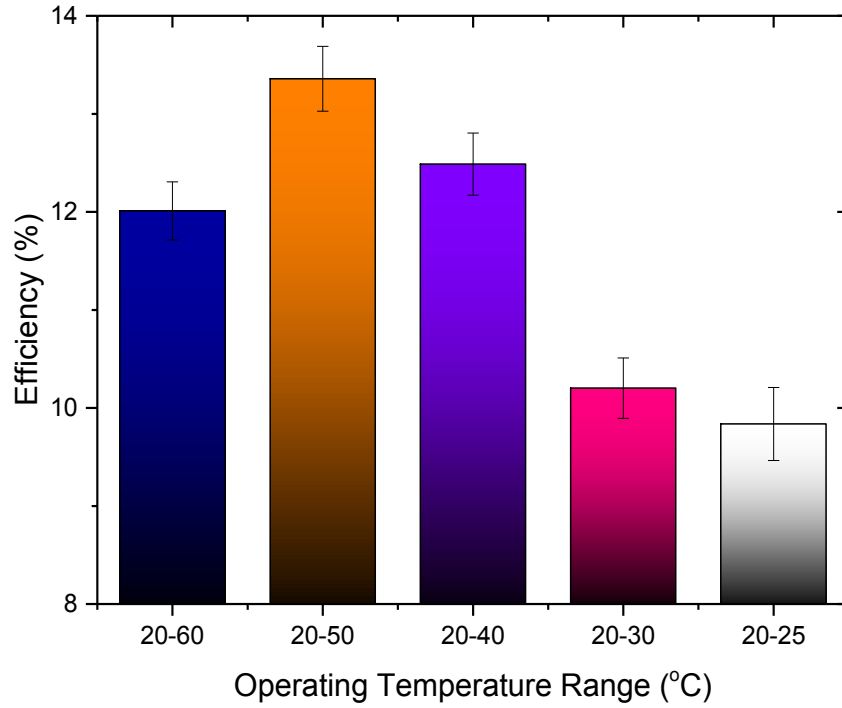
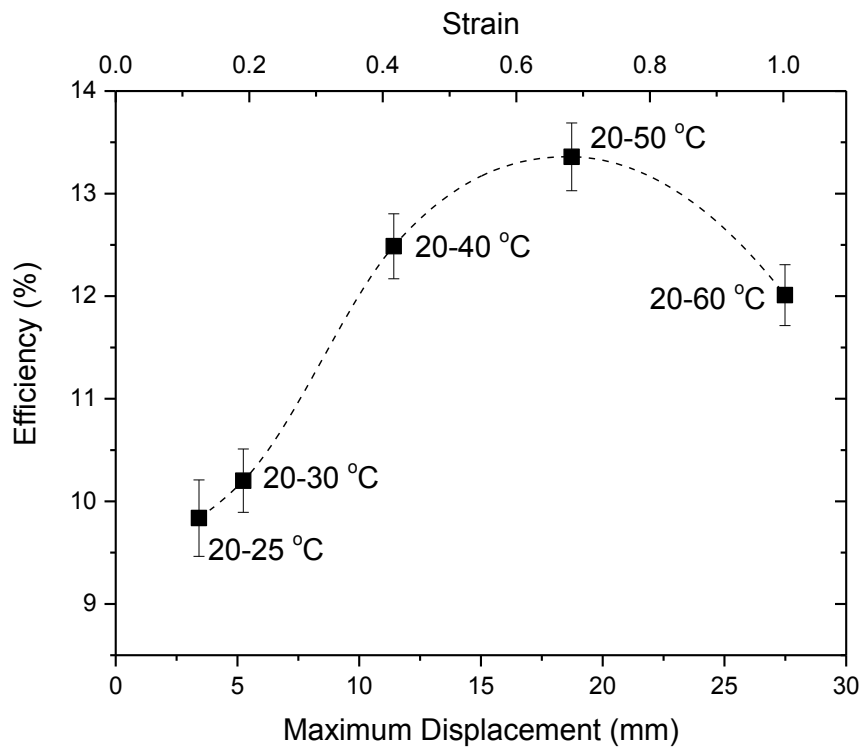**Figure 6. 13: System efficiency at various operating temperatures**

Figure 6. 14: System efficiency as a function of maximum displacement and strain

CHAPTER 7: Concluding Remarks and Future Direction

Metal hydrides have been studied, proposed and demonstrated for numerous applications as discussed in this article. The hydride materials originally received the attention from the research community because of their ability to store hydrogen at extraordinarily high density levels. It is this last quality, the storage capacity of metal hydrides, which had been coupled with most of the engineering systems proposed to generate desired output. Utilizing the heat evolved and absorbed during the reaction process, thermal systems such refrigerator, heat pump, heat storage were also demonstrated to perform at satisfactory level using laboratory scale models. In some cases, the physical properties of the materials were utilized in designing applications such as sensors. Onboard vehicular storage at higher gravimetric density is the ultimate problem that researchers will have to solve for the implementation of hydrogen as an alternative fuel. Besides, technology implementation and commercialization of such technology will require applicable codes and safety standards that need to be addressed once metal hydrides find its application in hydrogen powered systems in the future.

Comparing the two sorption cases, absorption and desorption, desorption reaction is realized to be faster than absorption at the operating temperatures used for this study. The process of hydrogen extraction can be slower if it is performed at a lower temperature than the case presented here. From this perspective it is hard to argue which process is slower or faster since the applicable temperatures for these processes are in the opposite extremes on the scale. If both the processes could be performed at same experimental boundary conditions such as temperature and pressure, more realistic conclusion could have been made regarding the pace of these to processes. Nevertheless, the model

presented for simulation agrees very well with the experimental results and can further be implemented for designing new hydride based application.

A successful demonstration has been made for the feasibility of metal hydride embedded actuator system, which can practically be implemented in industrial automation, robotics etc. Since hydrogen storage and extraction process are dominated by thermal energy extraction and supply respectively, Copper encapsulation and further compaction of the particles into pellets improves the conductivity of the storage material. Combination of the two thermal conductivity enhancement processes should greatly reduce the energy consumption to drive the system. Such efficient and compact energy source integrated to an actuator generating force/displacement for cyclic operation may actually hold pragmatic applications in research and industry. Different ranges of operating temperature can be applied depending on the actuation requirement. Strain generated by the actuator was found to be linear with the stress applied by desorbing hydrogen. This would simplify the integration of such actuator to an automatic control system. Temperature controlled operating procedure showed mostly steady pressure and displacement response during the forward stroke with respect to time. During return stroke the reduction of system pressure and displacement were observed to have fluctuations while observed from temperature frame of reference. But when the actuation process as well as system dependent variables such as pressure and displacement were observed from time frame of reference, proposed actuator demonstrated steady and smooth actuation even for repeated cycles. The stress vs. strain behavior of the system was very comparable to biological muscles, which makes the system a potential

candidate for application in biomimetic systems. Further investigation can be focused on improvement of cycle time from hydrogenation and actuation point of view.

The efficiency analysis of thermally driven metal hydride actuator showed very promising future for such concept. For worst case scenario, the efficiency turned out to be about 9.84%, which is still very impressive considering the efficiency of other soft robotic actuators. Braided pneumatic artificial muscles, for example, was found to have less than 1% first law efficiency [71] while coupled with metal hydride hydrogen storage system. For this system, it may be possible to minimize system loss and improve the system efficiency as high as approximately 54% or higher by integrating a heat recovery system. Since the hydriding and dehydriding process is reversible and involves evolution and absorption of heat respectively, a closed loop system can be created where heat evolved during absorption reaction will be stored and reused for subsequent cycle. In this way the system may partially compensate for its energy input requirement by recycling the waste heat. This may help design an actuator with efficiency as high as 54%, as projected, for which the relative energy distribution chart would be like Figure 7.1. This distribution was generated based on the assumption that 80% of the heat evolved during absorption reaction, would be recovered by integrating a heat recovery system.

Finally, dampers are not designed with flammable gas, which may explode in cases where the damper are subjected to high impact force. The extreme heat and compression may cause the gas to reach its combustion temperature during the operation. Neutral/inert gases are usually used for this purpose, which may still not be a cost effective concept to implement for general purpose. That is why, air is the best choice for any gas/pneumatic dampers since it is absolutely free from economic point of view and is totally free of fire

114

hazard. Integrating metal hydride to a damping system will unnecessarily complicate the system with increased cost and it may not serve the purpose of damping after all.
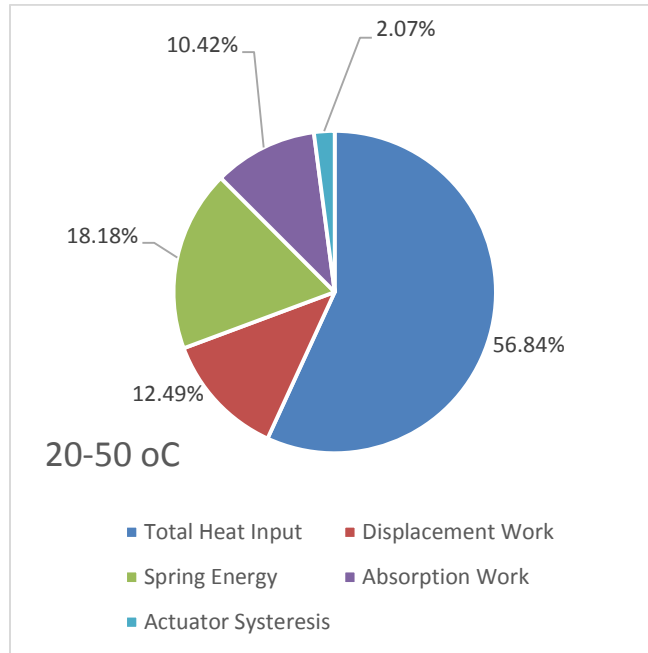

Figure 7. 1: Relative energy distribution for hypothetical scenario with heat recovery system, operating at 20-50 ^{o}C

Appendix – A: Monte Carlo Experiment – MATLAB Script

```matlab
% Metal Hydride Actuator's efficiency
quantification with uncertainty
% Based on the following guide lines:
% GUIDE TO THE EXPRESSION OF
UNCERTAINTY MEASUREMENT (GUM)
% ISO standard ISO/IEC guide 98-3

% Efficiency=(NUM1+NUM2)/(DEN1+DEN2)
% NUM1 : Displacement work
% NUM2 : Spring Energy
% DEN1 : Reaction Enthalpy
% DEN2 : Heat Loss
% For digital measurement, resolution can be
halved for analysis

clear all
clc
clf
M=210000;
%number of trial should be greater than 200,000
(95% conf. interval)

%variables – INPUT : type in the appropriate
numbers here
NUM1=1.3298;
NUM2=2.0511;
DEN1=27.2439;
DEN2=0.9059;

%SD – INPUT : type in the appropriate numbers
here
K=2;
sdNUM1=0.0189/K;
sdNUM2=0.0459/K;
sdDEN1=0.5176/K;
sdDEN2=0.0906/K;

%generating normal distribution
randn('state',0) % resets to initial state
ndNUM1 = sdNUM1*randn(1,M) + NUM1;
ndNUM2 = sdNUM2*randn(1,M) + NUM2;

ndDEN1 = sdDEN1*randn(1,M) + DEN1;
ndDEN2 = sdDEN2*randn(1,M) + DEN2;

%check distribution
subplot(221)
hist(ndNUM1,50)
title('Displacement Work')
hold on

subplot(222)
hist(ndNUM2,50)
title('Spring Energy')
hold on

subplot(223)
hist(ndDEN1,50)
title('Reaction Enthalpy')
hold on

subplot(224)
hist(ndDEN2,50)
title('Heat Loss')
hold on

%Evaluating Efficiency: the result
Efficiency=(ndNUM1+ndNUM2)./(ndDEN1+nd
DEN2);
figure(2)
hist(Efficiency,50)

%Report These values: mean, SD,low and high
end points for 95%,
disp(' MEAN Efficiency:')
mean(Efficiency)
disp(' Standard Deviation:')
std(Efficiency)
disp(' Low End Point for 95%:')
min(Efficiency)
disp(' High End Point for 95%:')
max(Efficiency)
disp('UNCERTAINTY (%, using MC method):')
2*std(Efficiency)/mean(Efficiency)*100
```

Appendix – B: Frequency distribution of measurand and efficiency

Operating Temperature 20-60 ⁰C					
Efficiency (absolute)	Standard Deviation	Low End Point for 95%	High End Point for 95%	Efficiency %	Relative UNCERTAINTY %
0.1201	0.0015	0.1137	0.1274	12.01	2.4721
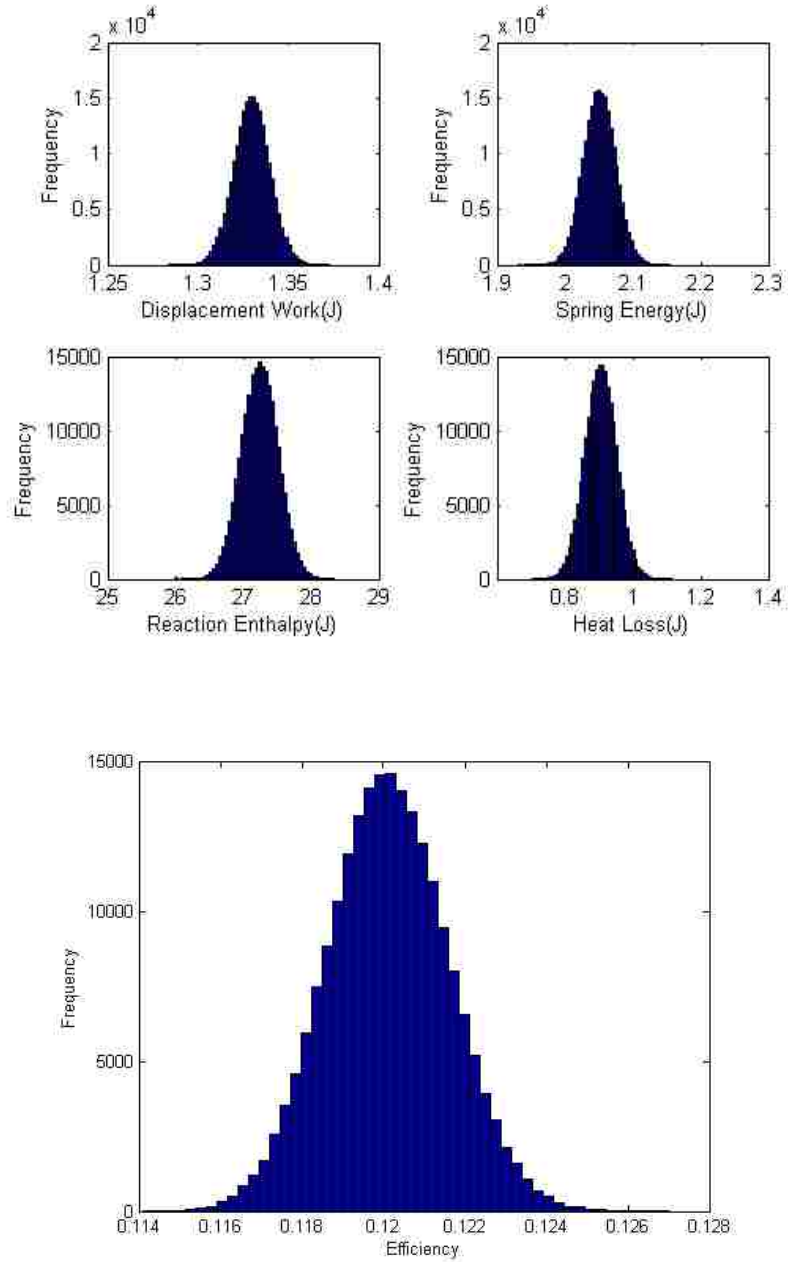
Operating Temperature 20-50 ^{o}C					
Efficiency (absolute)	Standard Deviation	Low End Point for 95%	High End Point for 95%	Efficiency %	Relative UNCERTAINTY %
0.1336	0.0017	0.1265	0.1418	13.36	2.4735
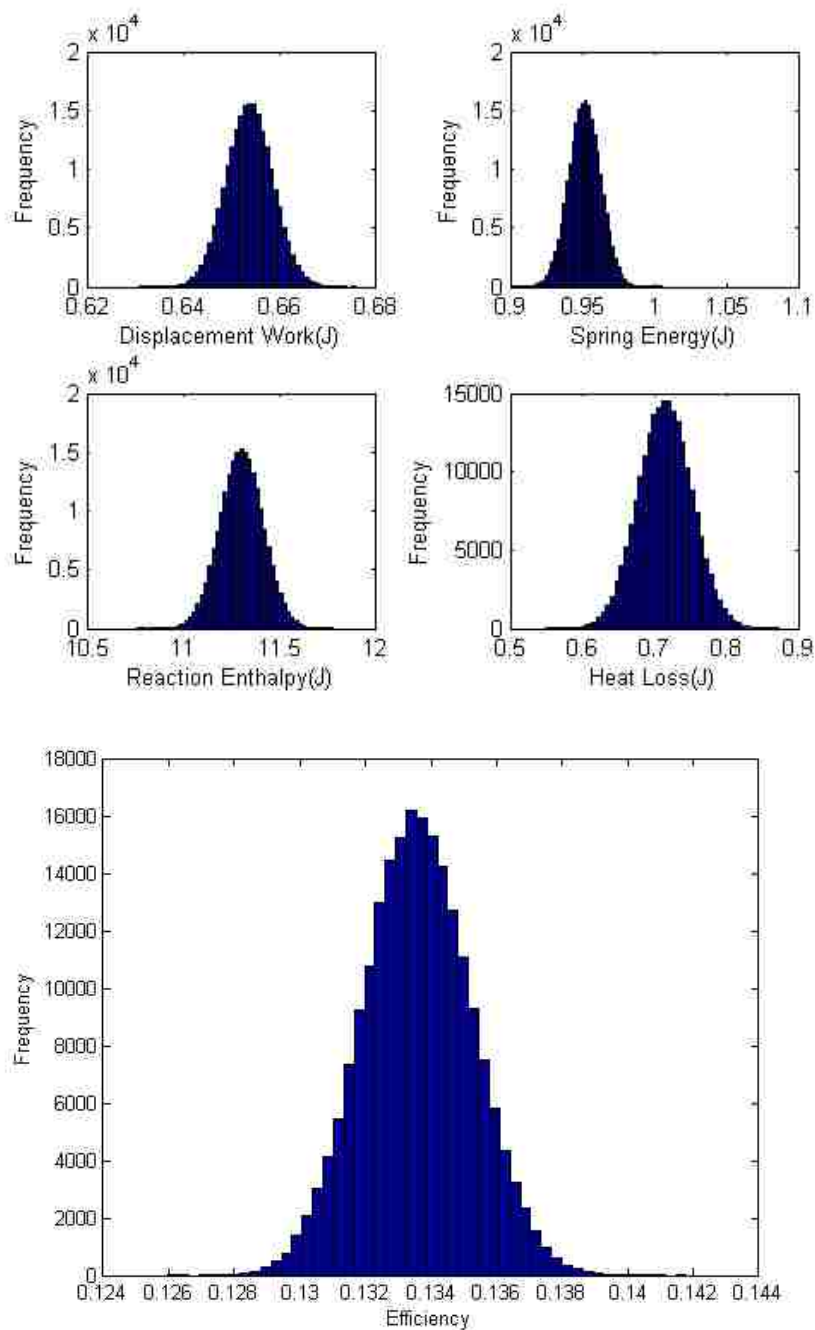
Operating Temperature 20-40 ^{o}C					
Efficiency (absolute)	Standard Deviation	Low End Point for 95%	High End Point for 95%	Efficiency %	Relative UNCERTAINTY %
0.1249	0.0016	0.1182	0.1319	12.49	2.5385

Operating Temperature 20-30 ^{o}C					
Efficiency (absolute)	Standard Deviation	Low End Point for 95%	High End Point for 95%	Efficiency %	Relative UNCERTAINTY %
0.1020	0.0015	0.0959	0.1090	10.2	3.0232

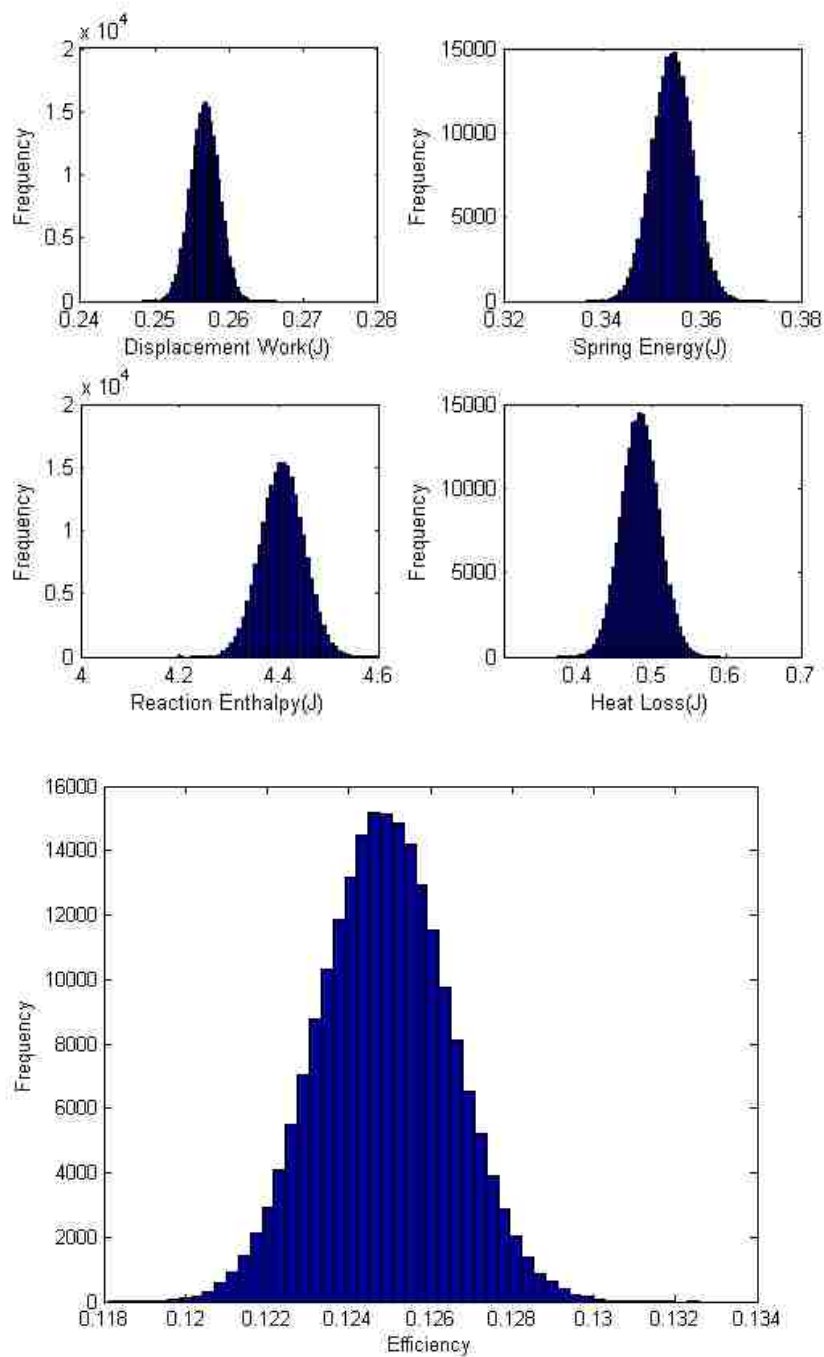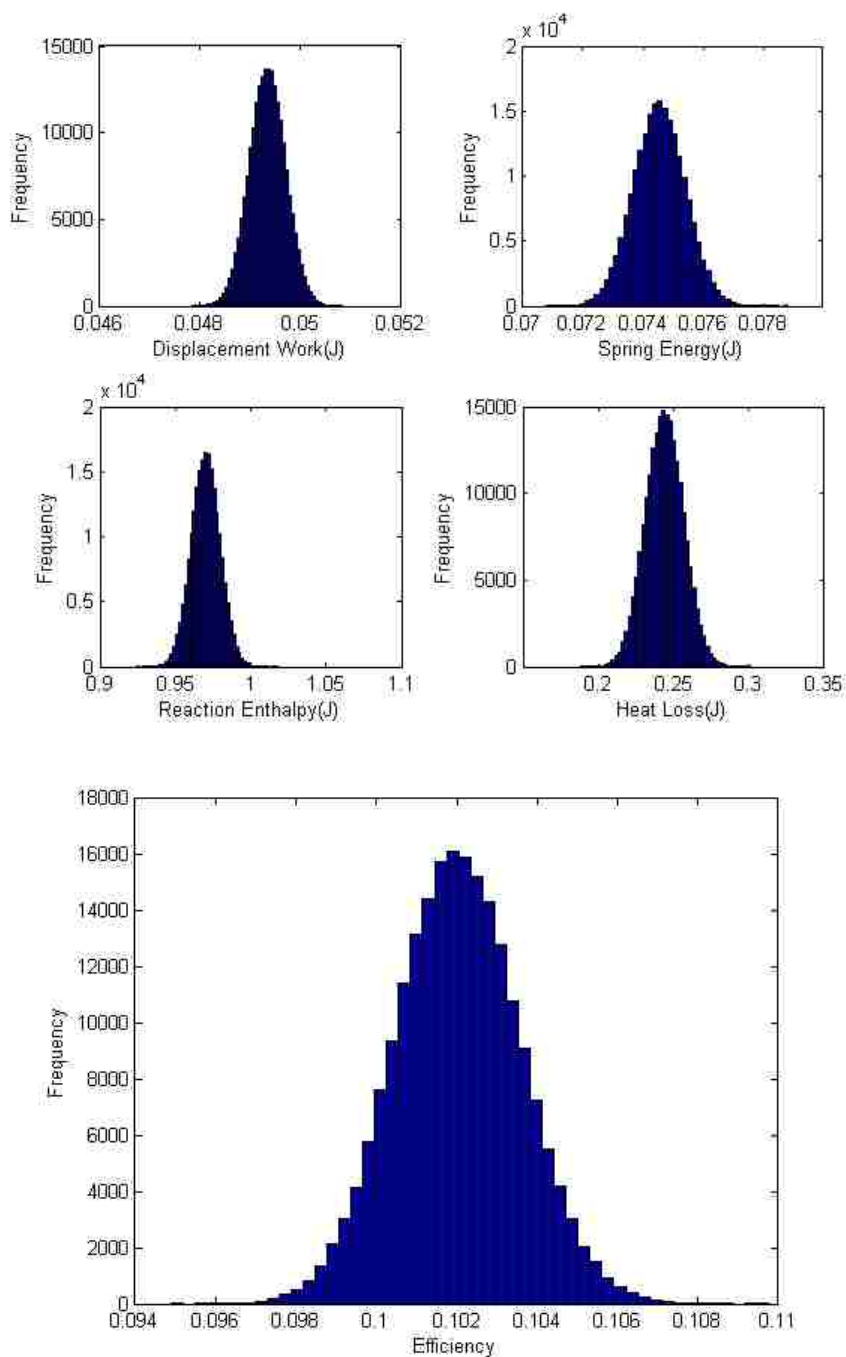| Operating Temperature 20-25 °C					
Efficiency (absolute)	Standard Deviation	Low End Point for 95%	High End Point for 95%	Efficiency %	Relative UNCERTAINTY %
0.0984	0.0019	0.0902	0.1074	9.84	3.7894
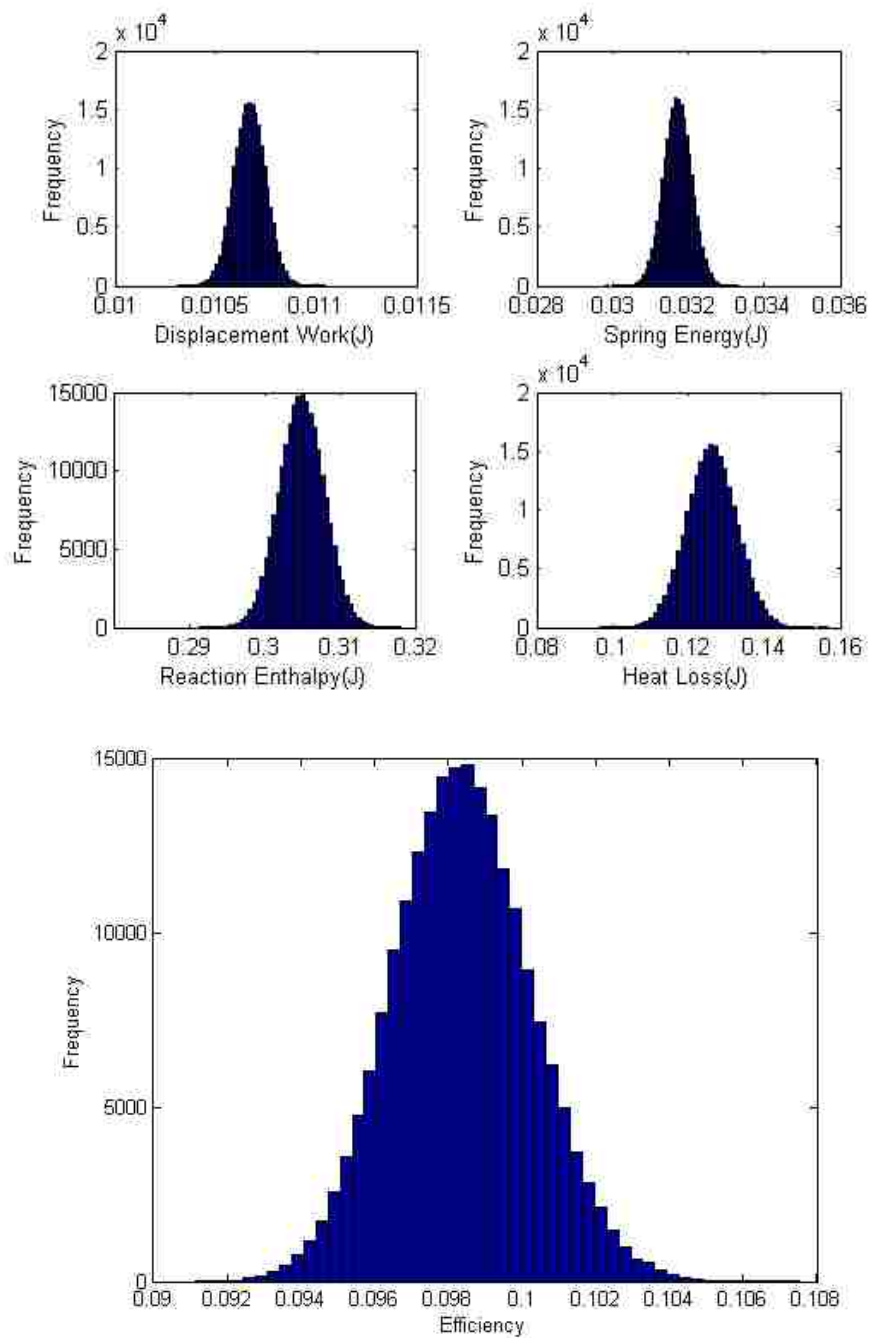
Appendix – C: Additional data for different operating temperature ranges

Temperature Range 20~60 °C
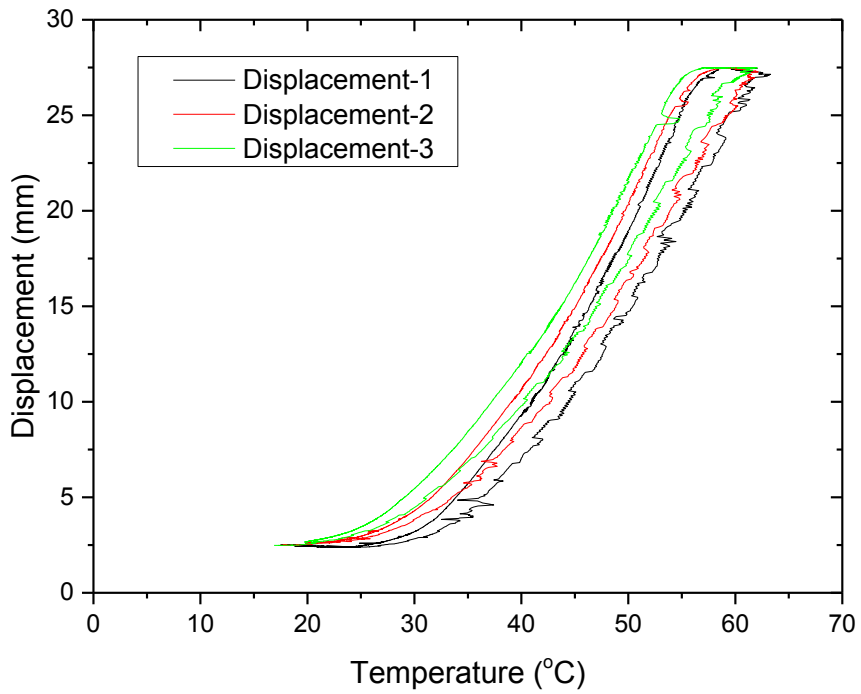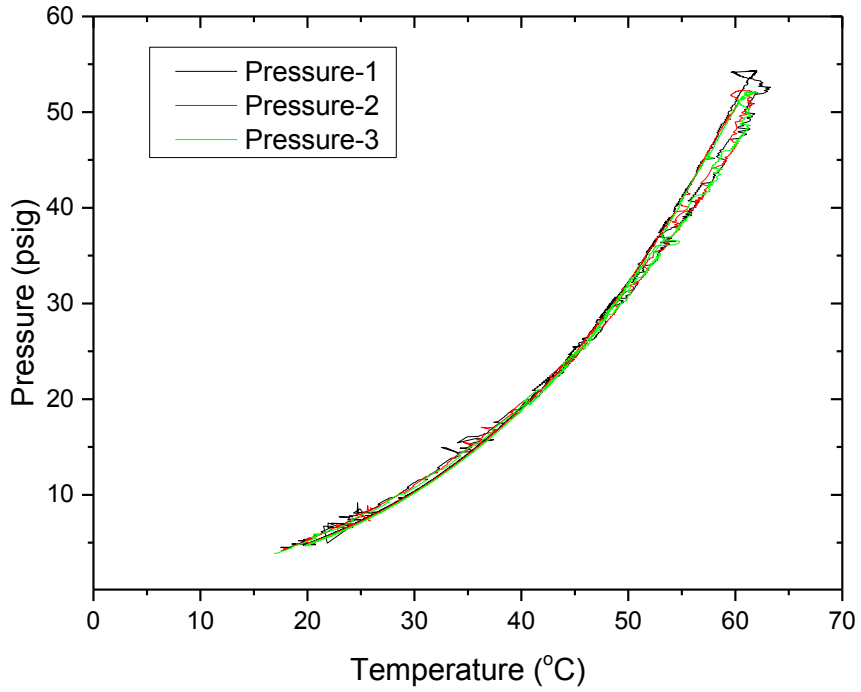
Temperature Range 20~50 °C
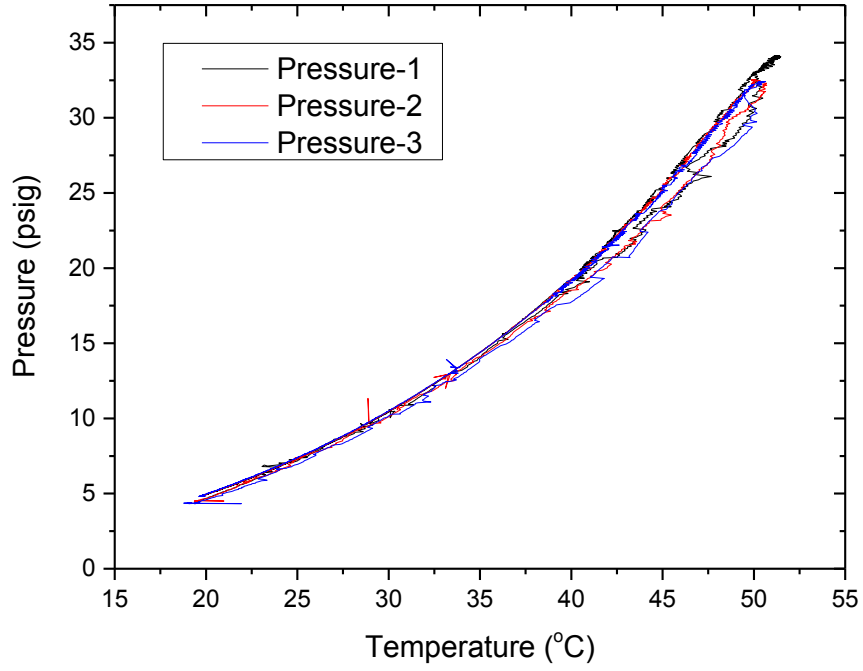
Temperature Range 20~40 °C
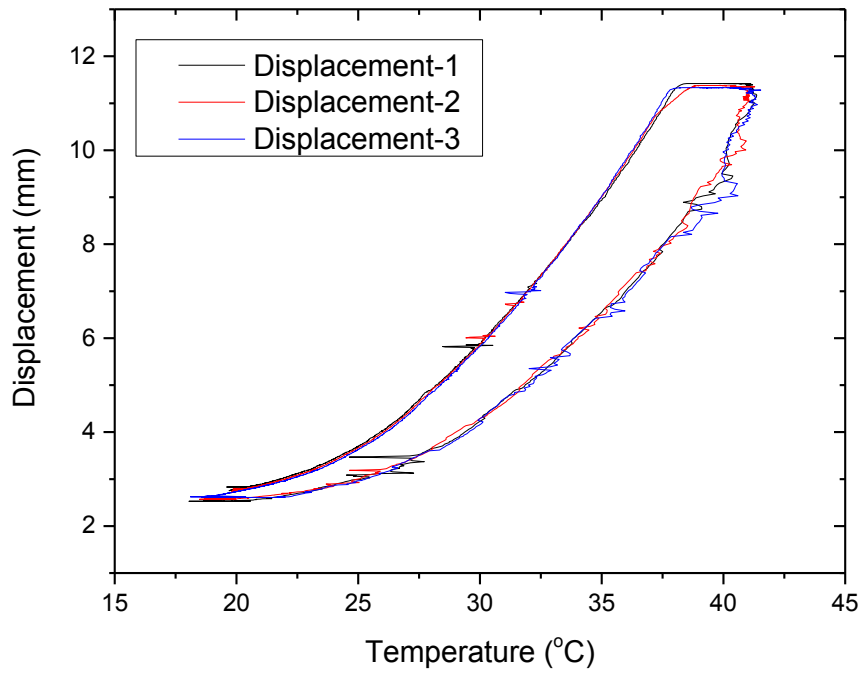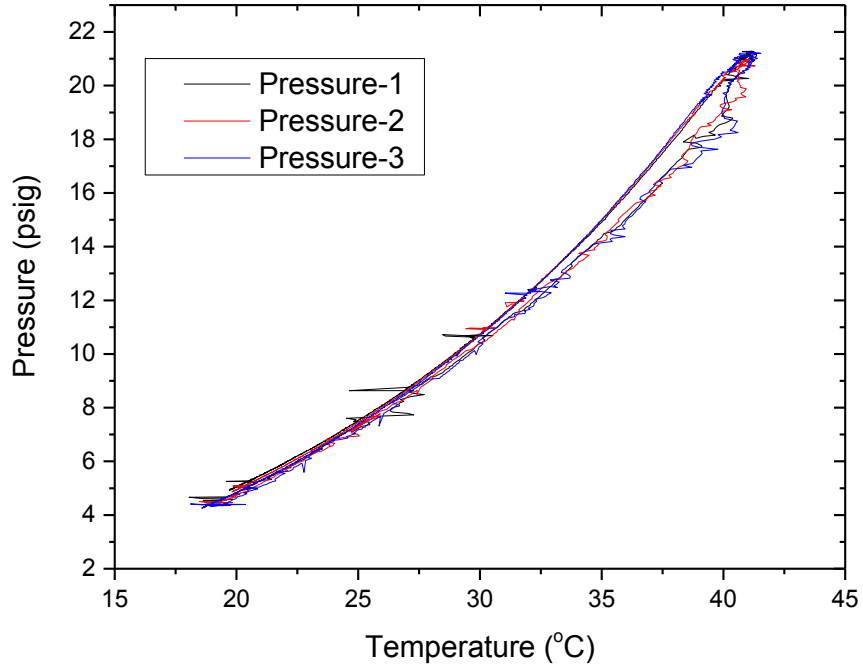
Temperature Range 20~30 $^{\circ}$C
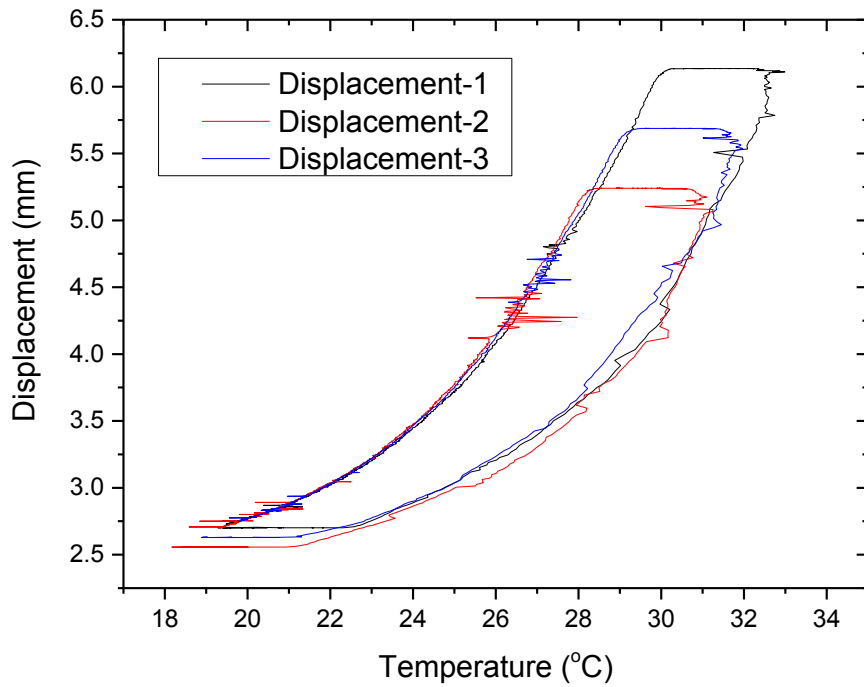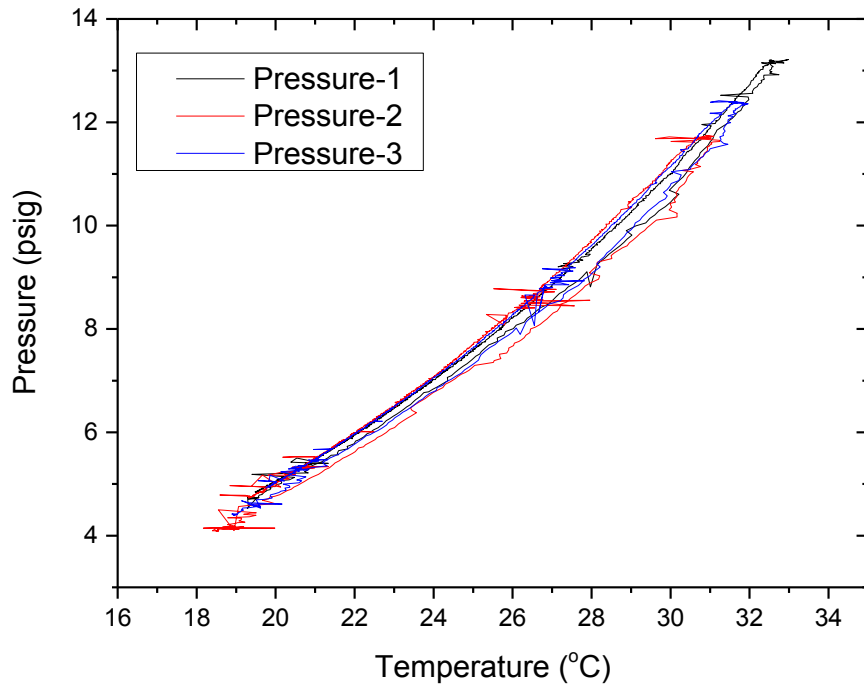
Temperature Range 20~25 °C
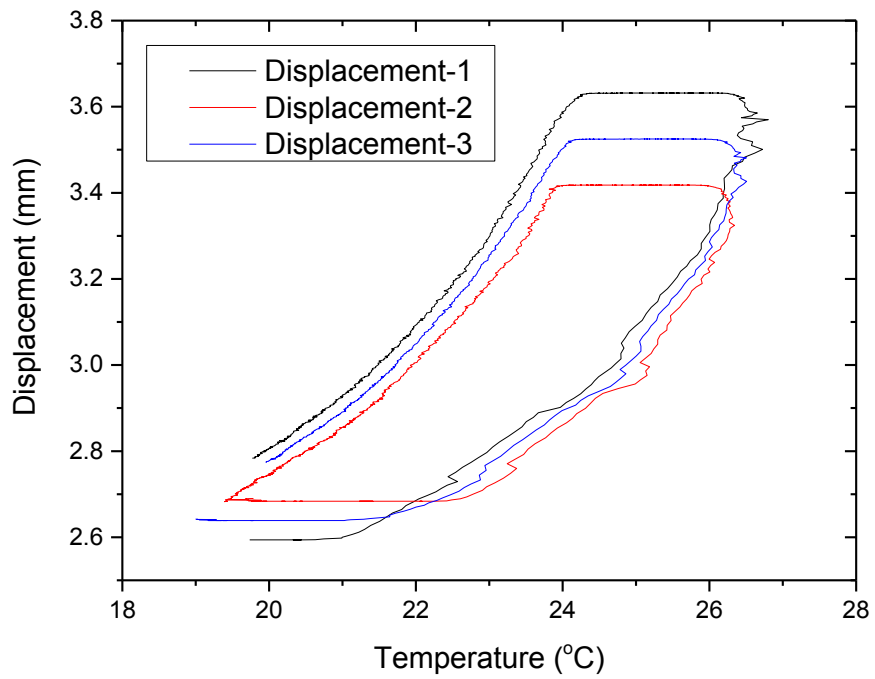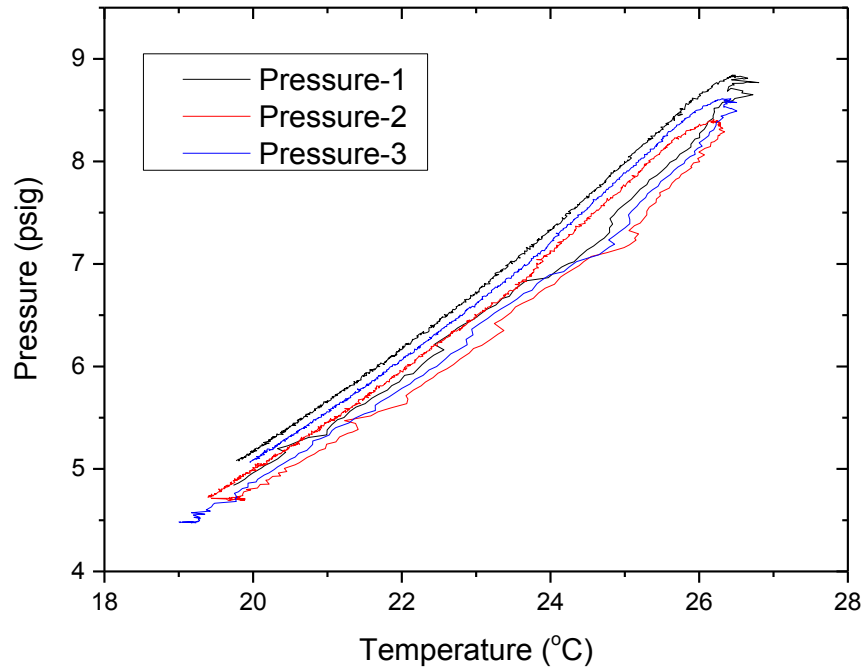
Cyclic Operation at 25-35 ᵒC
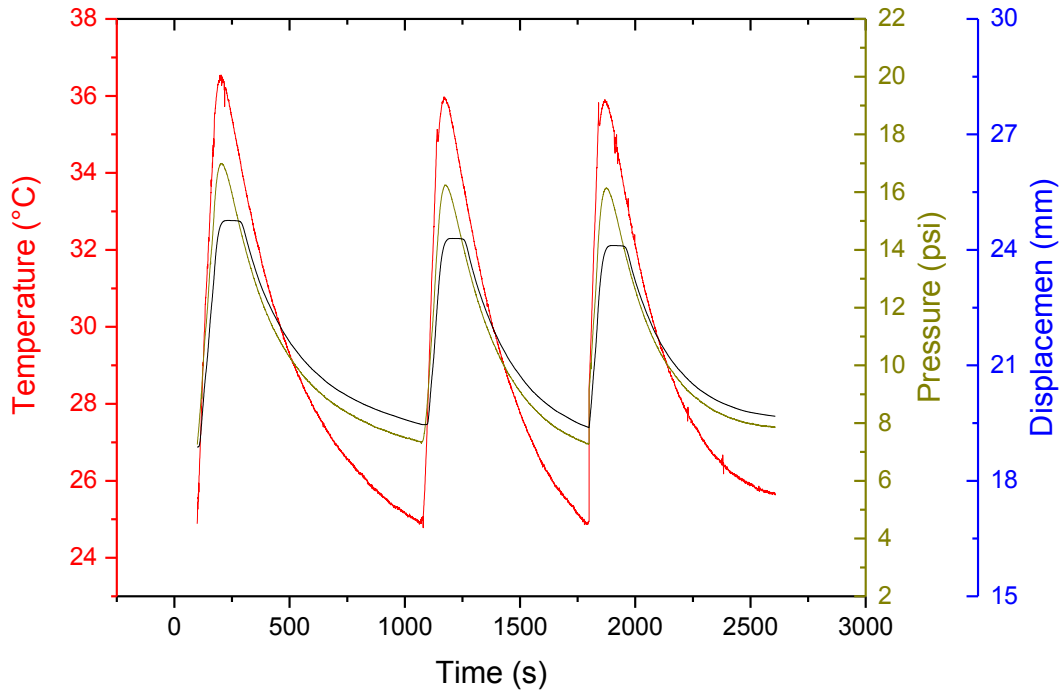
Cyclic Operation at 25-45 ᵒC
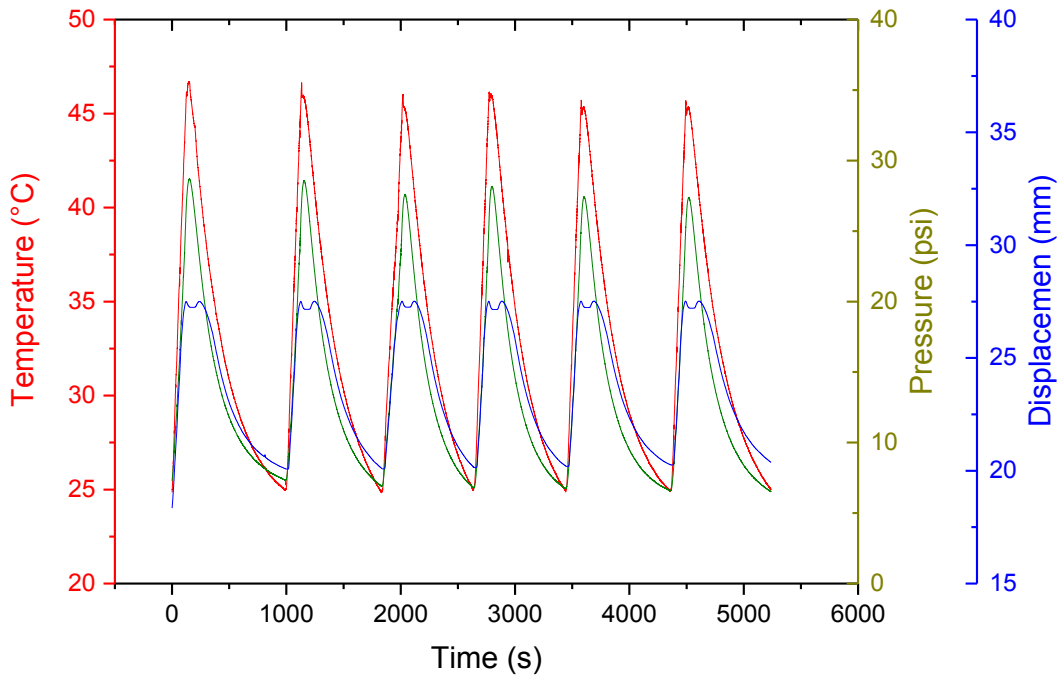
Appendix – E: Copyrights of the Figures used

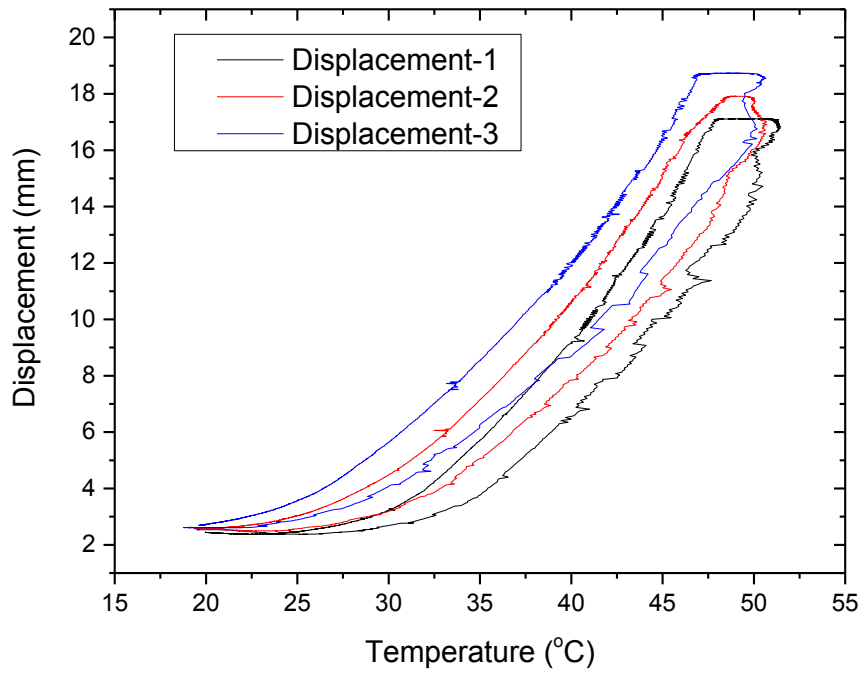| Figure	Reprinted from	Permission
Figure 1.1	Schlapbach, L., and Zuttel, A., 2001, Nature, 414(6861) pp. 353-358	Nature
Figure 1.2	Chandra, D., Reilly, J., and Chellappa, R., 2006 JOM, 58(2) p. 26	Springer
Figure 1.3	Schuth, F., Bogdanovic, B., and Felderhoff, M., 2004, Chemical Communications, 0(20) pp. 2249-2258	Royal Society of Chemistry
Figure 2.1	Lototskyy, M., Klochko, Y., Linkov, V., 2012, Energy Procedia, 29(0) pp. 347-356	Open Source
Figure 2.3	Nomura, K., Ishido, Y., and Ono, S., 1979, Energy Conversion, 19(1) pp. 49-57	Elsevier
Figure 2.5(a)	Kurosaki, K., Maruyama, T., Takahashi, K., 2004, Sensors and Actuators A: Physical, 113(1) pp. 118-123	Elsevier
Figure 2.6	DiMeo Jr., F., Chen, I., Chen, P., 2006, Sensors and Actuators B: Chemical, 117(1) pp.10-16	Elsevier
Figure 2.7	Anders, A., Slack, J. L., and Richardson, T. J., 2008, Thin Solid Films, 517(3) pp. 1021- 1026	Elsevier
Figure 2.10	Ito, Y., Takahashi, R., Mizusaki, S., 2006, Science and Technology of Advanced Materials, 7(4) pp. 369-372	Elsevier
Figure 2.11	Karazhanov, S. Z., Ulyashin, A. G., Vajeeston, P., 2008, Philosophical Magazine, 88(16) pp. 2461-2476	Taylor & Francis

N.B. All other figures, taken from published materials, were redrawn and properly cited to comply with copyright rules.

Appendix – F: Feasibility of Hydrides in Damping Application

The feasibility of integrating metal hydride to a damper for the purpose of dampening force/motion was investigated. Emphasis was given on pneumatic damping system, which is a close match and may have similar working principal as dampers embedded with hydrides. Active or semi active damping system was also be explored since integration of hydride may also mean controlling damping capabilities of the system by adjusting temperature of the hydride. Understanding fundamental principles of dampers would help explain how a system might actually behave while integrated with hydrides. Approximation of the working principal of a metal hydride embedded damping system might hold the key to unleash the potential of such system. Hence, efforts were made in determining probable working principle of a mechanical damper connected to hydride within the system.

Damping generally refers to prevention of oscillatory motion of a vibrating system. The device that dampens the motion is known as damper. Dampers resist motion via viscous friction. The resulting force is proportional to the velocity, which acts in the opposite direction and slows the motion by dissipating energy. Pneumatic dampers are generally used in conjunction with spring which acts to resist displacement. In this segment the feasibility of integrating metal hydride into a damping system would be assessed.

Figure F1 shows a conceptual diagram of a damper, which is combined with hydrogen storage system. When a spring loaded damping system is attached to a metal hydride system, possible working principle can be illustration with steps involved as tabulated in Table F1. Initially the cylinder may be assumed to be filled with hydrogen

gas and the storage material is depleted or partially filled with hydrogen. As a force is applied, the spring will gradually start to get compressed as the actuation rod moves into the cylinder. From the table, number 1 marks the beginning of the process and 2 and 3 marks the intermediate steps during the motion. 4 represents the maximum contraction the damper may experience for this hypothetical situation. Since metal hydrides can absorb or desorb at any given temperature, pressurizing the gas connected to a storage system will help it get absorbed in the storage material and form hydride phase during step 2 and 3. Thus, instead of dampening the motion the gas would escape the cylinder and get absorbed into the metallic particles and form hydride. This completely contradicts the working principle of the damper. As a damper, the gas must not escape the cylinder, instead build up pressure it to resist the motion of the piston. When the damper is connected to a metal hydride storage system, the gas will definitely escape the control volume without producing any resistance to the motion. Hence, damping effect would not occur while a metal hydride reactor is connected to a hydrogen filled spring loaded damper.
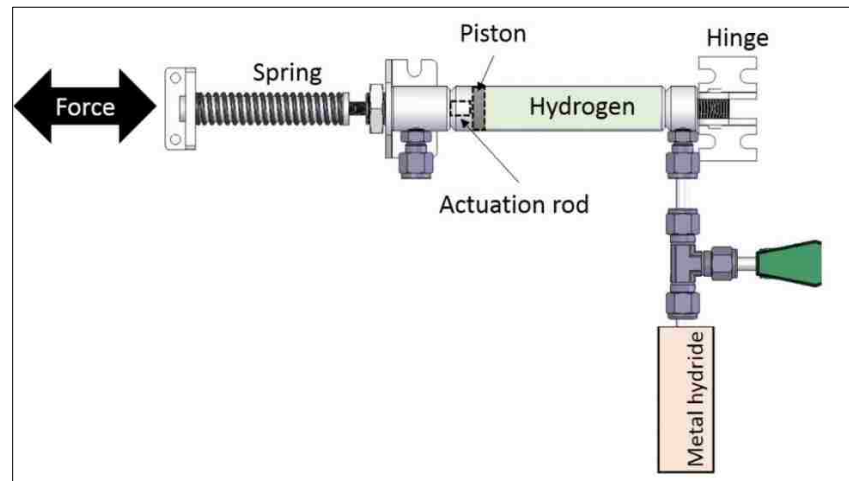
Figure F1: Metal hydride reactor integrated with a damper

The only way this concept may work is by making the storage material unstable with the application of heat that would make the hydride phase unstable. In that way it would be possible to resist hydrogen from getting absorbed into the storage material and may force it to stay inside the cylinder and build up pressure to resist motion as the piston moves inward. This can obviously be done also by closing the valve to hydrides and stop hydrogen from coming into contact to the hydride material. So, it may seem that attachment of metal hydride to a damper is completely unnecessary if the only way damping may happen is by making the hydride unstable and resist hydrogen from getting absorbed.

Once after the piston reaches the extreme end and the spring force pulls the actuation rod out of the cylinder, the working states may be illustrated using the right column of Table F1. Here the retraction steps will follow the sequence 5-6-7-8. The important thing to realize is that during this process a vacuum will be created as the actuation rod moves out with the help of spring force. This situation is very favorable for desorption process to occur. It means that instead of resisting the motion during the return stroke, desorbed hydrogen will actually help the piston move in the direction it is poised to move. Again, it contradicts the purpose of damping.

The only way a hydrogen filled damper connected with a MH hydrogen storage reactor may work is by refraining the hydrogen from getting absorbed into the storage material. Theoretically, hydrogen can get absorbed or desorbed at any given temperature. The direction of the reaction solely depends on the gas pressure above hydride material. Using hydrogen in a damping system for resisting motion by resisting the gas from getting absorbed in to the material, can be done only by making the storage system

unstable. It will require application of heat to a level that the temperature of the hydride reaches the critical point (T_c) or above as shown in Figure F2. This will ultimately make the storage material unstable, which will help gaseous hydrogen in the damper build pressure against the piston as the piston moves in and, hence, dampen the motion.

Table F1: MH reactor integrated with a damper
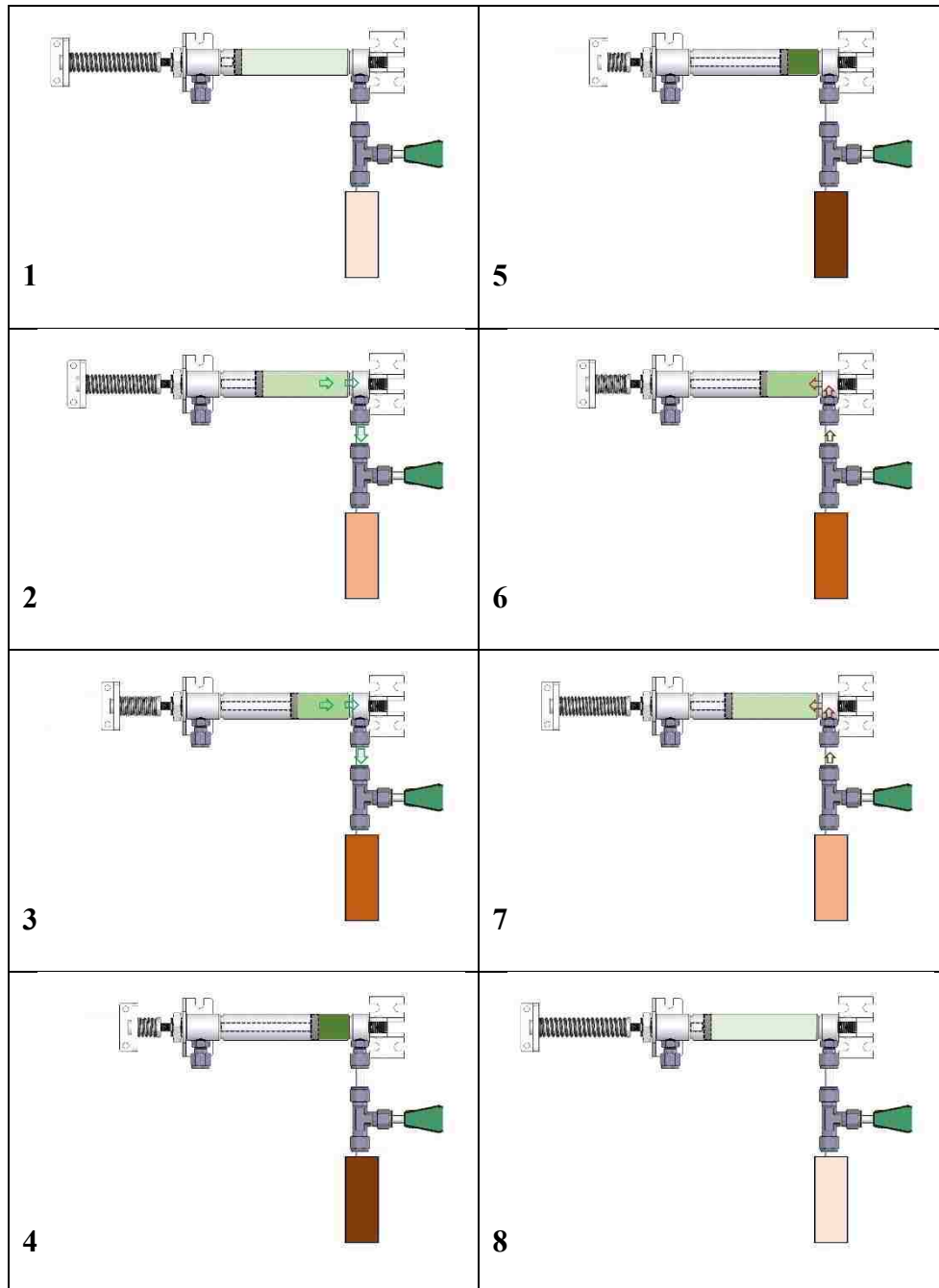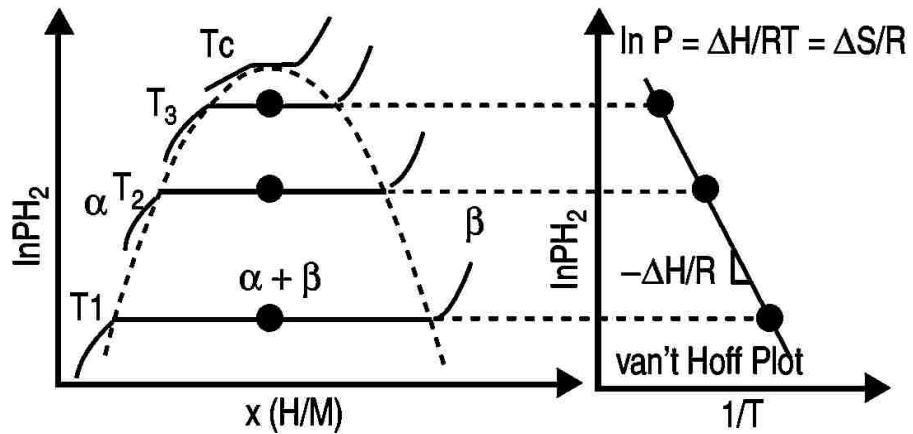
Figure F2: Pressure concentration isotherms of a typical metal hydride [20]

According to the hypothesis provided in earlier sections, metal hydrides may not have any usefulness if integrated to a damping system. It may overly complicate the system and may not support the damping purpose at all. Besides, flammable gases are never used in the damper since there is always a possibility of explosion under any operating condition. Since air is free and safe to use, even in high pressure conditions, pneumatic dampers utilizing air have found wide spread application in all sort of damping system.

REFERENCES

[1] Klebanoff, L., and Keller, J., 2013, "5 Years of Hydrogen Storage Research in the US DOE Metal Hydride Center of Excellence (MHCoE)," International Journal of Hydrogen Energy, .

[2] Miura, S., Fujisawa, A., and Ishida, M., 2012, "A Hydrogen Purification and Storage System using Metal Hydride," International Journal of Hydrogen Energy, **37**(3) pp. 2794-2799.

[3] Kim, J., Park, I., Kim, K. J., 2008, "A Hydrogen-Compression System using Porous Metal Hydride Pellets Of," International Journal of Hydrogen Energy, **33**(2) pp. 870-877.

[4] Li, H., Wang, X., Dong, Z., 2010, "A Study on 70 MPa Metal Hydride Hydrogen Compressor," Journal of Alloys and Compounds, **502**(2) pp. 503-507.

[5] Tae Kyu Kwon and Du Yeol Pang and Kwang-Hun Choi and Yong Yook Kim and Seong Cheol Lee and Nam,Gyun Kim, 2006, "Development of a SMH Actuator System using Hydrogen-Absorbing Alloys," Smart Materials and Structures, **15**(5) pp. N117.

[6] Kawamura, M., Ono, S., and Mizuno, Y., 1983, "Dynamic Characteristics of a Hydride Heat Storage System," Journal of the Less Common Metals, **89**(2) pp. 365-372.

[7] Kelly, N. A., and Girdwood, R., 2012, "Evaluation of a Thermally-Driven Metal-Hydride-Based Hydrogen Compressor," International Journal of Hydrogen Energy, **37**(14) pp. 10898-10916.

[8] Groll, M., Nonnenmacher, A., and Supper, W., 1985, "Experimental Investigation of Reaction Beds for Metal-Hydride Heat Transformers," Journal of Heat Recovery Systems, **5**(5) pp. 466.

[9] Sandrock, G., and Bowman Jr., R. C., 2003, "Gas-Based Hydride Applications: Recent Progress and Future Needs," Journal of Alloys and Compounds, **356–357**(0) pp. 794-799.

[10] Hopkins, R. R., and Kim, K. J., 2010, "Hydrogen Compression Characteristics of a Dual Stage Thermal Compressor System Utilizing LaNi5 and Ca0.6Mm0.4Ni5 as the Working Metal Hydrides," International Journal of Hydrogen Energy, **35**(11) pp. 5693-5702.

[11] Wang, X., Chen, R., Zhang, Y., 2006, "Hydrogen Storage Alloys for High-Pressure Suprapure Hydrogen Compressor," Journal of Alloys and Compounds, **420**(1–2) pp. 322-325.

[12] Reilly J. J. , Sandrock G. D., 1980, "Hydrogen Storage in Metal Hydrides," Scientific American , **242**pp. 118-129.

[13] Laurenczy, G., Dalebrook, A. F., Gan, W., 2013, "Hydrogen Storage-Beyond Conventional Methods," Chem.Commun., .

[14] Schlapbach, L., and Zuttel, A., 2001, "Hydrogen-Storage Materials for Mobile Applications," Nature, **414**(6861) pp. 353-358.

[15] Park, I., Kim, J., Kim, K. J., 2009, "Investigation of Coupled AB5 Type High-Power Metal Hydride Reactors," International Journal of Hydrogen Energy, **34**(14) pp. 5770-5777.

[16] Wang, X. H., Bei, Y. Y., Song, X. C., 2007, "Investigation on High-Pressure Metal Hydride Hydrogen Compressors," International Journal of Hydrogen Energy, **32**(16) pp. 4011-4015.

[17] Schuth, F., Bogdanovic, B., and Felderhoff, M., 2004, "Light Metal Hydrides and Complex Hydrides for Hydrogen Storage," Chemical Communications, **0**(20) pp. 2249-2258.

[18] Pasini, J. M., Corgnale, C., van Hassel, B. A., 2013, "Metal Hydride Material Requirements for Automotive Hydrogen Storage Systems," International Journal of Hydrogen Energy, **38**(23) pp. 9755-9765.

[19] Sakintuna, B., Lamari-Darkrim, F., and Hirscher, M., 2007, "Metal Hydride Materials for Solid Hydrogen Storage: A Review," International Journal of Hydrogen Energy, **32**(9) pp. 1121-1140.

[20] Chandra, D., Reilly, J., and Chellappa, R., 2006, "Metal Hydrides for Vehicular Applications: The State of the Art," JOM, **58**(2) pp. 26-32.

[21] Tozzini, V., and Pellegrini, V., 2013, "Prospects for Hydrogen Storage in Graphene," Physical Chemistry Chemical Physics, **15**(1) pp. 80-89.

[22] Mori, D., and Hirose, K., 2009, "Recent Challenges of Hydrogen Storage Technologies for Fuel Cell Vehicles," International Journal of Hydrogen Energy, **34**(10) pp. 4569-4574.

[23] SANDROCK, G.D., and SNAPE, E., 1980, AMERICAN CHEMICAL SOCIETY, pp. 293-322.

[24] Durbin, D. J., and Malardier-Jugroot, C., "Review of Hydrogen Storage Techniques For on board Vehicle Applications," International Journal of Hydrogen Energy, (0) .

[25] Semadeni, M., 2004, "Encyclopedia of Energy,"Elsevier, New York, pp. 719-738.

[26] US Department of Energy, September 2009, "Targets for Onboard Hydrogen Storage Systems for Light-Duty Vehicles." Office of Energy Efficiency and Renewable Energy and the FreedomCAR and Fuel Partnership, .

[27] Folonari, C., Iemmi, G., Manfredi, F., 1980, "Metal Hydride Fuel Cells: A Feasibility Study and Perspectives for Vehicular Applications," Journal of the Less Common Metals, **74**(2) pp. 371-378.

[28] Anonymous 1998, "98/03329 Cooling Power/Efficiency Diagrams for a Compressor-Driven Metal Hydride Heat Pump: Lloyd, G. M. Et Al. ASHRAE Trans., 1997, 103, (1), 384–391," Fuel and Energy Abstracts, **39**(4) pp. 307.

[29] Talagañis, B. A., Esquivel, M. R., and Meyer, G., 2009, "A Two-Stage Hydrogen Compressor Based on (La,Ce,Nd,Pr)Ni5 Intermetallics obtained by Low Energy Mechanical Alloying – Low Temperature Annealing Treatment," International Journal of Hydrogen Energy, **34**(4) pp. 2062-2068.

[30] Laurencelle, F., Dehouche, Z., Morin, F., 2009, "Experimental Study on a Metal Hydride Based Hydrogen Compressor," Journal of Alloys and Compounds, **475**(1–2) pp. 810-816.

[31] Muthukumar, P., Prakash Maiya, M., and Srinivasa Murthy, S., 2005, "Experiments on a Metal Hydride Based Hydrogen Compressor," International Journal of Hydrogen Energy, **30**(8) pp. 879-892.

[32] Feng, Z., Deyou, B., Lijun, J., 1995, "Metal Hydride Compressor and its Application in Cryogenic Technology," Journal of Alloys and Compounds, **231**(1–2) pp. 907-909.

[33] Muthukumar, P., Prakash Maiya, M., and Murthy, S. S., 2002, "Parametric Studies on a Metal Hydride Based Single Stage Hydrogen Compressor," International Journal of Hydrogen Energy, **27**(10) pp. 1083-1092.

[34] Muthukumar, P., Prakash Maiya, M., and Srinivasa Murthy, S., 2008, "Performance Tests on a Thermally Operated Hydrogen Compressor," International Journal of Hydrogen Energy, **33**(1) pp. 463-469.

[35] Luo, G., Chen, J. P., Li, S. L., 2010, "Properties of La0.2Y0.8Ni5−xMnx Alloys for High-Pressure Hydrogen Compressor," International Journal of Hydrogen Energy, **35**(15) pp. 8262-8267.

[36] Lototskyy, M., Klochko, Y., Linkov, V., 2012, "Thermally Driven Metal Hydride Hydrogen Compressor for Medium-Scale Applications," Energy Procedia, **29**(0) pp. 347-356.

[37] Mazumdar, S., Ram Gopal, M., and Bhattacharyya, S., 2005, "Thermodynamic Analysis and Optimization of Compressor-Driven Metal Hydride Cooling Systems," International Journal of Hydrogen Energy, **30**(6) pp. 631-641.

[38] Chernikov, A. S., Izhvanov, L. A., Solovey, A. I., 2002, "An Installation for Water Cooling Based on a Metal Hydride Heat Pump," Journal of Alloys and Compounds, **330–332**(0) pp. 907-910.

[39] Sajid Ahmed, S., and Srinivasa Murthy, S., 2004, "Analysis of a Novel Metal Hydride Cycle for Simultaneous Heating and Cooling," Renewable Energy, **29**(4) pp. 615-631.

[40] Kim, K. J., Feldman Jr, K. T., Lloyd, G., 1997, "Compressor-Driven Metal-Hydride Heat Pumps," Applied Thermal Engineering, **17**(6) pp. 551-560.

[41] Satheesh, A., Muthukumar, P., and Dewan, A., 2009, "Computational Study of Metal Hydride Cooling System," International Journal of Hydrogen Energy, **34**(7) pp. 3164-3172.

[42] Klein, H. -., and Groll, M., 2002, "Development of a Two-Stage Metal Hydride System as Topping Cycle in Cascading Sorption Systems for Cold Generation," Applied Thermal Engineering, **22**(6) pp. 631-639.

[43] Ni, J., and Liu, H., 2007, "Experimental Research on Refrigeration Characteristics of a Metal Hydride Heat Pump in Auto Air-Conditioning," International Journal of Hydrogen Energy, **32**(13) pp. 2567-2572.

[44] Linder, M., Mertz, R., and Laurien, E., 2010, "Experimental Results of a Compact Thermally Driven Cooling System Based on Metal Hydrides," International Journal of Hydrogen Energy, **35**(14) pp. 7623-7632.

[45] Choi, H., and Mills, A. F., 1990, "Heat and Mass Transfer in Metal Hydride Beds for Heat Pump Applications," International Journal of Heat and Mass Transfer, **33**(6) pp. 1281-1288.

[46] Yang, F. S., Wang, G. X., Zhang, Z. X., 2010, "Investigation on the Influences of Heat Transfer Enhancement Measures in a Thermally Driven Metal Hydride Heat Pump," International Journal of Hydrogen Energy, **35**(18) pp. 9725-9735.

[47] Satheesh, A., and Muthukumar, P., 2010, "Performance Investigation of Double-Stage Metal Hydride Based Heat Pump," Applied Thermal Engineering, **30**(17–18) pp. 2698-2707.

[48] Satheesh, A., and Muthukumar, P., 2010, "Simulation of Double-Stage Double-Effect Metal Hydride Heat Pump," International Journal of Hydrogen Energy, **35**(3) pp. 1474-1484.

[49] Jang, K. -., Fateev, G. A., Park, J. -., 2001, "Simulation of the Metal Hydride Heat Pump System with the Single and Double Reactors," International Journal of Hydrogen Energy, **26**(3) pp. 237-241.

[50] Park, J., Han, S., Jang, H., 2002, "The Development of Compressor-Driven Metal Hydride Heat Pump (CDMHHP) System as an Air Conditioner," International Journal of Hydrogen Energy, **27**(9) pp. 941-944.

[51] Park, J., Jang, K., Lee, P. S., 2001, "The Operating Characteristics of the Compressor-Driven Metal Hydride Heat Pump System," International Journal of Hydrogen Energy, **26**(7) pp. 701-706.

[52] Libowitz, G. G., Feldman Jr., K. T., and Stein, C., 1997, "Thermodynamic Properties of Metal Hydrides for a Novel Heat Pump Configuration," Journal of Alloys and Compounds, **253–254**(0) pp. 673-676.

[53] Suda, S., 1993, "What is Required for the Commercialization of Metal Hydride Refrigerators and Heat Pumps: Surface Engineering can Solve the Application Problems," Heat Recovery Systems and CHP, **13**(4) pp. 309-314.

[54] Payá, J., Linder, M., Mertz, R., 2011, "Analysis and Optimization of a Metal Hydride Cooling System," International Journal of Hydrogen Energy, **36**(1) pp. 920-930.

[55] Muthukumar, P., and Groll, M., 2010, "Erratum to "Metal Hydride Based Heating and Cooling Systems: A Review" [International Journal of Hydrogen Energy (2010) 35: 3817–3831]," International Journal of Hydrogen Energy, **35**(16) pp. 8816-8829.

[56] Muthukumar, P., and Groll, M., 2010, "Metal Hydride Based Heating and Cooling Systems: A Review," International Journal of Hydrogen Energy, **35**(8) pp. 3817-3831.

[57] Ram Gopal, M., and Srinivasa Murthy, S., 1995, "Performance of a Metal Hydride Cooling System," International Journal of Refrigeration, **18**(6) pp. 413-420.

[58] Gopal, M. R., and Murthy, S. S., 1995, "Prediction of Metal-Hydride Refrigerator Performance Based on Reactor Heat and Mass Transfer," International Journal of Hydrogen Energy, **20**(7) pp. 607-614.

[59] Lloyd, G., Razani, A., and Feldman Jr, K. T., 1998, "Transitional Reactor Dynamics Affecting Optimization of a Heat-Driven Metal Hydride Refrigerator," International Journal of Heat and Mass Transfer, **41**(3) pp. 513-527.

[60] Yang, F. S., Zhang, Z. X., and Bao, Z. W., 2012, "An Extensive Parametric Analysis on the Performance of a Single-Stage Metal Hydride Heat Transformer," International Journal of Hydrogen Energy, **37**(3) pp. 2623-2634.

[61] Werner, R., and Groll, M., 1991, "Two-Stage Metal Hydride Heat Transformer Laboratory Model: Results of Reaction Bed Tests," Journal of the Less-Common Metals, **172-174**(PART 3) pp. 1122-1129.

[62] Saitou, T., and Sugiyama, K., 1995, "Hydrogen Purification with Metal Hydride Sintered Pellets using Pressure Swing Adsorption Method," Journal of Alloys and Compounds, **231**(1–2) pp. 865-870.

[63] Block, F. R., Dey, A., Kappes, H., 1987, "Hydrogen Purification with Metal Hydrides in a New Kind of Reactor," Journal of the Less Common Metals, **131**(1–2) pp. 329-335.

[64] Fujisawa, A., Miura, S., Mitsutake, Y., "Simulation Study of Hydrogen Purification using Metal Hydride," Journal of Alloys and Compounds, (0) .

[65] Fan, C. Q., Rivera, H., Rao, U., 2012, "Applications of Metal Hydride-Based Bipolar Electrodes," Electrochimica Acta, **59**(0) pp. 470-473.

[66] Renquist, J. V., Dickman, B., and Bradley, T. H., 2012, "Economic Comparison of Fuel Cell Powered Forklifts to Battery Powered Forklifts," International Journal of Hydrogen Energy, **37**(17) pp. 12054-12059.

[67] Kim, T., 2012, "Fully-Integrated Micro PEM Fuel Cell System with NaBH4 Hydrogen Generator," International Journal of Hydrogen Energy, **37**(3) pp. 2440-2446.

[68] Zhu, L., Kim, D., Kim, H., 2008, "Hydrogen Generation from Hydrides in Millimeter Scale Reactors for Micro Proton Exchange Membrane Fuel Cell Applications," Journal of Power Sources, **185**(2) pp. 1334-1339.

[69] Jiang, Z., Dougal, R. A., Liu, S., 2005, "Simulation of a Thermally Coupled Metal-Hydride Hydrogen Storage and Fuel Cell System," Journal of Power Sources, **142**(1–2) pp. 92-102.

[70] Kurosaki, K., Maruyama, T., Takahashi, K., 2004, "Design and Development of MH Actuator System," Sensors and Actuators A: Physical, **113**(1) pp. 118-123.

[71] Alexandra Vanderhoff and Kwang, J. K., 2009, "Experimental Study of a Metal Hydride Driven Braided Artificial Pneumatic Muscle," Smart Materials and Structures, **18**(12) pp. 125014.

[72] Lloyd, G. M., and Kim, K. J., 2007, "Smart Hydrogen/Metal Hydride Actuator," International Journal of Hydrogen Energy, **32**(2) pp. 247-255.

[73] Sato, M., Hosono, M., Yamashita, K., 2011, "Solar Or Surplus Heat-Driven Actuators using Metal Hydride Alloys," Sensors and Actuators B: Chemical, **156**(1) pp. 108-113.

[74] Ram Gopal, M., and Srinivasa Murthy, S., 1992, "Prediction of Heat and Mass Transfer in Annular Cylindrical Metal Hydride Beds," International Journal of Hydrogen Energy, **17**(10) pp. 795-805.

[75] Mayer, U., Groll, M., and Supper, W., 1987, "Heat and Mass Transfer in Metal Hydride Reaction Beds: Experimental and Theoretical Results," Journal of the Less Common Metals, **131**(1–2) pp. 235-244.

[76] Wakao, S., Sekine, M., Endo, H., 1983, "A Heat Storage Reactor for Metal Hydrides," Journal of the Less Common Metals, **89**(2) pp. 341-350.

[77] Jemni, A., and Nasrallah, S. B., 1995, "Study of Two-Dimensional Heat and Mass Transfer during Absorption in a Metal-Hydrogen Reactor," International Journal of Hydrogen Energy, **20**(1) pp. 43-52.

[78] Da-Wen, S., and Song-Jiu, D., 1989, "Study of the Heat and Mass Transfer Characteristics of Metal Hydride Beds: A Two-Dimensional Model," Journal of the Less Common Metals, **155**(2) pp. 271-279.

[79] Yu, W., Dianbo, X., Jianmei, F., 2010, "Research on Sealing Performance and Self-Acting Valve Reliability in High-Pressure Oil-Free Hydrogen Compressors for Hydrogen Refueling Stations," International Journal of Hydrogen Energy, **35**(15) pp. 8063-8070.

[80] Arteconi, A., Hewitt, N. J., and Polonara, F., 2012, "State of the Art of Thermal Storage for Demand-Side Management," Applied Energy, **93**(0) pp. 371-389.

[81] Bogdanović, B., Ritter, A., Spliethoff, B., 1995, "A Process Steam Generator Based on the High Temperature Magnesium Hydride/Magnesium Heat Storage System," International Journal of Hydrogen Energy, **20**(10) pp. 811-822.

[82] Cabeza, L.F., 2012, "Comprehensive Renewable Energy,"Elsevier, Oxford, pp. 211-253.

[83] Reiser, A., Bogdanović, B., and Schlichte, K., 2000, "The Application of mg-Based Metal-Hydrides as Heat Energy Storage Systems," International Journal of Hydrogen Energy, **25**(5) pp. 425-430.

[84] Sakai, T., Honda, N., and Yonezu, I., 1986, "Metalhydride Container and Metal Hydride Heat Storage System," Journal of Heat Recovery Systems, **6**(1) pp. vii.

[85] Felderhoff, M., and Bogdanović, 2009, "High Temperature Metal Hydrides as Heat Storage Materials for Solar and Related Applications," International Journal of Molecular Science, **10**(1) pp. 325-344.

[86] Nomura, K., Ishido, Y., and Ono, S., 1979, "A Novel Thermal Engine using Metal Hydride," Energy Conversion, **19**(1) pp. 49-57.

[87] Ovshinsky, S. R., Fetcenko, M. A., and Ross, J., 1993, "A Nickel Metal Hydride Battery for Electric Vehicles," Science, **260**(5105) pp. 176-181.

[88] Li, L., Tang, X., Luo, Z., 2010, "A Novel Parameter for Evaluation on Power Performance of Ni–MH Rechargeable Batteries," International Journal of Hydrogen Energy, **35**(7) pp. 2847-2851.

[89] Nei, J., 2012, "Multi-Component AB2 Metal Hydride Alloys for Nickel Metal Hydride Battery Applications," ProQuest Dissertations and Theses, .

[90] Bäuerlein, P., Antonius, C., Löffler, J., 2008, "Progress in High-Power Nickel–metal Hydride Batteries," Journal of Power Sources, **176**(2) pp. 547-554.

[91] Nan, J., Han, D., Yang, M., 2006, "Recovery of Metal Values from a Mixture of Spent Lithium-Ion Batteries and Nickel-Metal Hydride Batteries," Hydrometallurgy, **84**(1–2) pp. 75-80.

[92] Cuscueta, D. J., Ghilarducci, A. A., and Salva, H. R., 2010, "Design, Elaboration and Characterization of a Ni–MH Battery Prototype," International Journal of Hydrogen Energy, **35**(20) pp. 11315-11323.

[93] Su, G., He, Y., and Liu, K., 2012, "Effects of Co3O4 as Additive on the Performance of Metal Hydride Electrode and Ni–MH Battery," International Journal of Hydrogen Energy, **37**(16) pp. 11994-12002.

[94] Kopera, J.J.C., 2004, "Inside the Nickel Metal Hydride Battery," COBASYS, .

[95] ART., 04/18/2013, "Fuel Cell: Proton Exchange Membrane Fuel Cell <http://Kids.Britannica.Com/Comptons/Art-106689>," Britannica Online for Kids, .

[96] Anonymous 2010, "Linde MH Delivers Fuel Cell Forklifts to Linde Gases," Fuel Cells Bulletin, **2010**(3) pp. 4.

[97] Nice, Karim, and Jonathan Strickland, " "How Fuel Cells Work" 18 September 2000. HowStuffWorks.Com. <http://Auto.Howstuffworks.Com/Fuel-Efficiency/Alternative-Fuels/Fuel-Cell.Htm> 18 April 2013." .

[98] Anonymous 2002, "Metal Hydride Artificial Muscles," Smart Materials Bulletin, **2002**(7) pp. 14.

[99] Ino, S., Sato, M., Hosono, M., 2009, "Development of a Soft Metal Hydride Actuator using a Laminate Bellows for Rehabilitation Systems," Sensors and Actuators B: Chemical, **136**(1) pp. 86-91.

[100] Marie-Charlotte Crevier and Martin Richard and D Matheson Rittenhouse and Pierre-Olivier Roy,and St, 2007, "Artificial Exomuscle Investigations for Applications—metal Hydride," Biomedical Materials, **2**(1) pp. S1.

[101] Choe, K., Kim, K. J., Kim, D., 2006, "Performance Characteristics of Electro-Chemically Driven Polyacrylonitrile Fiber Bundle Actuators," Journal of Intelligent Material Systems and Structures, **17**(7) pp. 563-576.

[102] DiMeo Jr., F., Chen, I., Chen, P., 2006, "MEMS-Based Hydrogen Gas Sensors," Sensors and Actuators B: Chemical, **117**(1) pp. 10-16.

[103] Slaman, M., Dam, B., Pasturel, M., 2007, "Fiber Optic Hydrogen Detectors Containing mg-Based Metal Hydrides," Sensors and Actuators B: Chemical, **123**(1) pp. 538-545.

[104] Karazhanov, S.Zh. and Ulyashiny, A.G., 2010, "Similarity of Optical Properties of Hydrides and Semiconductors for Antireflection Coatings," Philosophical Magazine, **90**(21) pp. 2925.

[105] Kirby, D. J., Chang, D. T., Stratton, F. P., 2009, "A Differential Capacitive Thin Film Hydrogen Sensor," Sensors and Actuators B: Chemical, **141**(2) pp. 424-430.

[106] Huiberts, J. N., Griessen, R., Rector, J. H., Wijngaarden, R. J., Dekker, J. P., de Groot, D. G., Koeman, N. J, 1996/03/21, "Yttrium and Lanthanum Hydride Films with Switchable Optical Propertie," Nature, **380**(6571) pp. 231-234.

[107] Mongstad, T., Platzer-Björkman, C., Karazhanov, S. Z., 2011, "Transparent Yttrium Hydride Thin Films Prepared by Reactive Sputtering," Journal of Alloys and Compounds, **509, Supplement 2**(0) pp. S812-S816.

[108] Anders, A., Slack, J. L., and Richardson, T. J., 2008, "Electrochromically Switched, Gas-Reservoir Metal Hydride Devices with Application to Energy-Efficient Windows," Thin Solid Films, **517**(3) pp. 1021-1026.

[109] Miura, S., Fujisawa, A., Tomekawa, S., "A Hydrogen Purification and Storage System using CO Adsorbent and Metal Hydride," Journal of Alloys and Compounds, (0) .

[110] Brodowsky, H., 1968, "Book Review: The Palladium-Hydrogen System. by F. A. Lewis," Angewandte Chemie International Edition in English, **7**(6) pp. 487-487.

[111] Heung, L. K., Tran, R. S., and Stoner, K. J., 1991, "Metal Hydride Compacts for Hydrogenisotope Separation," Journal of the Less Common Metals, **172–174, Part 3**(0) pp. 1313-1319.

[112] Choppin, G.R., Liljenzin, J., and Rydberg, J., 2002, "Radiochemistry and Nuclear Chemistry (Third Edition),"Butterworth-Heinemann, Woburn, pp. 11-40.

[113] Krishtalik, L. I., and Tsionsky, V. M., 1971, "Mechanism of the Elementary Act of Proton Transfer. Preexponential Factor and Hydrogen Isotope Separation Factor," Journal of Electroanalytical Chemistry and Interfacial Electrochemistry, **31**(2) pp. 363-374.

[114] Ito, Y., Takahashi, R., Mizusaki, S., 2006, "Magnetic Field Effects on the Hydrogen Isotope Separation with Metal Hydrides," Science and Technology of Advanced Materials, **7**(4) pp. 369-372.

[115] Vajeeston,S.Zh.Karazhanov and A.G.Ulyashin and P.Ravindran and P., 2008, "Semiconducting Hydrides," EPL (Europhysics Letters), **82**(1) pp. 17006.

[116] Karazhanov, S. Z., Ulyashin, A. G., Vajeeston, P., 2008, "Hydrides as Materials for Semiconductor Electronics," Philosophical Magazine, **88**(16) pp. 2461-2476.

[117] Leephakpreeda, T., 2012, "Mathematical Modeling of Pneumatic Artificial Muscle Actuation Via Hydrogen Driving Metal Hydride-LaNi5," Journal of Bionic Engineering, **9**(1) pp. 110-118.

[118] M M Barreiro and D R Grana and G A Kokubu and M I Luppo and S Mintzer and,G.Vigna, 2010, "Titanium Compacts Produced by the Pulvimetallurgical Hydride–dehydride Method for Biomedical Applications," Biomedical Materials, **5**(2) pp. 025010.

[119] Van Houten, R., 1974, "Selected Engineering and Fabrication Aspects of Nuclear Metal Hydrides (Li, Ti, Zr, and Y)," Nuclear Engineering and Design, **31**(3) pp. 434-448.

[120] Konashi, K., and Yamawaki, M., 2012, "Environmentally Friendly Application of Hydrides to Nuclear Reactor Cores," Advances in Applied Ceramics: Structural, Functional & Bioceramics, **111**(1) pp. 106-111.

[121] Lee, M., Kim, K. J., Hopkins, R. R., 2009, "Thermal Conductivity Measurements of Copper-Coated Metal Hydrides (LaNi5, Ca0.6Mm0.4Ni5, and LaNi4.75Al0.25) for use in Metal Hydride Hydrogen Compression Systems," International Journal of Hydrogen Energy, **34**(7) pp. 3185-3190.

[122] Ron, M., Bershadsky, E., and Josephy, Y., 1991, "The Thermal Conductivity of Porous Metal Matrix Hydride Compacts," Journal of the Less Common Metals, **172–174, Part 3**(0) pp. 1138-1146.

[123] Kim, K.J., "Multi-staged Thermal Compression of Hydrogen Utilizing Geothermal Energy - Final Technical Report, National Renewable Energy Laboratory, The United State Department of Energy September 16, 2011 .

[124] Dhaou, H., Mellouli, S., Askri, F., 2007, "Experimental and Numerical Study of Discharge Process of Metal–hydrogen Tank," International Journal of Hydrogen Energy, **32**(12) pp. 1922-1927.

[125] Sun, D., and Deng, S., 1990, "Numerical Solution of the Two-Dimensional Non-Steady Heat and Mass Transfer Problem in Metal Hydride Beds," International Journal of Hydrogen Energy, **15**(11) pp. 807-816.

[126] Jemni, A., and Nasrallah, S. B., 1995, "Study of Two-Dimensional Heat and Mass Transfer during Desorption in a Metal-Hydrogen Reactor," International Journal of Hydrogen Energy, **20**(11) pp. 881-891.

[127] Muthukumar, P., Satheesh, A., Madhavakrishna, U., 2009, "Numerical Investigation of Coupled Heat and Mass Transfer during Desorption of Hydrogen in Metal Hydride Beds," Energy Conversion and Management, **50**(1) pp. 69-75.

[128] Yoo, H., Ko, J., and Ju, H., 2013, "A Numerical Investigation of Hydrogen Absorption Phenomena in Thin Double-Layered Annulus ZrCo Beds," International Journal of Hydrogen Energy, **38**(18) pp. 7697-7703.

[129] Yoo, H., Ko, J., Yun, S., 2013, "A Numerical Investigation of Hydrogen Desorption Phenomena in ZrCo Based Hydrogen Storage Beds," International Journal of Hydrogen Energy, **38**(14) pp. 6226-6233.

[130] Majer, G, Kaess, U,Bowman, RC, 1998, "Nuclear Magnetic Resonance Studies of Hydrogen Diffusion in LaNi5.0H6.0 and LaNi4.8Sn0.2H5.8," PHYSICAL REVIEW B, **57**(21) pp. 13599-13603.

[131] Dantzer, P., and Orgaz, E., 1986, "Thermodynamics of Hydride Chemical Heat pump—II. how to Select a Pair of Alloys," International Journal of Hydrogen Energy, **11**(12) pp. 797-806.

[132] Bhuiya, M. M. H., Lee, C. Y., Hopkins, R., 2011, "A High-Performance Dual-Stage Hydrogen Compressor System Using Ca0.2Mm0.8Ni5 Metal Hydride," Smart Materials, Adaptive Structures and Intelligent Systems, Anonymous ASME, **1,** pp. 745-751.

CURRICULUM VITA

Graduate College
University of Nevada, Las Vegas

Md. Mainul Hossain Bhuiya

Education

MS, Mechanical Engineering, University of Nevada, Reno   **12.2008**

BS, Mechanical Engineering, Bangladesh Univ. of Engineering & Technology   **08.2005**

Professional Registration

Nevada Board of Engineers, License # OT6625   **12.2011**

Journal Publications

[1] "Heat Transfer Measurement During Dropwise Condensation Using Micro/Nano-Scale Porous Surface". *International Journal of Heat and Mass Transfer*, Vol. 65, p. 619–626 (**2013**)

[2] "Transparent Actuator Made with Few Layer Graphene Electrode and Dielectric Elastomer, for Variable Focus Lens". *Applied Physics Letters* 103, 023106 (**2013**)

[3] "High-Performance Heat Sink Composites Incorporating Micron-sized Inorganic Fillers and Sn/In Metal particles". *Polymer Engineering and Science,* Volume 52, Issue 11, Nov. **2012**

[4] "Pool Boiling Heat Transfer with Nano-Porous Surface". *International Journal of Heat and Mass Transfer*, Vol. 53, p. 4274 (**2010**)

Conference Proceedings

[5] "Development of Smart Heat Sink Composites Using Hybrid Fillers". Conference Proceedings*,* Society of Plastics Engineers (SPE)*.* 16 July **2012**

[6] "A High-Performance Dual-Stage Hydrogen Compressor System Using $Ca_{0.2}Mm_{0.8}Ni_5$ Metal Hydride", ASME Conference Proceedings*, SMASIS*, September **2011**, Phoenix, Arizona.

Dissertation Title

Design and Analysis of Hydrogen Powered Actuator Integrating Metal Hydride Storage System

Dissertation Examination Committee

Kwang J. Kim, Ph.D., Committee Chair

Brendan O'Toole, Ph.D., Committee Member

Dong-Chan Lee, Ph.D., Committee Member

Woosoon Yim, Ph.D., Committee Member

Jacimaria R. Batista, Ph.D., Graduate College Representative